

**Astrometric search  
for extrasolar planets  
in stellar multiple systems**

Dissertation

submitted in partial fulfillment  
of the requirements for the degree of  
doctor rerum naturalium (*Dr. rer. nat.*)

submitted to the  
faculty council for physics and astronomy  
of the Friedrich-Schiller-University Jena

by graduate physicist  
Tristan Alexander Röhl,  
born at 30.01.1981 in Friedrichroda.

**Referees:**

1. Prof. Dr. Ralph Neuhäuser (FSU Jena, Germany)
2. Prof. Dr. Thomas Preibisch (LMU München, Germany)
3. Dr. Guillermo Torres (CfA Harvard, Boston, USA)

**Day of disputation:** 17 May 2011

In Memoriam

**Siegmund Meisch**

\* 15.11.1951      † 01.08.2009

*“Gehe nicht, wohin der Weg führen mag,  
sondern dorthin, wo kein Weg ist,  
und hinterlasse eine Spur ... ”*

Jean Paul





# Contents

<b>1. Introduction</b>	<b>1</b>
1.1. Motivation . . . . .	1
1.2. Aims of this work . . . . .	4
1.3. Astrometry - a short review . . . . .	6
1.4. Search for extrasolar planets . . . . .	9
1.5. Extrasolar planets in stellar multiple systems . . . . .	13
<b>2. Observational challenges</b>	<b>29</b>
2.1. Astrometric method . . . . .	30
2.2. Stellar effects . . . . .	33
2.2.1. Differential parallaxe . . . . .	33
2.2.2. Stellar activity . . . . .	35
2.3. Atmospheric effects . . . . .	36
2.3.1. Atmospheric turbulences . . . . .	36
2.3.2. Differential atmospheric refraction . . . . .	40
2.4. Relativistic effects . . . . .	45
2.4.1. Differential stellar aberration . . . . .	45
2.4.2. Differential gravitational light deflection . . . . .	49
2.5. Target and instrument selection . . . . .	51
2.5.1. Instrument requirements . . . . .	51
2.5.2. Target requirements . . . . .	53
<b>3. Data analysis</b>	<b>57</b>
3.1. Object detection . . . . .	57
3.2. Statistical analysis . . . . .	58
3.3. Check for an astrometric signal . . . . .	59
3.4. Speckle interferometry . . . . .	62

*Contents*

<b>4. Calibration</b>	<b>63</b>
4.1. Calibration clusters . . . . .	64
4.2. Iterative calibration cycle . . . . .	65
4.3. Geometric field distortions . . . . .	67
<b>5. Results</b>	<b>71</b>
5.1. Astrometric precision - lower limits . . . . .	72
5.2. Astrometric calibration cluster - 47 Tuc . . . . .	74
5.3. Target system - HD 19994 . . . . .	81
5.3.1. Relative astrometry . . . . .	82
5.3.2. Speckle Interferometry . . . . .	84
5.3.3. Radial velocity . . . . .	86
5.3.4. Companion HD 19994 C . . . . .	88
5.3.5. Comparison with theoretical models . . . . .	92
<b>6. Summary and outlook</b>	<b>97</b>
<b>A. Calculation of ephemerides</b>	<b>I</b>
<b>B. Calculation of atmospheric refraction index</b>	<b>V</b>
<b>C. HD 19994 BC - Complex visibilities</b>	<b>VII</b>
<b>D. HD 19994 C - Orbital solution</b>	<b>IX</b>
<b>E. HD 19994 C - <math>\chi^2</math> Maps</b>	<b>XV</b>
<b>F. Extended target list</b>	<b>XIX</b>
<b>G. Acknowledgment</b>	<b>XXXV</b>
<b>H. Ehrenwörtliche Erklärung</b>	<b>XXXVII</b>

# List of Figures

1.1.	Mass-orbit diagram of exoplanets . . . . .	11
1.2.	Properties of exoplanets around single stars and in stellar multiple systems . . . . .	20
1.3.	Statistical analysis of exoplanets around single stars and in stellar multiple systems . . . . .	21
1.4.	Properties of exoplanets in stellar multiple systems . . . . .	23
1.5.	Mass and multiplicity dependency of exoplanets in stellar multiple systems . . . . .	26
2.1.	Astrometric signal in a stellar binary . . . . .	31
2.2.	Reflex motion of the flux center around the common center of mass . . . . .	32
2.3.	Differential parallaxe effect for a binary . . . . .	34
2.4.	Turbulences of earth's atmosphere . . . . .	37
2.5.	Differential chromatic refraction . . . . .	42
2.6.	Uncertainty of the differential refraction correction . . . . .	44
2.7.	Uncertainty of the differential aberration correction . . . . .	48
3.1.	Analysis strategy . . . . .	60
3.2.	Examples of complex visibilities . . . . .	62
4.1.	Old globular cluster 47 Tuc . . . . .	64
4.2.	Iterative calibration cycle . . . . .	66
4.3.	Field distortions on the NACO S13 camera . . . . .	68
5.1.	Chosen cluster stars of 47 Tuc . . . . .	77
5.2.	Measurements of the <i>Master-Baseline</i> . . . . .	77
5.3.	Intrinsic instability of the chosen cluster stars . . . . .	79
5.4.	Binary measurements of HD 19994 . . . . .	82

*List of Figures*

5.5.	Visibilitiy and phase of HD 19994 BC for 2004 . . . . .	85
5.6.	Astrometric measurements of HD 19994 A&BC . . . . .	90
5.7.	Speckle measurements of HD 19994 B&C . . . . .	90
5.8.	Radial velocities of HD 19994 B&C . . . . .	91
5.9.	Influence of the Br $\gamma$ narrow band and the Ks broad band filter on brightness ratio measurements. . . . .	94
5.10.	Theoretical evolutionary tracks for HD 19994 B&C . . . . .	95
A.1.	Orbit of a celestial body . . . . .	II
C.1.	Complex visibilities of HD 19994 BC (2004 & 2006) . . . . .	VII
C.2.	Complex visibilities of HD 19994 BC (2007 - 2009) . . . . .	VIII
D.1.	HD 19994 A&BC - orbital solution . . . . .	X
D.2.	HD 19994 B&C - orbital solution . . . . .	XI
D.3.	HD 19994 B - astrometric reflex orbit . . . . .	XII
D.4.	HD 19994 B&C - binary orbit . . . . .	XII
D.5.	HD 19994 B&C - radial velocities . . . . .	XIII
E.1.	Two dimensional $\chi^2$ maps . . . . .	XV
E.4.	One dimensional $\chi^2$ maps . . . . .	XVIII

# List of Tables

1.1. Exoplanets in closer binaries . . . . .	15
1.2. Exoplanets in wider binaries . . . . .	16
1.3. Exoplanets in stellar systems with more than two components . . . . .	17
1.4. Multiplicity of exoplanet host stars . . . . .	18
1.5. Critical semi-major axis of close stellar binaries . . . . .	24
2.1. Astrometric jitter caused by stellar activity . . . . .	35
2.2. Parameter uncertainties regarding the differential refraction correction . . . . .	43
2.3. Parameter uncertainties regarding the differential aberration correction . . . . .	47
2.4. Maximum gravitational light deflection . . . . .	50
2.5. Stellar systems observed on the northern hemisphere . . . . .	54
2.6. Stellar systems observed on the southern hemisphere . . . . .	55
5.1. Summary of remaining astrometric uncertainties . . . . .	73
5.2. Lower limits for astrometric measurement precision . . . . .	73
5.3. Measurements of the <i>Master-Baseline</i> . . . . .	78
5.4. Separation correction terms . . . . .	80
5.5. Position angle correction terms . . . . .	80
5.6. HD 19994 A&B separation measurements . . . . .	83
5.7. HD 19994 A&B position angle measurements . . . . .	84
5.8. HD 19994 B&C speckle measurements . . . . .	86
5.9. Radial velocities of HD 19994 B&C . . . . .	87
5.10. HD 19994 corrected measurements . . . . .	89
5.11. Orbital elements of HD 19994 C . . . . .	91
5.12. Ks band magnitudes of the HD 19994 system . . . . .	94



# 1. Introduction

## 1.1. Motivation

Since the first indisputable extrasolar planet<sup>1</sup> around a solar like star was discovered in 1995 by Mayor and Queloz [116], more than 450 exoplanets are detected so far (Schneider [171]). Almost all of them were detected indirectly, mainly by the radial velocity (RV) method, where the Doppler shift in the spectra of a star (introduced by an orbiting object) is measured. Another very successful method is the transit method, which measures the decreasing star flux while an object is moving in front of the star through the line of sight. Both methods detected more than 90 % of all known exoplanets today and are a perfect example of how the combination of different observation techniques could gain much more information than each method on its own.

Due to the unknown orbital inclination of the planetary companion the RV method just measured its minimum mass, whereas transit measurements delivers the inclination angle and the radius of a surrounding object, but no information about its mass. Combining both techniques the true mass, the radius, and the density of the exoplanet can be obtained. That allows an insight into the interior structure

---

<sup>1</sup> An extrasolar planet (exoplanet) is a planetary object orbiting another star than our sun.

## 1. Introduction

of the exoplanet, which is an important key to distinguish and characterize them as e.g. solid earth-like or Jovian planets. However, transit measurements are only applicable for nearly edge-on<sup>2</sup> orbits and are mainly sensitive for exoplanets very close to their host star. Almost all transiting exoplanets have orbital periods of less than one week. Looking at the mass-orbit diagram of exoplanets found so far (Fig. 1.1), one can identify areas with a higher rate of exoplanet detections. The reason for that is not only an astrophysical background of planetary formation, but also different sensitivities of the detection methods. By improving the measurement precision and including other types of target stars one can enter neighboring regions in the parameter space (e.g. RV measurements recently entered the region of lower mass exoplanets with smaller orbital periods, especially around low mass stars). But exoplanets with larger orbital periods are still undiscovered. The reasons are the observational timeline of current search programs and the decrease of the sensitivity for RV measurements toward larger orbital periods.

As one can see by the lines of sensitivity in Fig. 1.1 that parameter region can be perfectly filled by astrometric observations. Astrometry is complementary to the RV technique and measures the two transverse dimensions instead of the radial dimension of the stellar reflex motion (also called wobble), which is induced by an orbiting exoplanet. In contrast to RV or transit observations astrometry is applicable for exoplanets with larger orbital periods and delivers the true planetary mass independently from its orbital inclination. Especially in order to detect planetary system similar to our own solar system one has to consider outer planets with larger orbital periods

---

<sup>2</sup> edge-on ... inclination angle of about  $90^\circ$



like Jupiter, Neptune or Saturn.

The formation of exoplanets is still a poorly understood process and knowledge from observations is strongly biased by the observation technique and selection criteria for the target stars. For example, by using our own planetary system as an archetype almost all exoplanet search programs so far excluded stellar multiple systems as target stars, although the multiplicity of solar like stars is determined to be about 50 % (Abt and Levy [1], Duquennoy and Mayor [46], Raghavan et al. [158]). Today, almost all multiplicity studies of exoplanet host stars (Mugrauer et al. [134], Eggenberger et al. [50], Chauvin et al. [29]) were carried out after an exoplanet detection, thus the original selection effects are still present in these samples. These studies measured an exoplanet host star multiplicity of about 20 %. As described above, selection effects have an influence on the multiplicity rate, but are they the only explanation for such different multiplicity rates?

From the theoretical point of view, there should be an interaction between the protoplanetary disk around a star and a close stellar companion (Kley et al. [88], Haghighipour and Raymond [71], and references therein). Up to now, no exoplanet in a stellar binary with a semi-major axis of less than 20 AU<sup>3</sup> is found. Previous studies of exoplanets in stellar multiple systems indicate, that a close stellar component affects the formation, the dynamical behavior, the evolution, and the stability of an exoplanet (Eggenberger et al. [48], Bonavita and Desidera [15], Desidera and Barbieri [39], Holman and Wiegert [81]). Hence, it seems very likely that the difference in the multiplicity rate is also a result of real restrictions for planet formation and not only of observational bias and selection effects.

---

<sup>3</sup> 1 AU (Astronomical Unit) = 149 598 000 km

## 1. Introduction

### 1.2. Aims of this work

The main goal of this work is to study the occurrence and the properties of exoplanets in stellar multiple systems by develop a suitable observation strategy to search for exoplanets in such systems. This work is especially concentrated on close binaries, where planet formation should theoretically be truncated or influenced at a certain lower binary separation of about 20 AU. In contrast to the most previous multiplicity studies this work searches for exoplanets in stellar multiple systems and not for stellar components around exoplanet host stars. That avoids to adopt already existing selection effects. Another project with a similar approach is the project by Desidera et al. [41], who are using the RV technique to search for exoplanets in stellar binaries.

As described before astrometric observations are useful to fill up currently unobservable regions in the exoplanet parameter space (Fig. 1.1). Furthermore, it is a suitable method to search for exoplanets in very close binaries. A binary with a separation of ten AU at a distance of 50 parsec<sup>4</sup> has an angular separation of 0.2 arcsec<sup>5</sup>, thus a high spatial resolution is needed to observe both stars separately. Normally, RV observations are limited to a lower stellar separation of about 2 arcsec, due to the size of the slit or fiber. Also, the spatial resolution of transit observations is usually not sufficient to resolve such close binaries.

The best astrometric performance will be obtained by space based observations like GAIA (Global Astrometric Interferometer for Astrophysics) with a proposed accuracy of 10  $\mu$ as (Lindgren [100], Quist

---

<sup>4</sup> 1 parsec (pc) =  $3.0857 \times 10^{16}$  m

<sup>5</sup> One arcsec (as) is 1/3600 of one degree.

[155]) or ground based interferometric observations like PRIMA (Phase Referenced Imaging and Microarcsecond Astrometry) with a proposed accuracy of  $20 \mu\text{as}$  (Delplancke [37], Launhardt [94]).

However, besides the fact that both projects are presently not available for the astronomical community, neither GAIA nor PRIMA will be able to resolve such close binaries. GAIA, which is an astrometric satellite build by ESA (European Space Agency) and the successor of the Hipparcos satellite, is designed to map billion of stars and not for high resolution imaging. Dual-beam interferometers like PRIMA, which is operated by ESO (European Southern Observatory) at the VLTI (Very Large Telescope Interferometer) on Paranal in Chile, are limited by an optical device called star separator to a lower stellar separation limit of about 2 arcsec (Launhardt [94]).

On the other hand, current optical large telescopes like the ESO-VLT in Chile or the SUBARU telescope operated by the NAOJ (National Astronomical Observatory of Japan) on Hawaii are equipped with 8 meter apertures and adaptive optics (AO) systems to correct the turbulences of earth's atmosphere. Depending on the atmospheric conditions these facilities achieve a spatial resolution down to about 0.1 arcsec, which is ideal for astrometric observations of close binaries.

In summary, there are the following three main aspects, which will be presented and discussed in this work.

1. Statistical analysis of exoplanets in stellar multiple systems.
2. Development of observation, calibration and analysis strategies for a long term exoplanet search program by ground based astrometric imaging.
3. Feasibility study of the designed astrometric search program.

### 1.3. Astrometry - a short review

Astrometry itself, as the position and velocity measure of celestial bodies, is one of the oldest branches in astronomy. In 1844, the German mathematician and astronomer Friedrich Wilhelm Bessel detected a periodic deviation of the nearby and bright star Sirius superposed on its stellar proper motion (Bessel [13]). He assumed an unseen companion as perturber, which was confirmed about 20 years later by a direct detection. Thus, Bessel did the first indirect detection of an astrometric companion. That astrometric detection started a controversy about stellar multiplicity.

Several groups of astronomers were fascinated by the idea that every star could be in fact a multiple system and in the first half of the 20th century, astrometry was a very popular method to study the multiplicity of stars (Lippincott [101] and references therein). Already in 1956, van de Kamp [193] proposed to search for planetary objects around nearby stars by measuring their reflex motion. Several years later, in 1963, he published the astrometric detection of a Jovian planet around the nearby M-dwarf Barnard's star (van de Kamp [194]). However, other groups like e.g. Gatewood and Eichhorn [66] could not redetect the published reflex motion of Barnard's star.

In 1973, Hershey [79] measured systematic effects for the astrometric properties of the "Sproul refractor", which was also used by van de Kamp for his observations of Barnard's star. Hence, van de Kamp's supposed astrometric detection was in fact caused by systematic errors, due to a change of the telescope optics. Today, several observations with current telescopes and modern instruments excluded the existence of Jovian planets around Barnard's star. Unfortunately, van

de Kamp never acknowledged any systematic errors and believed in his astrometric detection until he died in 1995 (van de Kamp [195]).

After an international discussion about this false detection astrometry was discarded as suitable method to find exoplanets and in the following decades efforts were concentrated on other techniques like e.g. the radial velocity technique. But with the realization of observational bias and selection effects the need of different observational techniques, in order to study the exoplanetary diversity, becomes more relevant in the last years.

The first successful application of astrometry regarding exoplanets was done by Benedict et al. [11] in 2002. The authors used the HST<sup>6</sup> to confirm the planetary nature of the RV planet candidate Gl876 b, detected by Marcy et al. [110] in 1998. The astrometric measurements were done with the FGS<sup>7</sup> of the telescope, which is a white light interferometer. Other confirmations of RV planet candidates using the HST are 55 Cnc d by McArthur et al. [118] in 2004 and  $\epsilon$  Eridani b by Benedict et al. [12] in 2006. Furthermore, some RV exoplanet candidates could be ruled out as planets by HST astrometry (e.g. HD 33636 b by Bean et al. [8]).

In addition to space based observations, also ground based astrometric observations are done to find exoplanets. One of these programs is STEPS<sup>8</sup> by Pravdo and Shaklan [149]. In 2009, Pravdo and Shaklan [150] claimed the first astrometric detection of an exoplanet around the nearby M-dwarf VB 10. However, RV follow up observations done by Bean et al. [9] have ruled out that proposed exoplanet. Furthermore, Lazorenko et al. [97], who perform astrometric observa-

---

<sup>6</sup> Hubble Space Telescope

<sup>7</sup> Fine Guiding Sensor

<sup>8</sup> STEllar Planet Survey

## 1. Introduction

tions at the  $\mu\text{as}$ <sup>9</sup> level using the optical imager FORS2<sup>10</sup> at the VLT (Lazorenko et al. [96]), did not measure the published reflex motion of VB 10.

Another ground based project is PHASES<sup>11</sup>, which uses the Palomar Testbed Interferometer (PTI). The PTI was operated from 2002 until 2008 and one outcome of the data was recently published by Muterspaugh et al. [137] at the end of 2010. The authors claim the detection of a Jovian planet in the nearby stellar binary HD 176051. This astrometric detection has now to be confirmed by other observational methods.

Besides the astrometric accuracy, the observational timeline has also to be taken into account for astrometric observations. In contrast to transiting exoplanets with orbital periods of usually less than one week astrometry is most sensitive for large orbital periods of several years or decades. Such kind of long-periodic exoplanets are still undetectable today (Fig. 1.1) because the reflex motion of their host stars is too slow for RV measurements and they are still not resolvable by direct imaging techniques. To determine the orbital elements of an astrometric companion the complete astrometric reflex orbit should be covered with measurements. Hence, the observational timeline needed for astrometric observations could be larger than the typical lifetime of satellite missions or instruments. Therefore, special observation and calibration strategies are needed for astrometric search programs.

---

<sup>9</sup>  $1 \mu\text{as} = 1/1000 \text{ mas}$

<sup>10</sup> FOcal Reducer/low dispersion Spectrograph 2

<sup>11</sup> Palomar High-precision Astrometric Search for Exoplanet Systems

## 1.4. Search for extrasolar planets

After the discovery of more than 450 exoplanets so far (Schneider [171]) the task to characterize them has started recently. Planet formation and evolution can now be studied by comparing the properties of exoplanets regarding also the environment of their origin. However, one question is still open today, namely the definition of an exoplanet. The most common and generally accepted criterion for an exoplanet is a mass less than the theoretical deuterium burning minimum mass (DBMM) of about  $13 M_{\text{Jup}}$ <sup>12</sup>. But especially the transition zone around this DBMM is a dispute. In fact, to specify substellar objects<sup>13</sup> one has to know the interior structure (e.g. density) and the origin of their formation (e.g. within a circumstellar disc or from a molecular cloud, by fragmentation or gravitational collapse).

However, working with exoplanet data one has to use a tentative definition. In this work the exoplanet definition from the *Extrasolar Planets Encyclopaedia* (called EPE) by Jean Schneider [171] is used, thus all objects listed there are exoplanets by definition. This includes all detected and confirmed substellar objects with a mass less than  $20 M_{\text{Jup}}$  within a  $2\sigma$  uncertainty. Because of a controversial planetary status and missing references in the EPE, GJ 433 b, GJ 676A b, GJ 667C b, HIP 12961 b and HD 28254 b are rejected as exoplanets in this work.

Analysing current exoplanet data one has to keep in mind observational bias and selection effects, especially with respect to global statistics.

---

<sup>12</sup>  $1 M_{\text{Jup}} = 1.899 \times 10^{27}$  kg... the mass of Jupiter

<sup>13</sup> A substellar object (brown dwarf or planet) has a mass less than  $0.08 M_{\odot}$  ( $1 M_{\odot} = 1.989 \times 10^{30}$  kg... the mass of our sun), which is not heavy enough for stable hydrogen fusion.

## 1. Introduction

### Selection effect

Taking our own solar system as an archetype almost all exoplanet search programs are concentrated on single and solar like stars, thus the majority of all detected exoplanets have such a host star. Recently, the target selection for RV and transit observations was enlarged, especially to lower mass (e.g. late-type) main sequence stars in order to detect lower mass planets.

### Observational bias

There are several different methods to search for exoplanets, whereas the RV and transit method are the very most productive ones. However, every method has pros and cons. Furthermore, every method delivers other information about the exoplanet and is sensitive for different exoplanet properties (Fig. 1.1). The transit method measures the decreasing star flux while an object is moving in front of the star through the line of sight. The decrease of the flux and the transit probability ( $p$ ) can be calculated as

$$\frac{\Delta F}{F} \simeq \left( \frac{R_{\text{pl}}}{R_{\star}} \right)^2, \quad p = \frac{R_{\star}}{a_{\text{pl}}} = \arccos(i_{\text{min}}). \quad (1.1)$$

The probability ( $p$ ) to detect a transit event is inverse proportional to the planetary semi-major axis ( $a_{\text{pl}}$ ), thus almost all transiting exoplanets have an orbital period of less than one week and are very close to their host star. Transit observations achieve no information about the planetary mass. Therefore, RV follow-up observations are needed, which can deliver (in combination with the orbital inclination and planetary radius by transit measurements) the true mass and the density of the exoplanet.



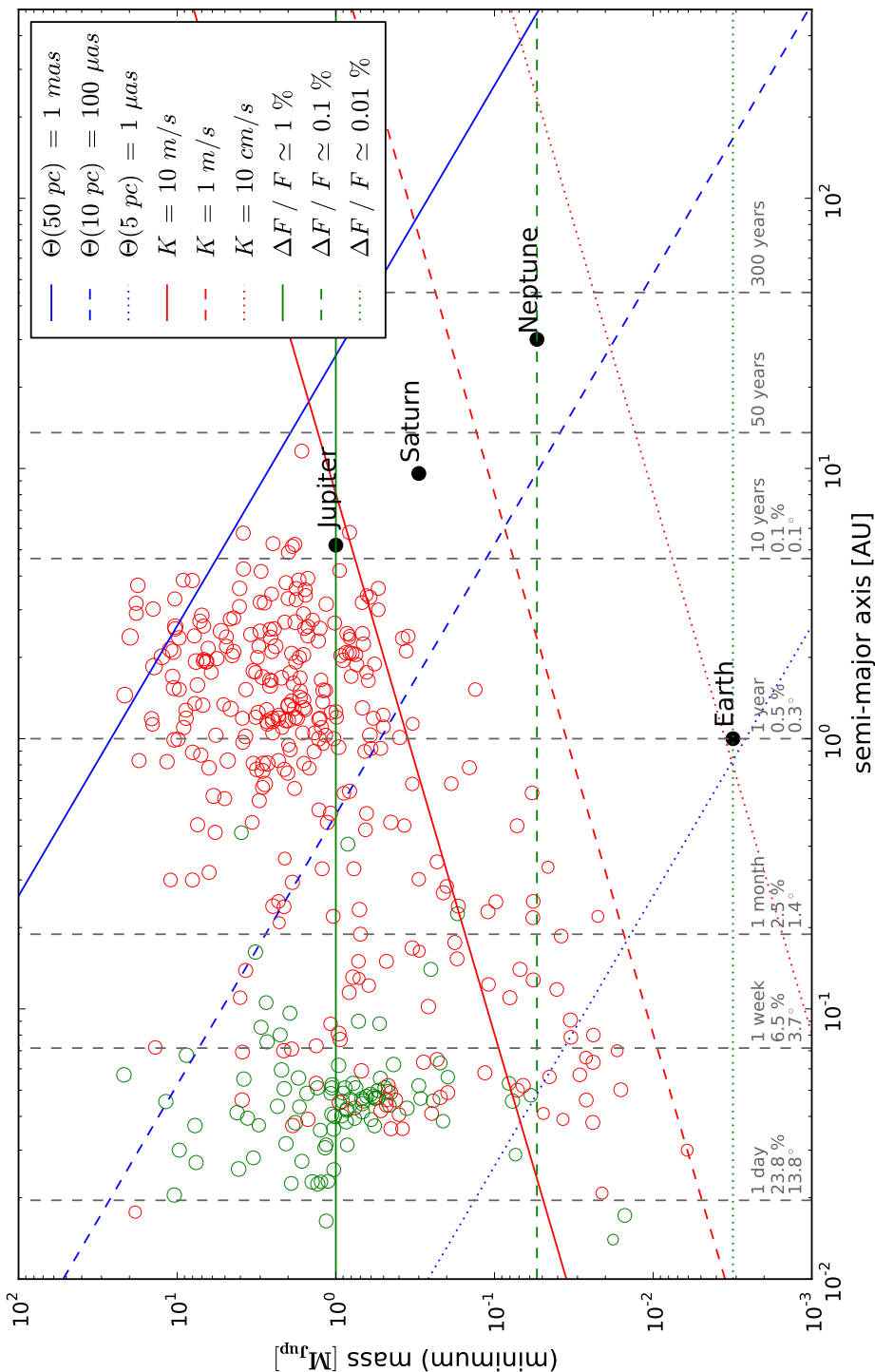


Fig. 1.1.: Planetary (minimum) mass over the semi-major axis for all exoplanets (data from the EPE, [171]) found by radial velocity (red circles) and transit (green circles) observations. The size of the markers represents the mass of the exoplanet host star. The gray numbers at the bottom of the diagram are the orbital period, the probability to detect a transit signal and the maximum allowed inclination deviation from an edge-on orbit for an exoplanet around a solar like star. Furthermore, the astrometric signal (blue lines), the radial velocity signal (red lines) as well as the transit signal (green lines) for an exoplanet in a circular orbit around a solar like star is shown. The black dots are planets from our own solar system.

## 1. Introduction

The RV method measures the radial velocity of an exoplanet host star, which can be determined by the Doppler shift of stellar spectral lines. That shift is caused by the periodic reflex motion of the exoplanet host star around the common center of mass. The RV signal  $K$  of an exoplanet can be calculated as

$$K \text{ [m/s]} = \frac{m_{\text{pl}} \sin(i)}{(M_{\star} + m_{\text{pl}})^{2/3}} \left( \frac{2\pi G}{P_{\text{pl}}} \right)^{1/3} (1 - e^2)^{-1/2}. \quad (1.2)$$

For shorter planetary periods ( $P_{\text{pl}}$ ) the radial velocity of its host star increases. Hence, the RV method is mostly sensitive for massive and short period exoplanets. Because the RV signal depends on the orbital inclination only the minimum mass  $m_{\text{pl}} \sin(i)$  of the exoplanet can be achieved, which is the reason why every RV exoplanet is a planet candidate until its inclination angle is determined.

The astrometric method is based on the same principle as the RV technique, but measures the spatial displacement (two transverse dimensions) of the host star's reflex motion and not the radial velocity. The astrometric signal of an exoplanet ( $\Theta$ ) is the reflex motion of the host star around the common center of mass and can be calculated for a circular orbit as

$$\Theta \text{ [mas]} = 1.91 \frac{m_{\text{pl}} [M_{\text{Jup}}]}{M_{\star} [M_{\odot}]} \frac{a_{\text{pl}} [\text{AU}]}{d [\text{pc}]} . \quad (1.3)$$

The astrometric signal is proportional to the planetary semi-major axis ( $a_{\text{pl}}$ ), thus astrometry is most sensitive for massive and long period planets. That makes astrometry complementary to the RV method and in contrast to RV and transit observations it delivers the true mass of the orbiting exoplanet independently from its inclination.

Every detection method produces a higher number of planet detections in a certain parameter region, where it is most sensitive. Hence, the distributions of exoplanets in Fig. 1.1 does not only reflect real planetary formation processes, but is also based on different detection methods. This effect is known as observational bias.

## 1.5. Extrasolar planets in stellar multiple systems

Speaking about exoplanets in stellar multiple systems one has to distinguish two types of configurations. The one is called “S-type” orbit and describes the common case of an exoplanet around one stellar component of a binary. In contrast to that, the “P-type” orbit describes a situation, where an exoplanet orbits the complete stellar binary. Such exoplanets are called circumbinary planets. It is not easy to find exoplanets in an “S-type” orbit, but it is much harder to detect a circumbinary planet. The most promising approach for that is the technique of “Transit Timing Variations” (TTV), which is only applicable for a nearly edge-on orbit of the stellar binary. The TTV method is still a new technique and measures the time of a transit event very precisely. A detected periodic deviation of the mid-transit time can then be modelled as a gravitational influence of a further surrounding object. Today, just three systems with a circumbinary planet are known, namely NN Serpentis (Beuermann et al. [14]), DP Leo (Qian et al. [152]) and HW Vir (Lee et al. [98]). Of course, all of them still have to be confirmed by other techniques. Because both orbit types has to be observed by different techniques this work concentrates on exoplanets in the commonly “S-type” orbits, which are detectable by astrometric imaging.

## 1. Introduction

Similar to the definition of an exoplanet one needs a criterion if two or more stars form a multiple system or not. Basically, no closer stellar companion around an exoplanet host star should exist, because such systems were excluded as target stars in the past. But multiplicity studies done in the last years (Eggenberger et al. [48], Mugrauer et al. [129], Raghavan et al. [157], Chauvin et al. [29], Desidera and Barbieri [39], Daemgen et al. [35]) reveal a lot of former believed single host stars to be in fact a member of a stellar multiple system. Such multiplicity studies are not complete, thus the multiplicity rate of host stars will increase in future by further detections of stellar companions.

The final proof for a bound membership of two objects is the presence of orbital motion. However, due to the large orbital periods of visible binaries, it is usually impossible to measure such orbital motion. Hence, a common proper motion is usually accepted as a sufficient proof for multiplicity. In this work, the multiplicity of an exoplanet host star is defined by either a published common proper motion or an entry in the CCDM<sup>14</sup> by Dommanget and Nys [44].

Working with observational catalogues one has to deal with incompleteness and false detections. Especially the order of multiplicity given for some stars in the CCDM are strange and arguable. However, to abide the definition of multiplicity declared above the information from the CCDM are adopted in this work. But if the stellar companion is only mentioned in the CCDM this host star is especially marked by the symbol ‡ in the tables 1.1, 1.2 and 1.3.

By searching the literature and matching the host stars of exoplanets detected by transit or RV observations from the EPE with the

---

<sup>14</sup> Catalogue of Components of Double and Multiple Stars

1.5. Extrasolar planets in stellar multiple systems

Host-star	$N_{\text{pl}}$	$m_{\text{pl}} \sin i$ [ $M_{\text{Jup}}$ ]	$a_{\text{pl}}$ [AU]	$\rho_{\text{app}}^*$ [AU]	Reference	
1	$\gamma$ Cephei A	1	1.60	2.04	12.4	[28, 76, 141]
2	G186 A	1	4.01	0.11	20.7	[153, 127], †
3	HD 41004 A	1	2.54	1.64	21.5	[207, 157]
4	HD 41004 B	1	18.40	0.02	21.5	[206, 157]
5	tau Boo A	1	3.90	0.05	45.2	[21, 157]
6	GJ 3021 A	1	3.37	0.49	66.9	[139, 133]
7	GJ 743.2 A	1	1.28	1.00	94.4	[198, 50]
8	WASP-2 A	1	0.91 $\sin i$	0.03	111.7	[27, 35]
9	HIP 64426 A	1	11.02	0.30	134.0	[93, 131]
10	GJ 4.2 A	1	1.03	1.00	138.2	[184, 157]
11	GJ 4130 A	1	1.13 $\sin i$	0.03	216.2	[19, 50]
12	HIP 12048 A	1	0.23	0.35	222.6	[111, 131]
13	TrES-2 A	1	1.20 $\sin i$	0.04	232.2	[145, 35]
14	HIP 110852 A	1	0.45	0.04	233.2	[102, 128]
15	HIP 84856 A	1	10.45	0.99	249.9	[182, 128]
16	eps Ret A	1	1.28	1.18	251.2	[23, 157, 29], §
17	HIP 64459 A	1	0.82	2.08	280.0	[24, 157]
18	HIP 31246 A	1	0.25	0.04	310.2	[111, 157]
19	HIP 61595 A	1	0.28	0.06	489.7	[59, 39]
20	HIP 43177 A	1	0.42	0.05	621.4	[192, 157]
21	HIP 97769 A	1	1.26	1.19	676.0	[113, 157]
22	HD 16760 A	1	14.3	1.13	737.9	[20], ‡
23	TrES-4 A	1	0.92 $\sin i$	0.05	756.6	[106, 35]
24	HD 142022 A	1	4.40	2.80	793.6	[49, 157]

Tab. 1.1.: Extrasolar planets detected with transit or RV observations in closer binaries ( $\rho_{\text{app}}^* \leq 1000$  AU), sorted by the increasing apparent separation of the binary ( $\rho_{\text{app}}^*$ ).

‡... multiplicity is only mentioned in the CCDM [44]

†... B component is a white dwarf, see Mugrauer and Neuhäuser [127]

§... B component is a white dwarf, see Chauvin et al. [29]

## 1. Introduction

Host-star	$N_{\text{pl}}$	$m_{\text{pl}} \sin i$ [ $M_{\text{Jup}}$ ]	$a_{\text{pl}}$ [AU]	$\rho_{\text{app}}^*$ [AU]	Reference
1 GJ 81.1 A	2	0.11 & 0.61	0.23 & 3.34	1010	[25, 157]
2 HD 121504 A	1	1.22	0.33	1030	[117], ‡
3 55 Cnc A	5	0.02 ... 3.84	0.04 ... 5.77	1050	[157]
4 HIP 45982 A	1	3.94 $\sin i$	0.45	1203	[21, 112, 118, 157]
5 30 Ari B	1	9.88	1.00	1521	[70]
6 HAT-P-1 B	1	0.52 $\sin i$	0.06	1557	[4]
7 rho CrB A	1	1.04	0.22	1559	[143, 144], ‡
8 61 Vir A	3	0.02 ... 0.07	0.05 ... 0.48	1968	[200], ‡
9 GJ 3683 A	1	0.30	0.30	2227	[104, 134]
10 HIP 50786 A	1	7.99	0.89	2457	[90, 130]
11 GJ 777 A	2	0.06 & 1.50	0.13 & 3.92	3312	[140, 199, 157]
12 HIP 111143 A	1	4.50	2.03	3909	[166, 131], †
13 kappa CrB A	1	1.80	2.70	4186	[83], ‡
14 GJ 620.1 A	1	1.00	1.26	4451	[117, 127, 147], §
15 HIP 116906 A	1	7.75	1.35	4746	[25, 157]
16 HIP 70123 A	3	0.06 ... 7.2	0.05 ... 4.2	4752	[60, 103, 128]
17 70 Vir A	1	7.44	0.48	5187	[109], ‡
18 HIP 75458 A	1	8.82	1.27	7969	[63], ‡
19 eps Tau A	1	7.60	1.93	8626	[168], ‡
20 HIP 15527 A	1	1.90	1.38	9072	[86, 39]
21 6 Lyn A	1	1.90	1.38	10219	[169], ‡
22 HIP 27253 A	2	0.78 & 17.70	0.13 & 3.69	11928	[56, 58, 157]

Tab. 1.2.: Extrasolar planets detected with transit or RV observations in wider binaries ( $\rho_{\text{app}}^* > 1000$  AU), sorted by the increasing apparent separation of the binary ( $\rho_{\text{app}}^*$ ).

‡... multiplicity is only mentioned in CCDM [44]

†... closer B component listed in the CCDM was disproved by Mugrauer et al. [131]

§... B component is a white dwarf, see Porto de Mello and da Silva [147]

1.5. Extrasolar planets in stellar multiple systems

	Host-star	$N_{\text{pl}}$	$N_{\star}$	$m_{\text{pl}} \sin i$ [ $M_{\text{Jup}}$ ]	$a_{\text{pl}}$ [AU]	$\rho_{\text{app}}^*$ [AU]	Reference
1	HD 196885 A	1	3	2.58	2.37	23.1	[32, 29, 53], ‡
2	HD 19994 A	1	3	1.68	1.42	51.5	[117, 157, 161]
3	HIP 100970 A	1	3	3.70	0.14	130.6	[55, 157], ‡
4	HD 33564 A	1	3	9.10	1.10	218.4	[65], ‡
5	HIP 38558 A	1	3	1.21	1.37	249.2	[117, 134]
6	HD 62509 A	1	7	2.90	2.90	306.1	[75, 77], ‡
7	WASP-8 A	1	3	$2.25 \sin i$	0.08	348.0	[154] ‡
8	HD 3651 A	1	3	0.20	0.28	477.3	[57, 132], †, ‡
9	83 Leo B	1	3	0.11	0.12	506.2	[113, 157], ‡
10	HIP 101806 A	1	3	3.00	2.50	511.2	[85, 131, 50]
11	HD 164922 A	1	3	0.36	2.11	689.9	[25], ‡
12	ups And A	3	4	$0.69 \dots 11.6$	$0.06 \dots 2.55$	702.0	[22, 48], ‡
13	HD 178911 B	1	3	6.29	0.32	756.7	[205, 47]
14	16 Cyg B	1	3	1.68	1.68	859.7	[31, 157]
15	HD 192263 A	1	4	0.72	0.15	1345	[165, 167], ‡
16	GJ 893.2 A	1	5	2.90	0.30	2095	[122, 157], ‡
17	HIP 28767 A	1	3	3.32	0.81	6336	[58, 47, 133]
18	HD 81688 A	1	3	2.70	0.81	6826	[169], ‡
19	18 Del A	1	3	10.30	2.60	14488	[169], ‡
20	HD 110014 A	1	4	11.09	2.14	16902	[36], ‡

Tab. 1.3.: Extrasolar planets detected with transit or RV observations in stellar systems with more than two components, sorted by the increasing apparent separation of the host star and the nearest stellar component ( $\rho_{\text{app}}^*$ ).

‡... at least one component is only mentioned in the CCDM [44]

†... B component is a brown dwarf, see Mugrauer et al. [132]

## 1. Introduction

Host-star	exoplanets	planetary systems
Single	379	321
Multiple	79	66
Total	458	387
Multiplicity	17.25 %	17.1 %

Tab. 1.4.: Host star multiplicity of exoplanets detected with transit or RV observations obtained by matching the *Extrasolar Planets Encyclopaedia* with the *Catalogue of Components of Double and Multiple Stars* plus literature search (October 2010).

CCDM catalog a number of 66 stellar multiple systems harboring at least one exoplanet out of 387 planetary systems in total was found. These systems are listed in the tables 1.1, 1.2, and 1.3. The multiplicity rate of the exoplanet host stars is shown in table 1.4 and has a value of about 17 % . This is slightly less than the value obtained by Raghavan et al. [157] in 2006 of about 23 % . The reason for that are the transiting exoplanets, which are also included in addition to RV exoplanets in this work. Raghavan et al. [157] on the other hand just analysed exoplanets detected by the RV technique. Multiplicity studies of host stars of transiting exoplanets have just started recently in 2009 by e.g. Daemgen et al. [35]. This fact causes an underestimation of the host star multiplicity. The number of transiting exoplanets rises rapidly, especially due to satellite missions like COROT<sup>15</sup> (ESA) and KEPLER<sup>16</sup> (NASA). Hence, doing a statistical analysis of planetary properties, these exoplanets should be considered.

However, compared to the multiplicity rate of solar like stars of about 50 % (Abt and Levy [1], Fischer and Marcy [54], Duquennoy and Mayor [46]), the multiplicity of exoplanet host stars is quite low.

<sup>15</sup> “CONvection, ROTation and planetary Transits”, see Bordé et al. [16] and Lammer et al. [91]

<sup>16</sup> see Borucki et al. [18] and Torres et al. [186]



### 1.5. Extrasolar planets in stellar multiple systems

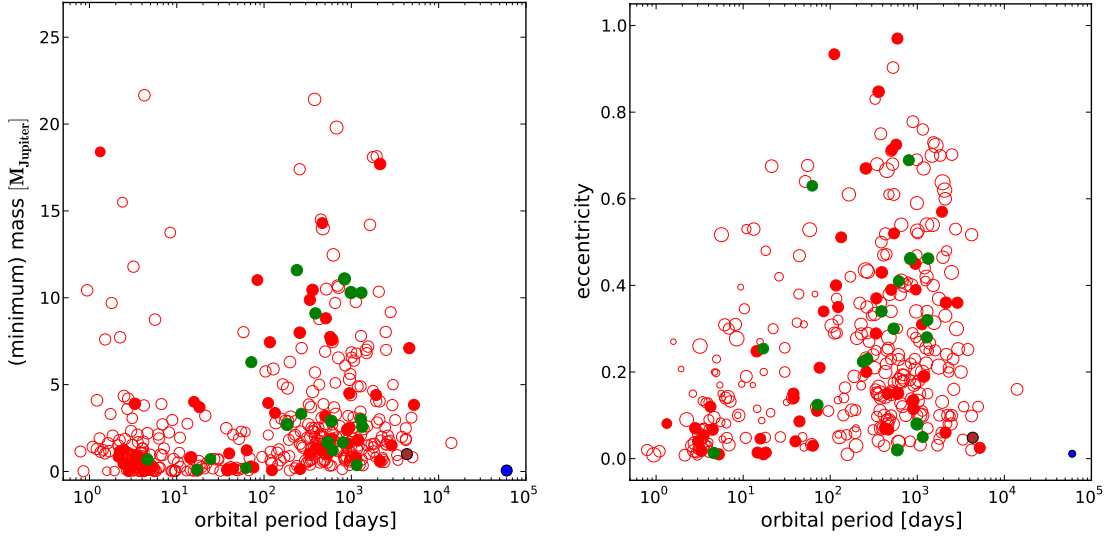
The most recent work done in the field of stellar multiplicity is the extensive study of nearby solar like stars by Raghavan et al. [158] using speckle and long-baseline interferometry as well as RV and direct imaging data. The authors determined a multiplicity rate for solar like stars of  $46\% \pm 2\%$ .

Does stellar multiplicity affect and inhibit the formation of planets or is the difference in the multiplicity rates only based on observational bias and selection effects? Of course, these effects have an influence on the multiplicity, but there is also a correlation between the binary and the planetary properties as one can see in Fig. 1.2, Fig. 1.3, and Fig. 1.5.

Very common diagrams to compare exoplanets around single stars and in multiple systems are the mass-period and the eccentricity-period diagram (Fig. 1.2) as published by e.g. Eggenberger et al. [48] in 2004 for all RV exoplanets detected so far. The authors conclude that high mass ( $m_{\text{pl}} \gtrsim 2 M_{\text{Jup}}$ ) and short period ( $P_{\text{pl}} \lesssim 40$  days) exoplanets are only present in stellar multiple systems. Another conclusion is that such short period planets in stellar multiple systems have nearly zero eccentricity. Following publications like Halbwachs et al. [72], Mugrauer et al. [131], Desidera and Barbieri [39], and Bonavita and Desidera [15] come to similar conclusions.

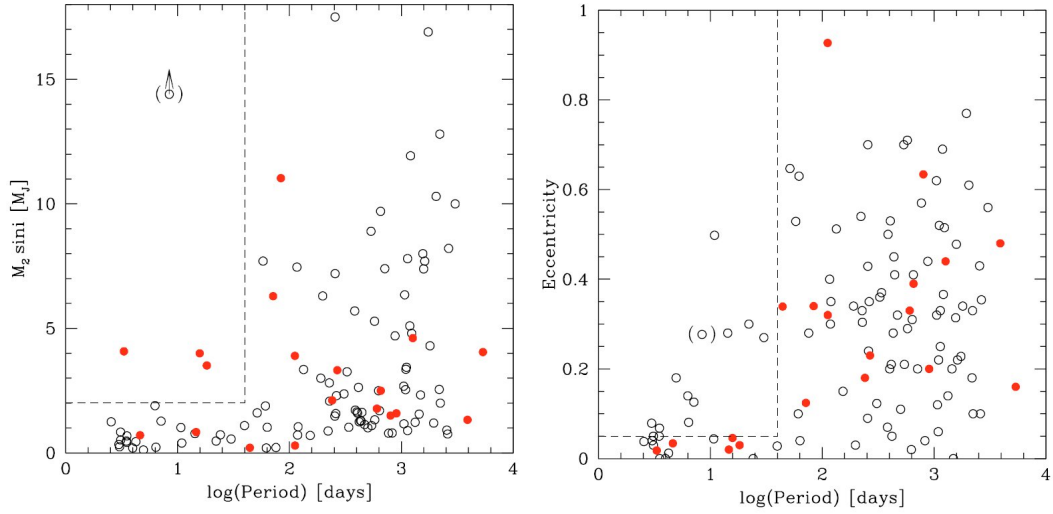
However, including also all exoplanets detected by transit observations into the analysis, the situation for the mass-period relation has changed dramatically due to the increasing number of the transiting exoplanets (Fig. 1.2). The region of high mass and short period planets is now dominated by exoplanets around single stars. The situation in the updated eccentricity-diagram is comparable to the conclusions of previous studies.

## 1. Introduction



(a) (Minimum) mass vs. orbital period of exoplanets. The size of the markers represents the mass of the exoplanet host star.

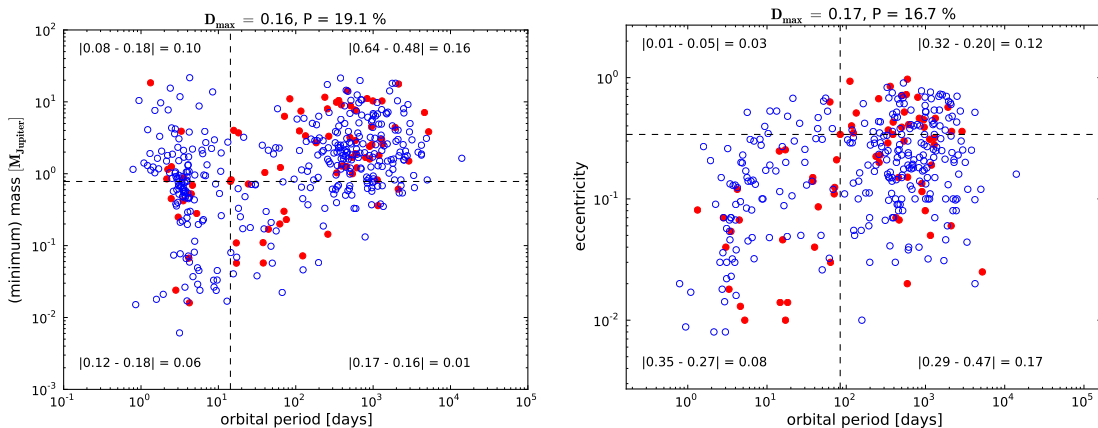
(b) Eccentricity vs. orbital period of exoplanets. The size of the markers represents the (minimum) mass of the exoplanet.



(c) Same diagrams as above by Eggenberger et al. [48] from 2004 based on RV exoplanet detections. The black circles are exoplanets around single stars while the red dots are exoplanets in a stellar multiple system.

Fig. 1.2.: Properties of exoplanets around single stars (red circles), in binaries (red dots) and in triple-stars (green dots). For comparison, Jupiter (brown dot) and Neptune (blue dot) are also shown. The upper two diagrams consists of current exoplanets (data from EPE, [171]) detected by RV or transit observations, while the lower two are only based on RV exoplanet candidates detected until 2004.

## 1.5. Extrasolar planets in stellar multiple systems



(a) Two-dimensional Kolmogorov-Smirnov test for the planetary mass-period relation.

(b) Two-dimensional Kolmogorov-Smirnov test for the planetary eccentricity-period relation.

Fig. 1.3.: Two-dimensional Kolmogorov-Smirnov test of exoplanets around single stars (blue circles) and in stellar multiple systems (red dots). The probability  $P$  that both samples have the same parent distribution is shown in the title of the diagrams and less than 20%. For further details on the two-dimensional Kolmogorov-Smirnov test see chapter 14 in Press [151].

To check if both samples (exoplanets around single stars and in stellar multiple systems) have the same parent distribution a two-dimensional Kolmogorov-Smirnov test was done (Fig. 1.3). The probability for that hypothesis is lower than 20%, thus it is very unlikely, that both samples have the same parent distribution. However, one has to keep in mind observational effects like the clump of transiting exoplanets, where multiplicity studies around their host stars have just recently started. For further details on the two-dimensional Kolmogorov-Smirnov test see chapter 14 in Press [151].

The largest difference in relative frequency between both samples (numbers in each quadrant of diagrams in Fig. 1.3) for the mass-period relation is the region of exoplanets more heavy than Jupiter and with orbital periods greater than ten days. This is not the region,

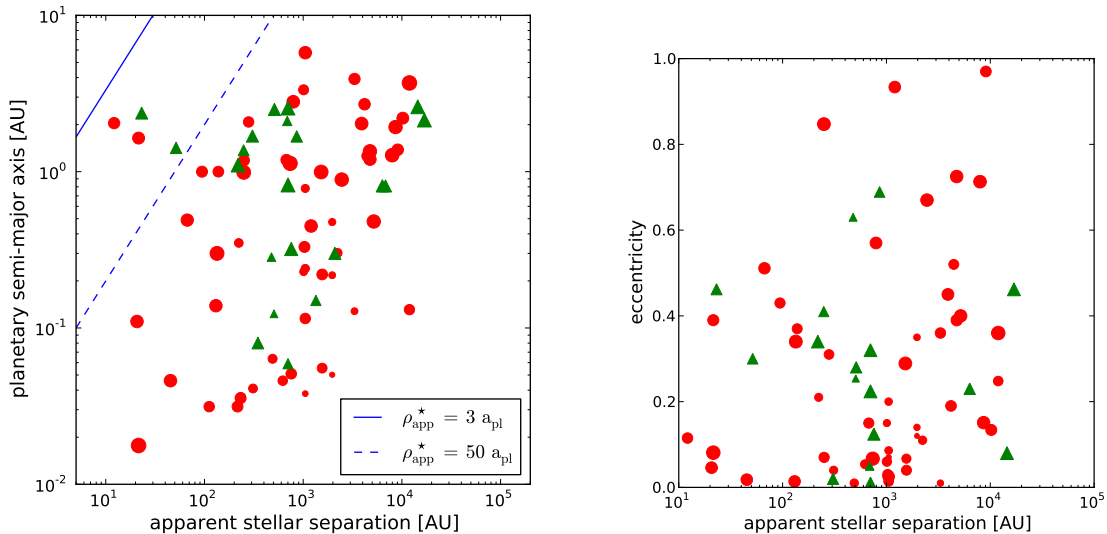
## 1. Introduction

where the clump of transiting exoplanets is located. Instead, it is the region with the most planets detected by RV observations. About 2/3 of all planets in stellar multiples systems, but only the half of all exoplanets around single stars are situated in this parameter region. That implicates a higher number of higher mass planets in stellar multiple systems as around single stars.

For the eccentricity-period relation the largest difference is present for larger orbital periods ( $P \gtrsim 100$  days) and smaller eccentricities ( $e \lesssim 0.3$ ). In this region about the half of all exoplanets around single stars, but only less than 1/3 of all planets in stellar multiples systems are located. Like for the mass-period relation that region in the eccentricity-period diagram is dominated by RV detections and not by transiting exoplanets. The large difference in that region seems to be a hint for dynamically instabilities of exoplanets with a higher ratio of planetary to stellar semi-major axis.

To unveil the reasons for these distinctions one has to take a closer look on the dependencies of the planetary properties and the characteristics of the stellar host system. The dynamical stability of a planetary orbit around one star of a binary depends among others on the masses, the planetary apastron, and the stellar periastron distance. For further details see Rabl and Dvorak [156], Holman and Wiegert [81], and Haghighipour and Raymond [71]. Thus, one has to know the whole set of orbital elements for the planetary and the stellar system. But normally, the stellar orbital elements are unknown, due to the large orbital period of visual binaries. To compare the properties of the exoplanet and the stellar system the apparent stellar separation, is used in this work to characterize the stellar multiple systems. Fig. 1.4(a) shows the planetary semi-major axis over the

### 1.5. Extrasolar planets in stellar multiple systems



(a) Planetary semi-major axis vs. apparent stellar separation.

(b) Planetary eccentricity vs. apparent stellar separation.

Fig. 1.4.: Properties of exoplanets in stellar multiple systems. The size of the markers represents the (minimum) mass of the exoplanet (dots are stellar binaries and triangles are stellar multiple systems with more than two components).

apparent separation between the host star and its nearest stellar companion. The four systems between the  $\rho_{\text{app}}^* = 2 a_{\text{pl}}$  and  $\rho_{\text{app}}^* = 50 a_{\text{pl}}$  relations are  $\gamma$  Cep, HD 196885, HD 41004 and HD 19994. According to Holman and Wiegert [81], the critical semi-major axis for a stable planetary orbit can be calculated by

$$\begin{aligned} \frac{a_{\text{crit}}}{a_{\text{bin}}} &= (0.464 \pm 0.006) + (-0.380 \pm 0.010) \mu_{\text{bin}} \\ &+ (-0.631 \pm 0.034) e_{\text{bin}} + (0.586 \pm 0.061) \mu_{\text{bin}} e_{\text{bin}} \\ &+ (0.150 \pm 0.041) e_{\text{bin}}^2 + (-0.198 \pm 0.074) \mu_{\text{bin}} e_{\text{bin}}^2 \end{aligned} \quad (1.4)$$

$$\mu_{\text{bin}} = M_{\text{comp}} / (M_{\text{host}} + M_{\text{comp}})$$

and varies from  $a_{\text{crit}} \simeq (0.02 \dots 0.45) a_{\text{bin}}$ , depending on the mass ratio  $\mu_{\text{bin}}$  and the eccentricity  $e_{\text{bin}}$  of the binary. To test if these planetary orbits are stable, the required orbital elements from the stellar

## 1. Introduction

Host star	$M_{\text{host}}$ [ $M_{\odot}$ ]	$M_{\text{comp}}$ [ $M_{\odot}$ ]	$\mu_{\text{bin}}$	$e_{\text{bin}}$	$a_{\text{bin}}$ [AU]	$a_{\text{crit}}$ [AU]	$e_{\text{pl}}$	$a_{\text{pl}}$ [AU]	$r_{\text{pl}}^{\text{apast}}$ [AU]	Ref.
$\gamma$ Cep A	1.4	0.41	0.23	0.41	20.2	3.86	0.05	2.0	2.1	[141]
HD 196885 A	1.3	0.45	0.25	0.42	21.0	3.84	0.48	2.6	3.85	[30]
HD 41004 A	0.7	0.42	0.38	0.40	20.0	3.38	0.39	1.6	2.28	[30]
HD 19994 A <sup>§</sup>	1.3	0.9	0.4	0.0	$\sim 100$	$\sim 31$	0.3	1.5	1.9	[162, 48]

Tab. 1.5.: Critical semi-major axis  $a_{\text{crit}}$  of close stellar binaries. Because all systems presented in this work are hierarchical, the exoplanet host star ( $M_{\text{host}}$ ) and its nearest stellar companion ( $M_{\text{comp}}$ ) can be treated as a binary system. The critical semi-major axis of all these systems are larger than the respective planetary semi-major axis, thus all planetary orbits are stable.

<sup>§</sup> ... less than 25% of the HD 19994 orbit is covered with measurements but the eccentricity seems to be zero and the semi-major axis is assumed to be about 100 AU;  $M_{\text{comp}}$  is determined in section 5.3

binaries and the exoplanets are gathered from the literature and listed in Table 1.5. After calculating the critical semi-major axis using Equ. 1.4, all exoplanets in these four systems appear to be long-term stable, because their critical semi-major axis is larger than the planetary semi-major axis. Considering the planetary eccentricity and comparing the apastron distance of the exoplanet ( $r_{\text{pl}}^{\text{apast}}$ ) with the critical semi-major axis ( $a_{\text{crit}}$ ) of the HD 196885 system that planet grazes an “unstable region” during the apastron passage. However, considering the age of the F8V host star HD 196885 A of  $2.0 \pm 0.5$  Gyr (Correia et al. [32]) the planetary system can be regarded as long-term stable.

The closest binaries observed so far harboring an exoplanet are  $\gamma$  Cep and Gl 86. For the binary  $\gamma$  Cep, Neuhäuser et al. [141] determined a semi-major axis of about 20 AU. Both systems are still a challenge for current planet formation theories, as mentioned by Kley and Nelson [87]. However, from the observations a binary semi-major axis of about 20 AU seems to be the lower limit for stable planet for-

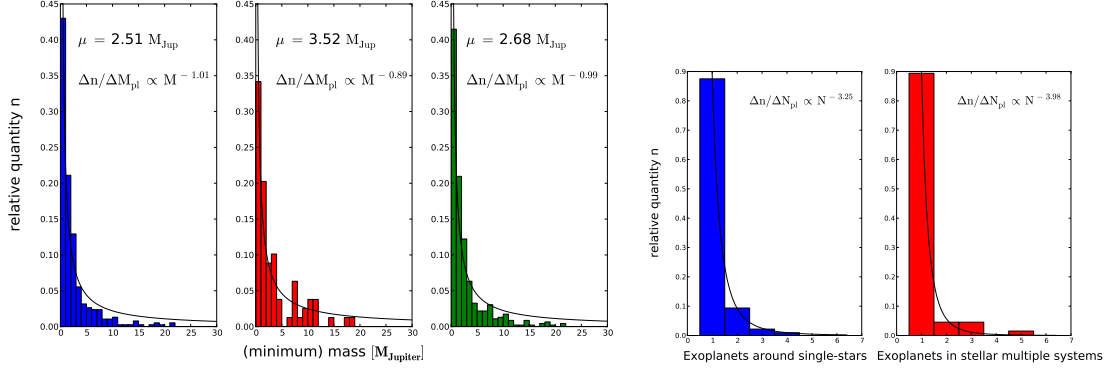
### 1.5. Extrasolar planets in stellar multiple systems

mation. A very interesting system is Gl 86, where the secondary is found to be a white dwarf by Mugrauer and Neuhäuser [127]. The evolution of a star to a white dwarf in such close binaries should have major impact to the evolution and stability of a planetary system.

Marcy et al. [107] fitted the histogram of all known RV exoplanet minimum masses in 2005 by a simple power law and yield an exponent of -1.07 for the mass distribution. In 2009, Mordasini et al. [125] could reproduce a similar value of -1.05 for a sample of synthetic exoplanets detectable by current RV observations. In this work, current RV planets and exoplanets found by transit observations are analysed. Using also a simple power law an exponent of -0.99 was determined, which is similar to the results of previous works. Splitting the sample of exoplanets into two subsamples by the criterion of a present stellar companion (Fig. 1.5), different values for the exponent were found. The exponent is -0.89 and -1.01 for exoplanets in stellar multiple systems, respectively around single stars. This also results in different values for the exoplanet mean masses, which are about  $2.5 M_{\text{Jup}}$  for exoplanets around single stars and  $3.5 M_{\text{Jup}}$  for the case of stellar multiplicity. Interesting is a second peak in the histogram of exoplanets in stellar multiple systems at about  $10 M_{\text{Jup}}$ .

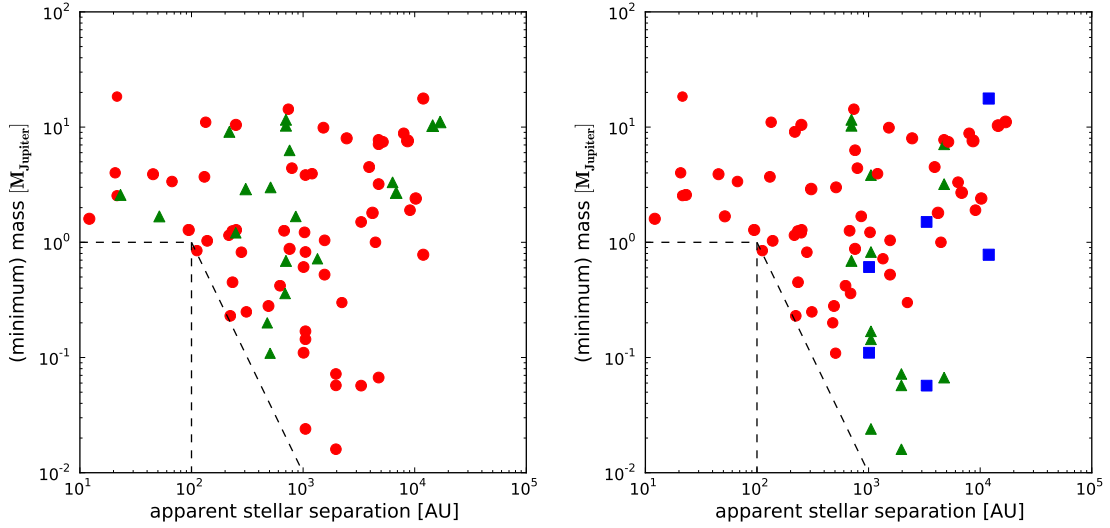
Furthermore, there is a slight difference between both exoplanet subsamples regarding the numbers of planets in one system. Fitting the planet occurrence histogram by a simple power law (Fig. 1.5), one gets an exponent of -3.25 for single host stars and -3.98 for multiple systems. Multiple planet systems seems to be truncated in the case of stellar multiplicity, which results in a higher number of single-planet systems. The reason for the preference of higher mass and single-planet systems seems to be the presence of a close stellar com-

## 1. Introduction



(a) Histogram of the (minimum) mass of exoplanets around single stars (left), in stellar multiple systems (middle) and for all exoplanets (right). The black line shown in the graph is a power-law fit and  $\mu$  is the mean mass.

(b) Histogram of the number of exoplanets around single stars (left) and in stellar multiple systems (right). The black line shown in the graph is a power-law fit.



(c) Planetary (minimum) mass vs. apparent stellar separation (red: binaries, green: triples or higher stellar multiplicity). The separation between the exoplanet host star and the nearest stellar component has a strong influence on the exoplanet mass, while the number of stellar components seems to be nonrelevant.

(d) Planetary (minimum) mass vs. apparent stellar separation (red: one exoplanet, blue: two exoplanets, green: three or more exoplanets). The separation between the exoplanet host star and the nearest stellar component has a strong influence on the mass and the number of exoplanets.

Fig. 1.5.: Mass and number of exoplanets in stellar multiple systems. In stellar systems with an apparent separation of the nearest stellar companion of less than 100 AU only high mass and single planet systems are found.



### 1.5. Extrasolar planets in stellar multiple systems

panion, as one can see in the figure 1.5(c) and 1.5(d). Stellar systems can be distinguished into four types. Very close systems with stellar apparent separations less than ten AU, close systems with separations between ten AU and 100 AU, intermediate systems between 100 AU and 1000 AU, and wide systems with apparent separations of more than 1000 AU. While exoplanets in wider systems are more or less uniformly distributed over the whole detectable mass regime no exoplanet is detected so far in very close systems. In close systems all detected exoplplanets have a mass greater than  $1 M_{\text{Jup}}$ . For intermediate systems, the planetary mass decreases with an increasing stellar separation. Furthermore, multi-planet systems are only present in stellar systems with a separation of more than 500 AU. For smaller separations, only single-planet systems are found. The order of the stellar multiplicity plays no important role for the properties of the planet. Due to the hierarchic structure, multiple systems can be treated as binaries consisting of the exoplanet host star and its nearest stellar companion.

However, one also should mentioned that observational bias and selection effects are still present in the analysed data. Thus, the reason for the presence of only high mass and single-planet systems in stellar systems with a separation less than 100 AU could also be an observational effect due to the influence of the close stellar companion, which perhaps obscures the RV signal of a possible planet. But, assuming a stellar binary with a total mass of one solar mass and a separation of 50 AU, the RV signal for a circular edge-on orbit would be about 4250 m/s with a period of about 350 years. Such a strong and long period signal should be easily distinguishable from a short period RV signal of an exoplanet.



## 2. Observational challenges

As described in chapter 1.5, there are differences between exoplanets in close binaries and around single stars, regarding their number and mass. To develop a method to observe and study such close systems is one of the main aspects of this work and will be presented in this chapter.

For an observation program two important facts have to be considered. First, in order to minimize observational bias and selection effects, it has to be a search for exoplanets in stellar multiple systems and not, like it was done so far, a search for stellar companions around exoplanet host stars. The reason is that all bias and selection effects are adopted from the original exoplanet search programs.

The second point is the requirement of a high spatial resolution to resolve close stellar systems. Close systems are binaries with an apparent separation of less than 100 AU. At a distance of 50 pc this results in an angular separation of less than 2 arcsec. Binaries at 50 pc with a separation of less than 20 AU, which is assumed to be the lower limit in semi-major axis for stable planet formation, would have an angular separation of less than 0.2 arcsec.

Spectrographs have typically a lower limit in the angular resolution of about 2 arcsec, due to the size of their slit or fiber. Space missions like Hipparcos or GAIA were designed to measure a lot of stars and not

## 2. *Observational challenges*

to resolve close systems. The ESPRI project<sup>1</sup> will also have a lower separation limit of about 2 arcsec, due to the star separator, which is needed for dual-beam interferometry. In contrast, imaging with the support of adaptive optics by ground based large apertures yield a spatial resolution of about 0.1 arcsec. This is sufficient to observe such close binaries, where planet formation should theoretically be inhibited by the stellar companion.

In this chapter the observation, analyse and calibration strategies of an astrometric search for exoplanets by ground based imaging will be presented. The astrometric search program described in this work consists of the observation of a target and a calibration system. The latter one is a specific field of an old globular cluster (see chapter 4). Hence, all effects presented in this chapter are discussed for both, the target and the calibration system.

### 2.1. **Astrometric method**

An unseen companion orbiting a star introduce a reflex motion (also called “wobble”) of its host star around the common center of mass. Whereas RV observations measure the radial dimension of this motion, astrometry observes the spatial displacement of the reflex motion. To reach the needed precision to detect an exoplanet, which is usually less than one mas, one has to do relative astrometry. Stellar positions are not known accurate enough to detect such a small reflex motion by absolute astrometry. Hence, the angular separation and the position angle of the host star to a reference star is measured over the time very precisely.

---

<sup>1</sup> “Exoplanet Search with PRIma” is an astrometric exoplanet search program using the dual-beam interferometric instrument PRIMA at the VLTI.



Fig. 2.1.: Sketch of a stellar binary harboring an unseen astrometric companion. While orbiting one stellar component of the binary, the astrometric companion causes a periodic deviation in the separation and position angle of the binary.

In this work stellar multiple systems are observed and the reference star is always one of the stellar components (e.g. the secondary of a binary). By observing the binary over the time very precisely, one can search for a periodic deviation in the separation and the position angle measurements of the binary. Such a periodic deviation could be the astrometric signal of an unseen companion around one of these stars (Fig. 2.1).

The astrometric signal depends on the mass ratio, the distance of the system, and the orbital period of the astrometric companion. For the case of zero eccentricity it is twice the semi-major axis of the reflex orbit ( $\theta = 2 a_{\star}$ ) and can be calculated as

$$\theta [\text{mas}] = 1.91 \frac{m_{\text{comp}} [M_{\text{Jup}}]}{M_{\star} [M_{\odot}]} \frac{a_{\text{comp}} [\text{AU}]}{d [\text{pc}]} \quad (2.1)$$

## 2. Observational challenges

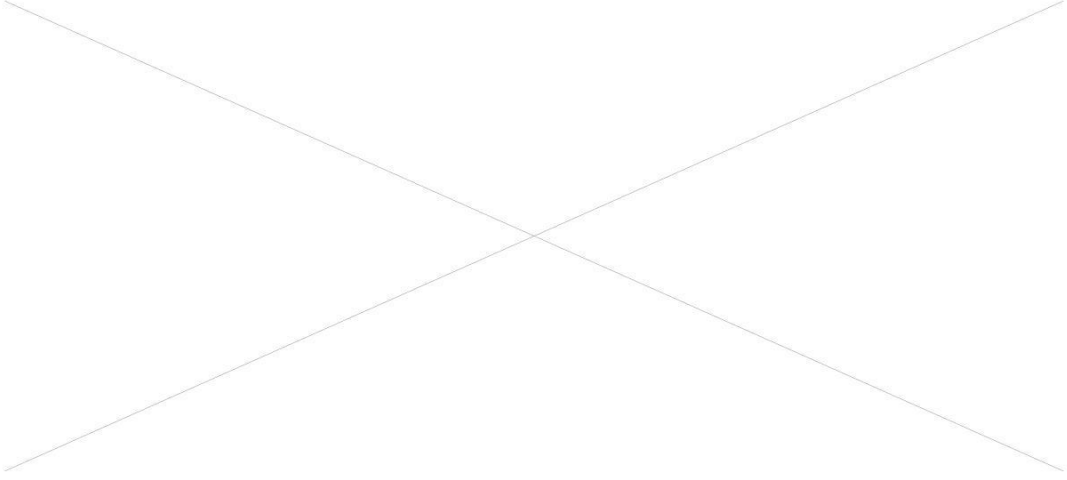


Fig. 2.2.: Sketch of a circular and unresolved binary. What is in fact observable is the reflex motion of the common flux center around the common center of mass.

However, what can be measured in reality is just the reflex orbit of the common flux center around the common center of mass (Fig. 2.2). A not resolvable binary with a given mass ratio can counterfeit the astrometric signal of a planetary companion, due to an unsuitable brightness ratio.

$$\begin{aligned}
 \tilde{M} &= \left(1 + \frac{M_{\star}}{m_{\text{comp}}}\right)^{-1} \\
 \tilde{F} &= \left(1 + \frac{F_{\star}}{F_{\text{comp}}}\right)^{-1} = (1 + 10^{0.4\Delta m})^{-1} \\
 \alpha_{\star} &= a_{\star} \left(1 - \frac{\tilde{F}}{\tilde{M}}\right)^{-1} = a_{\text{total}} (\tilde{M} - \tilde{F})
 \end{aligned} \tag{2.2}$$

In the case of a negligible brightness of the astrometric companion ( $F_{\star} \gg F_{\text{comp}} \Rightarrow \tilde{F} \simeq 0$ ) the orbital motion of the flux center can be equated with the orbital motion of the masses around the common center of mass ( $\alpha_{\star} = a_{\star}$ ).

## 2.2. Stellar effects

Stellar effects are based on the properties of the star itself or the observed stellar system. They could influence or even falsify astrometric measurements (e.g. stellar activity, distance and proper motion). Especially for the case of relative astrometry, effects like differential parallax and differential proper motion between the target and the reference star have to be considered. Furthermore, the stellar activity can produce an astrometric noise level or even a false astrometric signal in case of a stellar spot on the surface of a large rotating star.

In this section these stellar effects, which could influence ground based astrometric observations will be presented and discussed.

### 2.2.1. Differential parallax

In this work the astrometric reference star is always a stellar companion of the target system itself, which means both stars have more or less the same distance and proper motion. Using a background star as reference star one would have to consider differential parallax as well as differential proper motion effects. But, as one can see in Fig. 2.3, the effect of differential parallax is also present in binaries, especially in nearby and wide edge-on systems. In the case of a pole-on orbit ( $\text{inc} = 0^\circ$ ) this effect vanishes away. The differential parallax  $\Delta\pi$  is a result of the difference in the distances  $\Delta d$  between the target and the reference star.

$$\pi [\text{as}] = 1 \text{ AU}/d [\text{pc}], \quad \Delta\pi = \pi \frac{\Delta d}{d} \quad (2.3)$$

Fig. 2.3 illustrates the amount of the differential parallax for circular and edge-on binaries, which depends on the binary maximum

## 2. Observational challenges

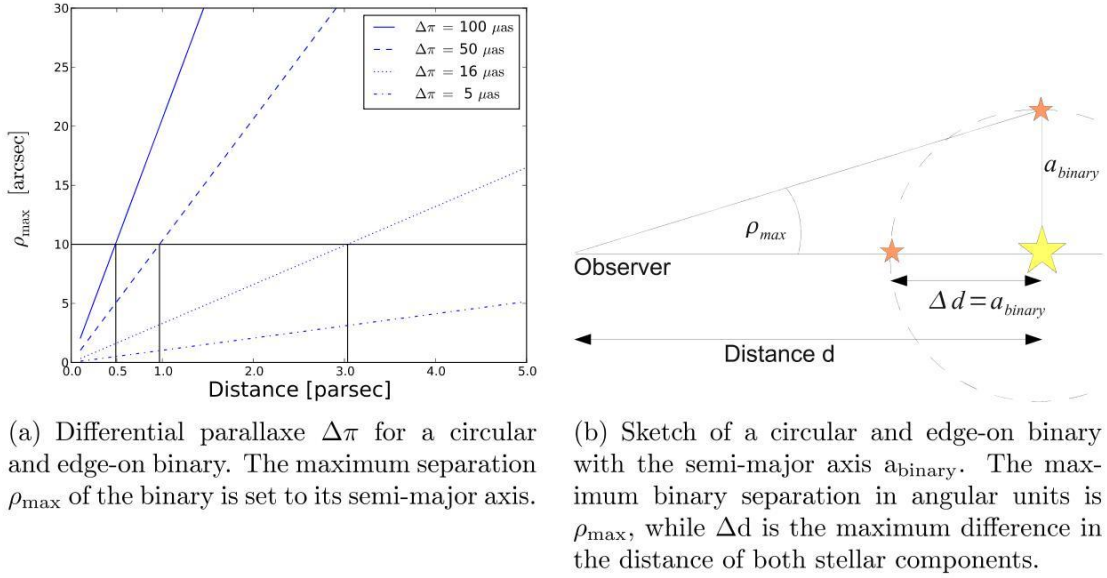


Fig. 2.3.: Effect of the differential parallaxe in a circular and edge-on binary.

separation and distance. All target systems observed in this work have an apparent separation of less than 10 as and are further away than 3 pc. Hence, assuming that the measured is similar to the maximum separation, the effect of differential parallaxe is always less than  $16 \mu\text{as}$ . Such a precision will not be achieved in this work, but future projects like ESPRI or GAIA will have to consider this effect.

The calibration clusters used in this work are very far away, namely about  $4.5 \text{ kpc}^2$  for 47 Tuc and 10 kpc for M 15 (see chapter 4). Due to this huge distances, the influence of the differential parallaxe is small, even considering the whole diameter of the clusters. The diameter of the old globular cluster 47 Tuc is assumed to be less than 200 parsec (Giersz and Heggie [67]), which results in a differential parallaxe of less than  $10 \mu\text{as}$ .

<sup>2</sup>  $1 \text{ kpc} = 1000 \text{ pc} = 3.0857 \times 10^{19} \text{ m}$



### 2.2.2. Stellar activity

For RV observations the stellar activity is one of the biggest problems. A present rotating stellar spot could counterfeit a RV signal of an exoplanet and has to be ruled out by special analyze methods (e.g. bisector analysis, see Povich et al. [148], Martínez Fiorenzano et al. [114]). However, stellar spots can also produce an artificial astrometric signal due to a periodic shift of the stellar flux center, which is called the astrometric jitter  $\Sigma$ . Eriksson and Lindegren [52] modeled the amount of this astrometric jitter for several spectral types and luminosity classes.

Spectral Type	$\Sigma$ [ $10^{-6}$ AU]	$\Sigma(10 \text{ pc})$ [ $\mu\text{as}$ ]
B8 V - M9 V	$\lesssim 30$	$\lesssim 3$
O0 III - M0 III	$\simeq 1 \dots 1400$	$\simeq 0.1 \dots 140$
M0 III - M5 III	$\simeq 1400 \dots 16000$	$\simeq 140 \dots 1600$
O I - M I	$\simeq 25 \dots 100000$	$\simeq 2.5 \dots 10000$

Tab. 2.1.: Astrometric jitter caused by stellar activity modeled for different spectral types by Eriksson and Lindegren [52].

As one can see in table 2.1 the astrometric jitter is dominant for giant stars, because it linearly depends on the stellar radius. The stellar radius affects the astrometric jitter even stronger than the effect of the spot filling factor, which is mainly based on the age and the spectral type of the star. For main sequence stars with a distance of more than three parsec the astrometric jitter is always less than  $10 \mu\text{as}$ . Such small perturbations of the stellar flux center are not detectable in this work, but have to be considered for future astrometric projects like ESPRI or GAIA.

## 2. *Observational challenges*

Most of the observable stars in the calibration clusters are not dwarf but giant stars. However, because of the huge distance of these clusters of more than 4 kpc (see chapter 4) the effect of the astrometric jitter is still very small. Assuming the presence of supergiants (luminosity class I) the astrometric jitter is less than 0.1 AU. In case of the old globular cluster 47 Tuc with a distance of about 4.5 kpc that results in an amount less than  $25 \mu\text{as}$ . The distance of the old globular cluster M 15 is 10 kpc, thus the astrometric jitter is always less than  $10 \mu\text{as}$ .

### 2.3. Atmospheric effects

One of the biggest problems for astrometric observations from the ground is the atmosphere of the earth. It is not constant, neither spatial nor temporal. Thus, the optical properties of the atmosphere, like the refraction index, will change in time. It depends on the observational site as well as on the climatic conditions, like the air temperature, the air pressure, and the relative humidity. The influence of earth's atmosphere regarding ground based astrometric observations will be discussed in this section.

#### 2.3.1. Atmospheric turbulences

Observing through earth's atmosphere is comparable to looking at a coin located at the ground of a fountain through the bumpy water. The apparent position of the coin will always changes just like the apparent position of a star observed through the disturbed atmosphere.

The turbulences of earth's atmosphere can be described by Fried's coherence length  $r_0$  (Fried [61]), the isoplanatic angle  $\theta_0$ , and the

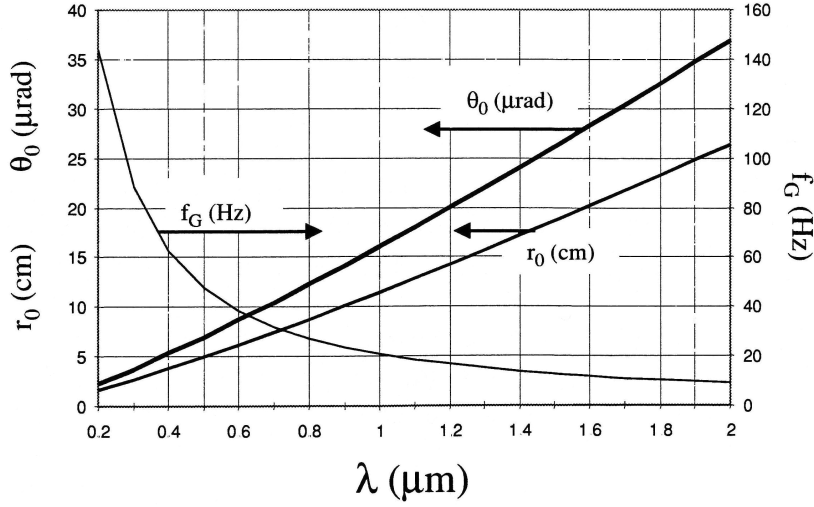


Fig. 2.4.: Relationship between the wavelength  $\lambda$  and the coherence length  $r_0$ , the isoplanctic angle  $\theta_0$ , and the Greenwood frequency  $f_G$  (Tyson [190]).

Greenwood frequency  $f_G$ . These parameters are, in simplification, the size of one turbulence cell (one cell has constant optical properties per definition), the angle where light passes through the same cell (thus it is disturbed the same way), and the velocity of the cell, which is the temporal behaviour of the turbulences (Equ. 2.4). The often used parameter *seeing* is defined as the wavelength divided by the coherence length ( $s = \lambda/r_0$ ) and describes the angular FWHM (Full Width at Half Maximum) of the stellar point spread function (PSF) blurred by the atmospheric turbulences.

$$\begin{aligned}
 r_0 &= \left[ 0.423 k^2 \sec \beta \int_{\text{path}} C_n^2(z) dz \right]^{-3/5} \propto \lambda^{6/5} \\
 \theta_0 &= \left[ 2.91 k^2 \sec^{8/3} \beta \int_{\text{path}} C_n^2(z) z^{5/3} dz \right]^{-3/5} \propto \lambda^{6/5} \\
 f_G &= 2.31 \lambda^{-6/5} \left[ \sec \beta \int_{\text{path}} C_n^2(z) V_{\text{wind}}^{5/3}(z) dz \right]^{3/5} \propto 1/r_0
 \end{aligned} \tag{2.4}$$

## 2. Observational challenges

As one can see in equation 2.4 all parameters described above depends on the wavelength  $\lambda$  (or the wave number  $k = 2\pi/\lambda$ ), the zenith angle  $\beta$ , and the so called atmospheric refractive structure constant  $C_n^2(z)$ . That constant describes the variations of the refraction index, thus the strength of the atmospheric turbulences. However, this constant is not constant, but it depends on the altitude  $z$  and the atmospheric conditions above the observational site. The most common model to calculate  $C_n^2(z)$  is the ‘‘Hufnagel-Valley-Boundary’’ (HVB) model which is defined as

$$C_n^2(z) = 5.94 \times 10^{-23} z^{10} e^{-z} W/27 + 2.7 \times 10^{-16} e^{-2z/3} + A e^{-10z}, \quad (2.5)$$

where  $W$  and  $A$  are adjustable parameter based on the current atmospheric conditions (for further details see Rasouli and Tavassoly [159], Tyson [190], Fried [61]).

An adaptive optics system is, in simple terms, a system consisting of a wavefront sensor (measuring the distortion of a wavefront), a computer, and a deformable mirror to correct all incoming light for the measured wavefront distortions. As shown in Fig. 2.4 the atmosphere gets less turbulent for longer wavelengths, thus the Greenwood frequency decreases by switching from optical to infrared observations. Because of the high Greenwood frequency of the turbulent atmosphere in the optical, AO systems are currently only operable for infrared observations.

However, atmospheric turbulences are very chaotic and the AO system just corrects the distortion of the atmosphere in front of that star observed by the wavefront sensor (called AO guide star). But this specific star can be behind another turbulent cell than the tar-

get star observed by the scientific instrument. The distortions of the wavefronts are only identical if both stars are within the isoplanatic angle, which is typically  $\theta_0 \simeq 10'' \dots 20''$  for the near infrared (NIR), depending on the atmospheric conditions.

The observation strategy chosen in this work can be described as NIR AO assisted lucky imaging, where the AO guide star is always one component of the observed stellar multiple systems. It is not important how the atmosphere disturbs and how the AO system corrects the stellar PSF, as long as these influences are identically for all observed stars. In that case, the relative astrometric measurements are not influenced by atmospheric turbulences. Hence, all stars of the multiple systems should be observed simultaneously and within the isoplanatic angle.

Lucky imaging is an observation strategy, where the exposure time is decreased until it is less than the typical coherence time  $\tau_0$ . That coherence time is the corresponding period to the Greenwood frequency and a measure how long one turbulent cell is stable above the telescope. At the end, the frames with the best strehl ratio<sup>3</sup> will be selected and coadded. By doing so, nearly diffraction limited frames can be obtained and the resulting frame is barely blurred out by the atmosphere. For further information about lucky imaging, see Fried [62], Baldwin et al. [5], Law et al. [95], Tubbs [188] and references therein. For relative astrometry the selection criterion is not the strehl ratio, but the statistical behavior of the separation and position angle measurements. After the standard data reduction (bad pixel, dark, and flat-field correction) several thousand of single frame mea-

---

<sup>3</sup> The strehl ratio is defined by the ratio of the peak intensities of a real image and of a diffraction-limited image with the same total flux. For further information see Soummer and Ferrari [178]

## 2. Observational challenges

measurements of one binary are analysed using a Kolmogorov-Smirnov test (Wall and Jenkins [201]) in order to extract the Gaussian core of the measurements. At the end, the error of the mean is the standard deviation of the Gaussian distributed measurements divided by the square root of the number of measurements. This is a similar strategy as done for RV observations, where thousands of spectral lines of one spectrum are used to measure the Doppler shift with high precision.

### 2.3.2. Differential atmospheric refraction

As described above, the atmospheric refractive structure constant  $C_n^2$  is not constant but depends on the wavelength and changes in time and space. Hence, the atmospheric refraction is different for targets with different colors, zenith angles, and climatic conditions.

In general the refraction angle depends on the zenith angle  $Z$ , the wavelength  $\lambda$ , the air temperature  $T$ , the air pressure  $P$ , and the relative humidity  $H$ . According to Stone [180] the refraction angle  $R$  can be calculated for  $Z < 75^\circ$  as

$$\begin{aligned}
 R &= \kappa \gamma (1 - \beta) \tan(Z) - \kappa \gamma (\beta - \gamma/2) \tan^3(Z) \\
 \kappa &= 1 + 5.302 \times 10^{-3} \sin^2(\phi) \\
 &\quad - 5.83 \times 10^{-6} \sin^2(2\phi) - 3.15 \times 10^{-7} h
 \end{aligned} \tag{2.6}$$

$$\gamma(\lambda, T, P) = n(\lambda, T, P) - 1$$

$$\beta = 12.54 \times 10^{-4} \left( \frac{273.15 + T}{273.15} \right),$$

whereas  $\kappa$  considers the geographic coordinates of the observational site (latitude  $\phi$  and altitude  $h$ ),  $\gamma$  correlates with the atmospheric re-

fraction index  $n$ , and  $\beta$  with the air temperature  $T$ . The calculation of the atmospheric refraction index  $n$ , which is a function of the climatic conditions and the wavelength, can be found in appendix B.

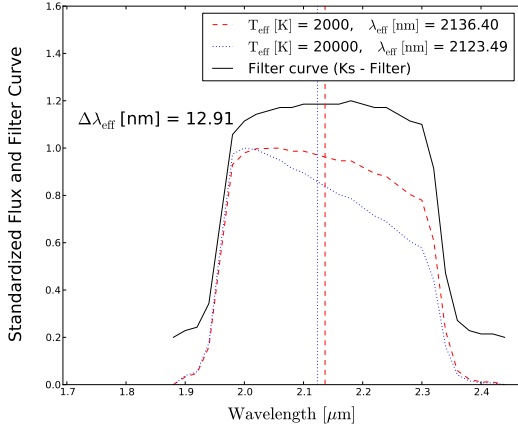
In case of relative astrometry the absolute refraction angle is not important, but the differential refraction angle between the target and the reference star have to be considered. The pointing of the telescope and the climatic conditions during the observation are saved and written to the FITS header<sup>4</sup> of each frame. With these information, the differential refraction based on different zenith angles and climatic conditions can be calculated.

In addition to the zenith angle and the climatic conditions different wavelenghts also cause a different atmospheric refraction angle. This effect is known as the differential chromatic refraction (DCR). However, the incoming stellar light onto the detector is a combination of the spectral type and the spectral properties of the star as well as of the used filter properties. But these information are in general not known with the needed accuracy. Thus, one has to choose an observation strategy, where the DCR can be neglected. By observing in the infrared with a narrow-band filter the DCR effect can be minimized to less than  $15 \mu\text{as}$  for the extrem case of two blackbodies with effective temperatures of 2 000 K and 20 000 K and for zenith angles of less than  $70^\circ$  (Fig. 2.5). For approaching spectral types, the DCR effect decreases. The filter curves for the Ks broad-band and NB2.17 narrow-band filter shown in Fig. 2.5 are obtained from the ESO website [138]. The largest zenith angles reached in this work are  $Z \simeq 50^\circ \dots 55^\circ$  for the observations of the astrometric calibration cluster 47 Tuc. Hence, a zenith angle larger than  $60^\circ$  will never

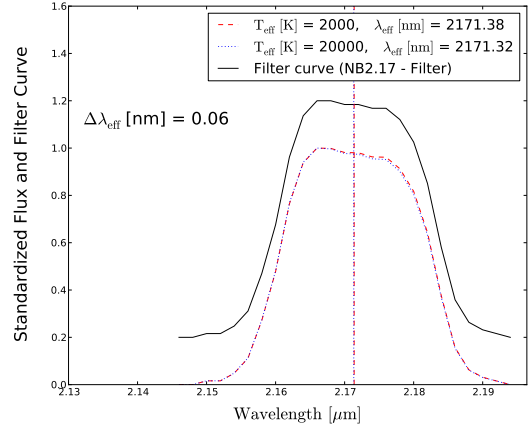
---

<sup>4</sup> Flexible Image Transport System, see Calabretta and Greisen [26]

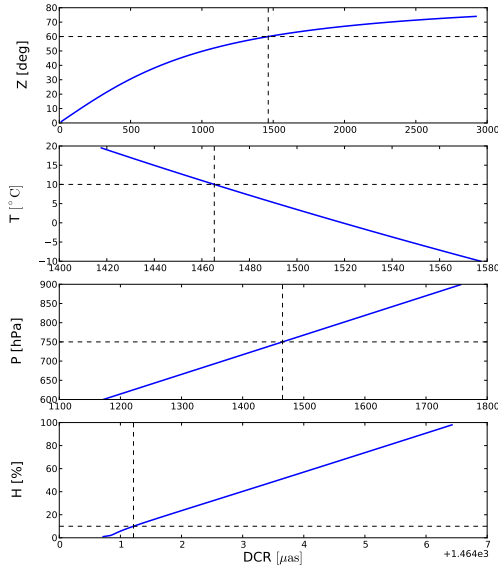
## 2. Observational challenges



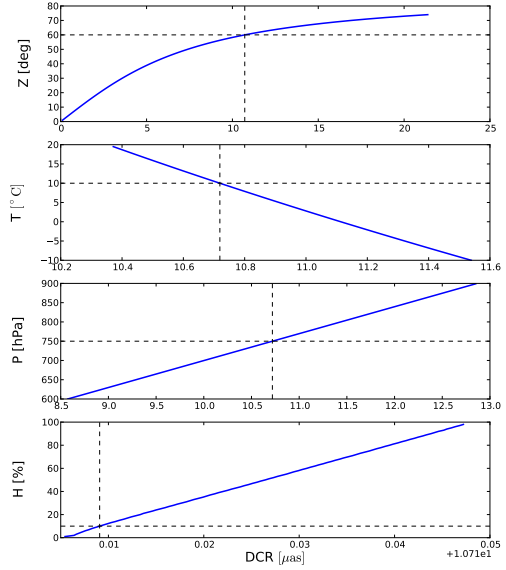
(a) Flux of two blackbodies folded with the ESO Ks broad-band filter curve (solid line). The effective temperatures of the blackbodies are 2000 K (dashed line) and 20000 K (dotted line). The effective wavelength reaching the detector is defined as the weighted mean of the folded flux (vertical lines). The difference of the effective wavelengths is about 13 nm.



(b) Flux of two blackbodies folded with the ESO NB2.17 narrow-band filter curve, (solid line). The effective temperatures of the blackbodies are 2000 K (dashed line) and 20000 K (dotted line). The effective wavelength reaching the detector is defined as the weighted mean of the folded flux (vertical lines). The difference of the effective wavelengths is less than 0.1 nm.



(c) DCR effect for the ESO Ks broad-band filter using the effective wavelengths from (a) and typical climatic conditions (dashed lines) for the ESO/VLT observational site on Paranal in Chile.



(d) DCR for the ESO NB2.17 narrow-band filter using the effective wavelengths from (b) and typical climatic conditions (dashed lines) for the ESO/VLT observational site on Paranal in Chile.

Fig. 2.5.: Transmission and DCR for the ESO Ks broad-band and the ESO NB2.17 narrow-band filter. Two extrem different blackbodies were chosen, with effective temperatures of 2000 K and 20000 K. While the DCR effect is several milli-arcsec using the Ks broad-band filter, it is always less than 15  $\mu\text{s}$  in case of using the NB2.17 narrow-band filter and for zenith angles of  $Z \lesssim 70^\circ$ .



### 2.3. Atmospheric effects

Parameter	47 Tuc	HD 19994	$\sigma$
	$\mu$		
wavelength [nm]	2167.35		0.05
pixel scale [mas/pixel]	13.24		0.1
separation of two stars [pixel]	1000	200	0.1
zenith angle	60°	50°	10''
difference of position and parallactic angle	0°		0.1°
air temperature [°C]	10		0.1
relative humidity [%]	10		1
air pressure [mbar]	750		0.1

Tab. 2.2.: All parameters needed to calculate the differential refraction for the binary HD 19994 and the astrometric calibration cluster 47 Tuc. Each parameter is assumed as a Gaussian distribution described by a mean value  $\mu$  and a standard deviation  $\sigma$ . The standard deviation is chosen conservatively and the weather conditions are typically values for the VLT on Paranal in Chile.

be reached in this work. It has to be mentioned that stars are not pure blackbodies, but the Br $\gamma$  emission line at  $2.17\mu\text{m}$ , for which the NB2.17 narrow-band filter was designed for, is mostly present in the case of accretion. Especially young stars still accreting material from their protoplanetary disk or contact binaries with a mass overflow have this spectral feature. Because this astrometric search program is concentrated on main-sequence stars such young stars are not be observed and using speckle interferometry one can check for close and brighter companions. This is done anyway in this work in order to analyze the brightness of a detected astrometric companion and will be described in section 3.4.

While the DCR effect can be neglected by using a NIR narrow-band filter, the shares in different zenith angles and climatic conditions have to be corrected (Equ. 2.7, Roe [160]). The differential refraction angle

## 2. Observational challenges

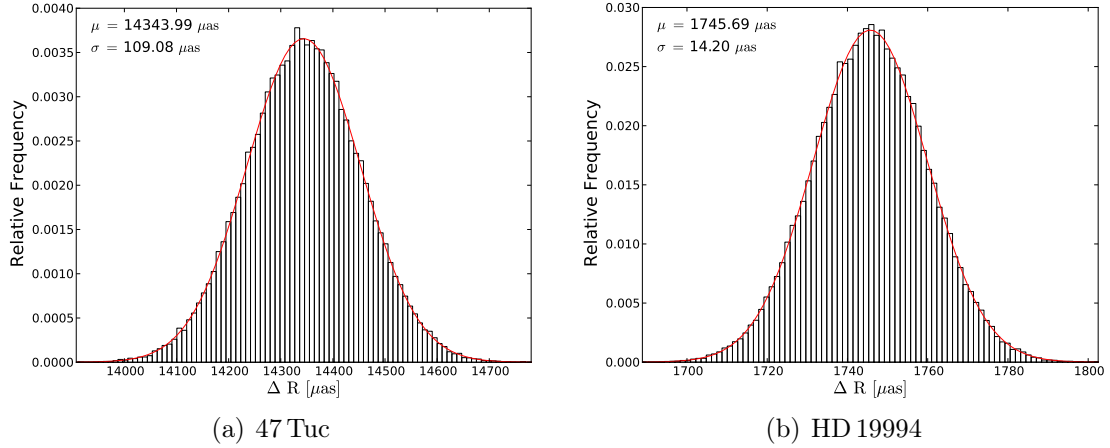


Fig. 2.6.: Monte-Carlo simulation to determine the influence of all parameter uncertainties listed in table 2.2 on the differential refraction correction for 47 Tuc (left) and HD 19994 (right). The mean value  $\mu$  is the correction term and the standard deviation  $\sigma$  is the correction uncertainty.

itself can be calculated by Equ. 2.6 presented earlier.

$$\begin{aligned}
 \Delta R & \dots \text{ differential refraction angle in mas} \\
 P & \dots \text{ position angle in degree} \\
 Q & \dots \text{ parallactic angle in degree} \\
 ps & \dots \text{ pixel scale in mas/pixel}
 \end{aligned} \tag{2.7}$$

$$\Delta X = \frac{\Delta R}{ps} \sin(P - Q), \quad \Delta Y = \frac{\Delta R}{ps} \cos(P - Q)$$

To determine the precision of the differential refraction correction a Monte-Carlo simulation is done. All needed parameters are listed in table 2.2 with conservatively chosen uncertainties. The influence of these parameters on the differential refraction correction is shown in Fig. 2.6. The final correction uncertainty is  $110 \mu\text{as}$  for the globular cluster 47 Tuc and less than  $15 \mu\text{as}$  for HD 19994.

## 2.4. Relativistic effects

Another source of interference are relativistic effects, which are mainly based on the finite speed of light as well as on a deformation of the space caused by high gravitational masses. These effects and their influence on ground based astrometric observations will be presented and discussed in this section.

### 2.4.1. Differential stellar aberration

Because of the finite speed of light and the permanent motion of the observer relatively to the star a displacement between the true and the apparent stellar position in the sky occurs. This effect, called stellar aberration, is mainly based on the earth revolution around the sun and depends on the world coordinates of the star and the exact observational time.

As described in the *Astronomical Almanac* [191] the differential effect of the stellar annual aberration can be calculated by the following equation.

$$\begin{aligned}\alpha_{\text{corr}} &= a \Delta\alpha + b \Delta\delta \\ \delta_{\text{corr}} &= c \Delta\alpha + d \Delta\delta\end{aligned}\tag{2.8}$$

The corrections  $\alpha_{\text{corr}}$  and  $\delta_{\text{corr}}$  are in units of 0.001 seconds and 0.01 arcsec, while the separation of two stars ( $\Delta\alpha$  and  $\Delta\delta$ ) are in units of 1 minute and 1 arcmin.

## 2. Observational challenges

The coefficients a,b,c, and d are correlated to the observation time and the world coordinates. They can be calculated as

$$\begin{aligned}
 a &= -5.701 \cos(H + \alpha) \sec(\delta) \\
 b &= -0.380 \sin(H + \alpha) \sec(\delta) \tan(\delta) \\
 c &= 8.552 \sin(H + \alpha) \sin(\delta) \\
 d &= -0.570 \cos(H + \alpha) \cos(\delta),
 \end{aligned} \tag{2.9}$$

whereas H is defined by

$$\begin{aligned}
 H \text{ [hours]} &= 23.4 - D/15.2 \\
 D &\dots \text{ day of the year.}
 \end{aligned} \tag{2.10}$$

After calculating the correction terms  $\alpha_{\text{corr}}$  and  $\delta_{\text{corr}}$  one can correct the pixel position of the target star relatively to the reference star using Equ. 2.11.

$$\begin{aligned}
 \Delta X &= \frac{\alpha_{\text{corr}}}{\text{ps}} \cos(\delta) \cos(180^\circ - \eta) + \frac{\delta_{\text{corr}}}{\text{ps}} \sin(\eta) \\
 \Delta Y &= \frac{\alpha_{\text{corr}}}{\text{ps}} \cos(\delta) \sin(180^\circ - \eta) + \frac{\delta_{\text{corr}}}{\text{ps}} \cos(\eta).
 \end{aligned} \tag{2.11}$$

$\eta$  ... detector orientation in degree

$\delta$  ... declination in degree

ps ... pixel scale in mas/pixel

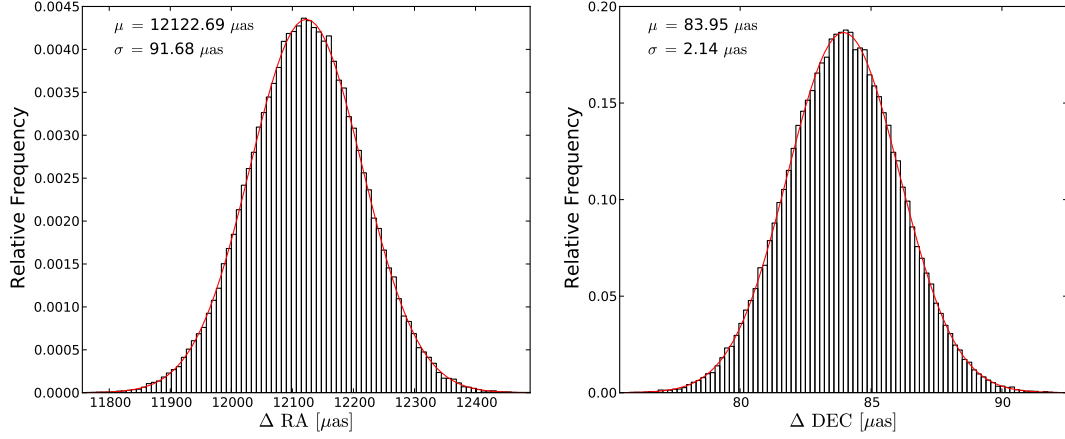
#### 2.4. Relativistic effects

Similar to the differential refraction one has to determine the final precision of the differential aberration correction, which is influenced by the uncertainties of the parameters listed in Tab. 2.3. This is done by a Monte-Carlo simulation and the results are presented in Fig. 2.7. The final correction uncertainty is  $95 \mu\text{as}$  for the globular cluster 47 Tuc and less than  $5 \mu\text{as}$  for HD 19994.

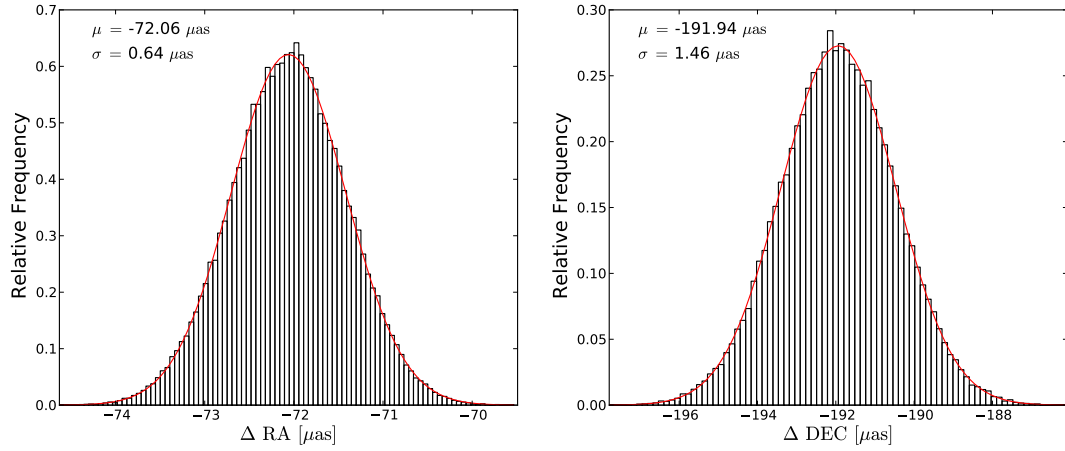
Parameter	47 Tuc	HD 19994	$\sigma$
	$\mu$		
pixel scale [mas/pixel]	13.24		0.1
stellar separation [pixel]	1000	200	0.1
position angle	$0^\circ$	$200^\circ$	$0.1^\circ$
RA [h:min:sec]	+00 : 24 : 06	+03 : 12 : 46	$10''$
DEC [d:m:s]	-72 : 04 : 53	+01 : 11 : 46	$10''$

Tab. 2.3.: All parameters needed to calculate the differential stellar aberration for the binary HD 19994 and the astrometric calibration cluster 47 Tuc. Each parameter is assumed as a Gaussian distribution described by a mean value  $\mu$  and a standard deviation  $\sigma$ , which is chosen conservatively.

## 2. Observational challenges



(a) Monte-Carlo simulation to estimate the influence of all parameters uncertainties listed in Tab. 2.3 on the correction of the differential stellar aberration for the calibration cluster 47 Tuc.



(b) Monte-Carlo simulation to estimate the influence of all parameters uncertainties listed in Tab. 2.3 on the correction of the differential stellar aberration for the HD 19994 system.

Fig. 2.7.: Monte-Carlo simulation to estimate the influence of all parameters uncertainties (Tab. 2.3) on the correction of the differential stellar aberration for the calibration cluster 47 Tuc (upper panel) and the HD 19994 system (lower panel). The mean value  $\mu$  is the correction term and the standard deviation  $\sigma$  is the correction uncertainty.

### 2.4.2. Differential gravitational light deflection

The absolute deflection angle caused by the gravitational mass of a deflecting body can be calculated by the following formula given in Turyshev [189]. The Eddington parameter describes the deflecting strength of the gravitational mass and is equal to one for the theory of general relativity.

$$\Delta\chi = -(\gamma + 1) \frac{G}{c^2} \frac{M}{r} \frac{1 + \cos(\chi)}{\sin(\chi)}$$

$\gamma$  ... Eddington parameter ( $\gamma = 1$ )  
 $M$  ... mass of the deflecting body  
 $r$  ... distance to the deflecting body  
 $\chi$  ... angle between star and deflecting body

(2.12)

In general our sun is the strongest deflecting body for ground based observations because of its mass. The deflecting angle of a target observed  $20^\circ$  away from the sun is about 24 mas. However, for relative astrometry the absolute deflecting angle is not relevant, but relative measurements between the target and the astrometric reference star are affected by the different angular separations to the deflecting body. According to Turyshev [189] the differential deflecting angle of two objects can be calculated as

$$\delta\chi = (\gamma + 1) \frac{G}{c^2} \frac{M}{r} \frac{\cos[(\chi_2 - \chi_1)/2]}{\sin(\chi_1/2) \sin(\chi_2/2)},$$
(2.13)

whereas  $\chi_1$  and  $\chi_2$  are the angular separations to the deflecting body.

## 2. Observational challenges

Object	$\chi$	$\Delta\chi$ in $\mu\text{as}$	$\delta\chi$ in $\mu\text{as}$	$\chi_{\min}$
Sun	$20^\circ$	23500	10	$20^\circ$
Jupiter	$20'$	340	8.3	$18.2'$
Saturn	$20'$	50.1	1.2	$6.8'$
Moon	$20'$	21.3	0.6	$4.4'$

Tab. 2.4.: Maximum absolute ( $\Delta\chi$ ) and differential ( $\delta\chi$ ,  $\chi_2 - \chi_1 = 30''$ ) gravitational light deflection for the strongest deflecting bodies in our solar system. Furthermore, the minimum angular separation  $\chi_{\min}$ , where the differential gravitational light deflection is  $\delta\chi = 10 \mu\text{as}$  in maximum is shown in the last column.

In table 2.4 the strongest deflecting bodies in our solar system are listed. As an absolute distance the smallest possible distance to the earth is chosen as well as an angular separation of  $\chi_2 - \chi_1 = 30''$ . The field of view of the NIR imager used in this work is about  $15'' \times 15''$ . Hence, the values listed in table 2.4 are a worst case scenario.

For ground based and nightly observations the angular separation to the sun will always be larger than  $20^\circ$ . Furthermore, the apparent diameter of the moon is about 30 arcmin, which is much larger than the minimum separation of  $\chi_{\min} = 4.4$  arcmin. That minimum separation corresponds to a differential deflecting angle of  $\delta\chi = 10 \mu\text{as}$ . The apparent diameters of Jupiter and Saturn are about 50 arcsec and 20 arcsec, but due to their brightness they usually are observed at a larger angular separation than their  $\chi_{\min}$  values. In contrast to space based observations the earth plays no role as a deflecting body for ground based observations. Hence, the influence of differential gravitational light deflection caused by a body of the solar system is always less than  $10 \mu\text{as}$ .



## 2.5. Target and instrument selection

In this section the criteria for a suitable instrument as well as the target selection criteria are discussed. Some of these criteria were already addressed in previous sections, but their will be summarized here.

### 2.5.1. Instrument requirements

An instrument used for an astrometric search program for exoplanets in close binaries by ground based imaging have to provide the following properties due to the disturbing effects discussed in previous sections.

- NIR imager equipped with a narrow-band filter
- adaptive optics system and a high spatial resolution
- field of view equal or less than the isoplanatic angle
- fast read-out mode and low read-out noise level

These requirements lead to a large aperture with an AO assisted NIR imager like the large telescopes located on Mauna Kea (Hawaii) or on Paranal in Chile. For the astrometric search program in this work the instruments NACO<sup>5</sup> at the ESO/VLT on Paranal and CIAO<sup>6</sup> at the SUBARU telescope on Mauna Kea are chosen. Both telescopes have a mirror diameter of about eight meter and both instruments are AO assisted NIR imager with a pixel scale of about 13 mas/pixel. Furthermore, the instruments are available with a Br $\gamma$  narrow-band

---

<sup>5</sup> Nasmyth Adaptive Optics System with a Near-Infrared Imager and Spectrograph (Rousset et al. [163], Lenzen et al. [99])

<sup>6</sup> Coronagraphic Imager with Adaptive Optics (Murakawa et al. [136])

## 2. Observational challenges

filter. NACO is operable in the so called *cube-mode*. With that observation mode frames can be saved in a data container called *cube* with nearly no loss of time during the read-out. By doing so one can obtain about 2000 frames within 15 minutes for the minimum exposure time of 0.35 seconds. To reduce this minimum exposure time one can just read-out a specified window instead of the whole detector, which is possible for both detectors, NACO and CIAO.

In 2009, CIAO was decommissioned and the successor instrument Hi-CIAO<sup>7</sup> is still not available. Also NACO is expected to be decommissioned in 2011. However, because astrometric observations are ideal to search exoplanets with orbital periods larger than the typically lifetime of satellite missions and instruments a change of the instrument has to be considered already at the beginning of astrometric observations. As long as the requirements mentioned above are considered and the same stars of the same calibration cluster will be observed to monitor the astrometric stability (chapter 4), a real change of the instrument will then occur as a dramatic change of the astrometric properties of a fictive continuous instrument. These changes can be measured and used to combine the astrometric observations of different instruments.

---

<sup>7</sup> High-Contrast Instrument with Adaptive Optics (Suzuki et al. [181])

### 2.5.2. Target requirements

Not every star or binary is dedicated for astrometric observations. The target stars selected for the astrometric search program described in this work have to fulfill the following requirements. These requirements are needed, due to the sensitivity of the astrometric method itself as well as the observational constraints presented earlier in this chapter.

- stellar separation less than  $10''$
- distance less than 100 pc
- main sequence stars
- solar like or less mass stars
- suitable NIR brightness and contrast ( $K \lesssim 10^m$ ,  $\Delta K \lesssim 3^m$ )

Up to now, six stellar systems on the northern and six systems on the southern hemisphere have been observed in the course of this astrometric search program. The instrument CIAO at the SUBARU telescope on Mauna Kea (Hawaii), which was used for targets on the northern hemisphere, was decommissioned in 2009 and the successor HiCIAO is still not available. Hence, only two epoch observations for the northern targets could be done so far. Further epoch observations of the northern target systems are planned with the successor instrument HiCIAO.

For targets on the southern hemisphere the NIR imager NACO at the VLT on Paranal (Chile) is used. Currently, four target systems are observed once, one target system is observed two times so far and for one target system, namely HD 19994, already four observations

## 2. Observational challenges

Name	SpTy	d [pc]	Sep <sub>app</sub> [as]	Sep <sub>app</sub> [AU]	Epoch	Ref.
HD 200466	G5	43.8	5.0	$\simeq 220$	2	[40]
HD 186858	K3	20.0	3	$\simeq 60$	2	[115]
GJ 22 <sup>†</sup>	M2	10.2	4.3 / 0.5	$\simeq 44 / 5$	2	[43]
GJ 856	M0	16.1	1.7	$\simeq 28$	2	[175, 126]
GJ 2005	M6	7.7	1.5 / 0.35	$\simeq 12 / 3$	2	[173]
GJ 860	M2	4.0	2.4	$\simeq 10$	2	[115]

Tab. 2.5.: Already observed target systems on the northern hemisphere using the AO assisted NIR imager CIAO at the SUBARU telescope on Mauna Kea (Hawaii). The astrometric calibration cluster for the northern hemisphere is M 15. If the apparent separation Sep<sub>app</sub> has more than one value, the system consists of more than two components.

SpTy...spectral type

<sup>†</sup> GJ 22 is a triple system, where a fourth and very low mass component around GJ 22 B is assumed. [43]

are available. The used calibration clusters are the globular clusters M 15 for the northern, and 47 Tuc for the southern hemisphere.

The astrometric reference star is always one component of the observed stellar multiple system, thus differential parallax and proper motion effects can be neglected. However, the orbital motion of the components affects their separations and position angles. That influence is fitted as a second order polynomial and then subtracted from the separation and position angle measurements (chapter 3).

Because three measurements are necessary to fit that influence by a second order polynomial, at least four measurements are needed to check the data for the presence of an astrometric signal. However, for a faithful orbital solution of the astrometric companion more than four measurements are advised.

That is the reason, why in this work HD 19994 is the only system presented in more detail. At this time, with only one or two epoch

## 2.5. Target and instrument selection

Name	SpTy	d [pc]	Sep <sub>app</sub> [as]	Sep <sub>app</sub> [AU]	Epoch	Ref.
HD 19994 <sup>†</sup>	F8	22.6	2.3	≈ 52	4	[179, 117, 124]
GJ 2005	M6	7.7	1.5 / 0.35	≈ 12 / 3	2	[173]
HD 19063	F8	49.0	0.6	≈ 30	1	[82]
AT Mic	M4	10.2	2.7	≈ 28	1	[105]
GJ 568	M4	10.2	1.2	≈ 13	1	[176]
GJ 866*	M6	3.3	0.2	≈ 0.7	1	[185, 172]

Tab. 2.6.: Stellar systems already observed on the southern hemisphere using the AO assisted NIR imager NACO at the VLT on Paranal (Chile). The astrometric calibration cluster for the southern hemisphere is 47 Tuc. If the apparent separation Sep<sub>app</sub> has more than one value, the system consists of more than two components.

SpTy...spectral type

<sup>†</sup> HD 19994 A is known to harbor a RV exoplanet candidate [117]

\* GJ 866 A is a very close binary itself [185]

measurements for the other target systems, no conclusion about the existence of an astrometric signal can be made.

In 2004, Mayor et al. [117] published the detection of a RV planet candidate around the primary of the HD 19994 binary. This exoplanet candidate has a minimum mass of  $M \sin i \simeq 1.7 M_{\text{Jup}}$  and the expected astrometric signal is about (0.15... 1.5) mas, depending on the orbital inclination. Hence, the HD 19994 binary is an ideal target system to test the feasibility of the ground based astrometric search program developed and presented in this work.

All stellar systems listed in the tables 2.5 and 2.6 have a distance of less than 50 pc and their apparent separations are mostly less than 100 AU. Therefore, they are exactly those close systems of interest, where planetary formation is affected by the stellar companion.

This astrometric search program is planned as an ongoing and long term observation program. New suitable target systems will be con-

## 2. *Observational challenges*

tinuously included and other systems, where no deviation could be detected after five observations, will be excluded or postponed. By matching the *Gliese catalogue of nearby stars* (Gliese and Jahreiss [68]) with the CCDM (Dommanget and Nys [44]) more than 150 suitable stars can be found with a spectraltype later or equal than G0, a distance of less than 60 pc, and a stellar companion with an apparent separation between 0.1 arcec and 15 arcsec. That extended target list can be found in appendix F.

## 3. Data analysis

In this chapter the data analysis is presented. It consists of the usual standard data reduction for astronomical observations including dark subtraction, flat-field, and bad-pixel correction. Usually, NIR observations are dithered to subtract the sky, which is brighter in the infrared than in the optical. For several reasons the observations in this work are not dithered. First the flux of the sky background is less than the usual read-out noise per exposure and can be neglected. The second reason bases on the requirement of a large number of measurements for the statistical analysis. Dithering, which is a slightly movement of the telescope, will cause a time loss and thus a lower number of frames. Last but not least, regarding that one deals with non perfect optics, the target systems should be placed on the same detector region for every epoch observation. Further information about geometric distortions of the NACO S13 camera are presented in section 4.3.

### 3.1. Object detection

The pixel coordinates of all stars on the detector are determined with the IDL program *Starfinder* written by Diolaiti et al. [42]. It uses an empirical PSF obtained by averaging the best PSFs on the same

### 3. Data analysis

frame, e.g. the brightest point sources on the frame, to measure the position of a star on the detector. A PSF disturbed by the atmosphere and corrected by an AO system has not a Gaussian shape and the shape changes in time, depending on the atmospheric conditions and the AO performance. Hence, an empirical reference PSF obtained from the same frame is superior in measuring the pixel coordinates than a typical theoretical Gaussian like PSF.

As long as all stars are observed within the isoplanatic angle the perturbations of the different PSFs are identical and the astrometric measurements at the end can be described as a Gaussian distribution. If some frames are taken at worse atmospheric conditions, where the isoplanatic angle is smaller than the binary separation, both PSFs will be different in shape. In that case, the resulting separation and position angle measurements can be identified as systematic outliers in the Gaussian measurement distribution. At the end, more measurements results in a better measurement statistic, thus several thousand frames per target system are taken.

## 3.2. Statistical analysis

After standard data reduction the effects of differential refraction and aberration have to be corrected as described in the sections 2.3.2 and 2.4.1. Afterwards, the binary separation and position angle are measured on every frame, which results in several thousand separation and angle measurements per binary. Using a Kolmogorov-Smirnov test<sup>1</sup> in combination with a  $2\sigma$  clipping, all systematic outliers are excluded and the Gaussian distributed measurements are left. The

---

<sup>1</sup> see Wall and Jenkins [201] and chapter 14 Press [151] for further information



### 3.3. Check for an astrometric signal

standard deviation of this distribution correlates with the atmospheric conditions and the AO performance. The measurement error, which is the error of the mean value, can be calculated as the standard deviation divided by the square root of the number of Gaussian distributed measurements ( $\mu_{\text{error}} = \sigma_{\text{meas}}/\sqrt{N}$ ). This procedure has also been done for the observations of the calibration cluster.

Comparing the relative alignment of the cluster stars for all epoch observations the astrometric stability of the instrument can be monitored. Without such a monitoring it is not possible to combine single epoch measurements because the astrometric properties of the instrument and the telescope could change from one to another observation. If systematic effects between the epoch observations are detected, the corresponding astrometric correction terms are calculated. These correction terms will then be applied on the astrometric measurements of the target system (Fig. 3.1). Further information about the calibration strategy can be found in the next chapter.

### 3.3. Check for an astrometric signal

In order to detect the astrometric signal of an unseen companion the influence of the stellar orbital motion has to be removed from the data. Because of the huge orbital periods of visual double stars (typically more than several hundred years) the orbital elements of such binaries are not known accurate enough to calculate the orbital motion of the binary at a sub-mas level. But the change of the separation and position angle of such a double star will be just slightly curved over the observational timeline of several years. Hence, this influence can be fitted by a second order polynomial. After subtracting those

### 3. Data analysis

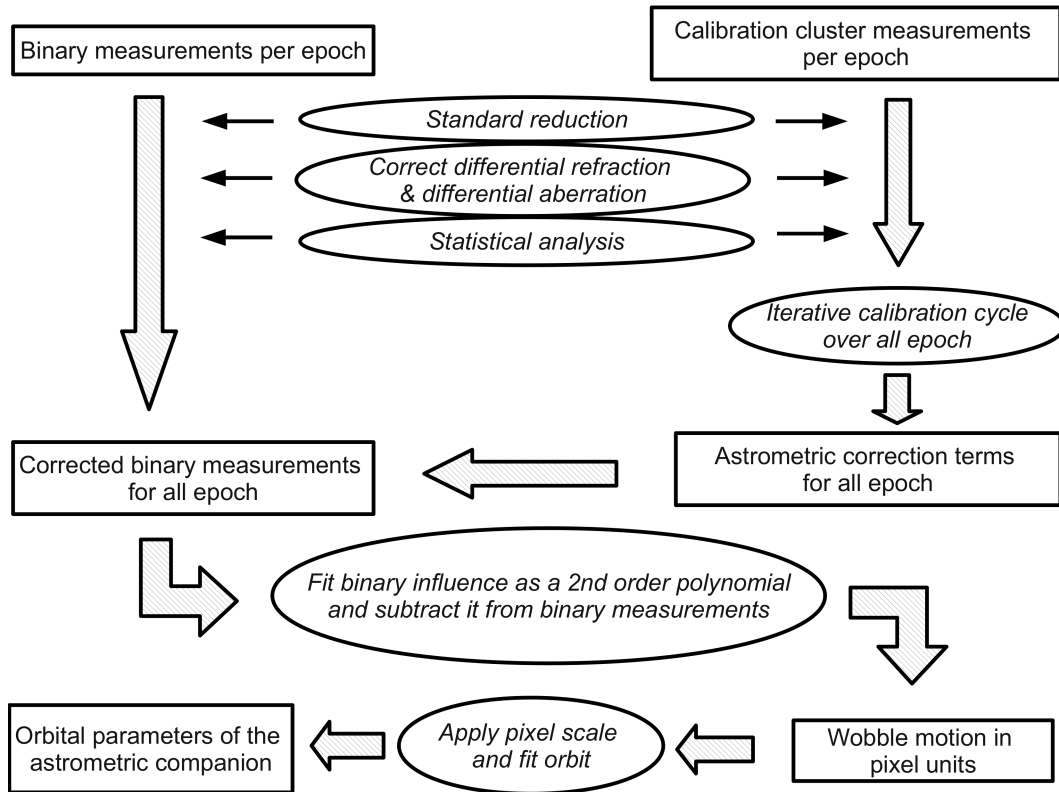


Fig. 3.1.: Analysis strategy developed in this work to search for an astrometric signal within the binary measurements. Because of the influence of the stellar orbital motion (which is fitted as a second order polynomial) at least four measurements are needed to search for an astrometric signal.

fitted values a present periodic deviation can be interpreted as an astrometric signal.

Up to now, all separation measurements as well as the fit of the influence by the stellar orbital motion are done in pixel units. The reason for that is the pixel scale, which is not known with an accuracy appropriate to search a sub-mas signal over the range of several pixel. For a pixel separation of 200 pixel, an accuracy of  $0.5 \mu\text{as}/\text{pixel}$  is needed to achieve a separation measurement error of  $0.1 \text{mas}$ , but such an accurate known (and stable) calibration system does not exist today.

### 3.3. Check for an astrometric signal

Published values for the pixel scale of the NACO S13 camera differs from (13.22...13.26) mas/pixel, while its accuracy varies from 50  $\mu$ as/pixel up to 200  $\mu$ as/pixel (e.g. Neuhäuser et al. [142], Schmidt et al. [170], Mugrauer et al. [135] and Correia et al. [33]). Because Schmidt et al. [170] considered a maximum possible orbital motion of their calibration binary the authors achieved the largest uncertainty of 200  $\mu$ as/pixel. Normally, the pixel scale of the NACO S13 camera is determined with an accuracy better than 0.1 mas per pixel. For this work, a conservatively chosen pixel scale of (13.24  $\pm$  0.1) mas/pixel is used.

The astrometric signal of an exoplanet is usually less than one milli-arcsec, which corresponds to less than a tenth of a NACO S13 pixel. By adopting the pixel scale after the subtraction of the fitted orbit motion influence the uncertainty of the pixel scale has much less impact on the final measurement precision. The difference of the measured and the fitted binary separation, which is the deviation caused by an astrometric companion, is converted in angular units using the pixel scale.

$$\begin{aligned} \tilde{\rho} &= ps \times \tilde{\varrho}, & \Delta\tilde{\rho} &= \sqrt{(ps \times \Delta\tilde{\varrho})^2 + (\Delta ps \times \tilde{\varrho})^2} \\ \tilde{\rho} &\dots \text{deviation in mas}, & \tilde{\varrho} &\dots \text{deviation in pixel} \\ ps &\dots \text{pixel scale in mas/pixel} \end{aligned} \tag{3.1}$$

A polynomial of second order has three parameters, thus with only three epoch observations one will never find a deviation between the measurements and the fitted influence of the binary orbit. At least four observations are needed to check for an astrometric signal. To determine all seven orbital parameters (see appendix A for further details) of a detected astrometric companion one has to fit

### 3. Data analysis

$7 + (2 \times 3) = 13$  parameters in total, thus the binary has to be observed at least seven times.

## 3.4. Speckle interferometry

As mentioned in section 2.1, the astrometric signal depends on the mass- and the brightness ratio of the star and its astrometric companion. Therefore, one has to check the brightness of a detected astrometric companion. This is done in this work with speckle interferometry using a program written by Rainer Köhler. The theory of speckle interferometry is complex and not part of this work. Further information about this topic and especially about the used program can be found in Köhler et al. [89].

In simple terms, the power spectrum<sup>2</sup> of a not resolvable binary is folded with the power spectrum of a single star. The resulting power spectrum is the brightness distribution of the binary and can be modeled with the theoretical visibility of a binary model. Fig. 3.2 demonstrates how the complex visibility (square root of the power spectrum) looks like for different kind of binaries.

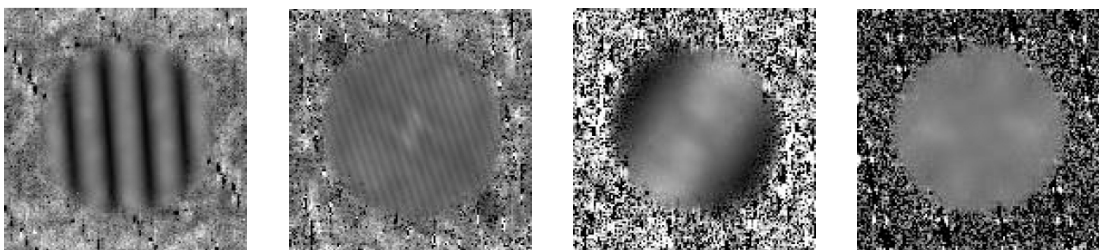


Fig. 3.2.: Examples of complex visibilities for different binaries (Köhler et al. [89]). The shown visibilities illustrates (from left to right) a wide and bright companion, a wide and faint companion, a bright and close companion, and a single star.

---

<sup>2</sup> square of the Fourier transform

## 4. Calibration

The calibration strategy chosen in this work is based on the same principle as used for the calibration of Hipparcos observations and which will be also used for JWST (van der Marel et al. [196]), GAIA (Lammers et al. [92]), and ESPRI (Elias et al. [51]), namely an iterative calibration strategy. That means that the astrometric measurements as well as the calibration system itself will be recalibrated after each new observation in order to identify systematic long-term trends concerning the astrometric properties of the instrument.

That iterative approach is owed to the fact that no absolute stable reference system exist. For example binaries and stellar clusters, which are often used for astrometric calibrations, have an orbital motion, respectively a velocity dispersion. The spectral calibration unit of a spectrograph is affected by pressure and temperature. Photometric calibrations are influenced by the stellar activity of the photometric standard star. At the end, every calibration system is unstable if one increases the needs of the precision far enough. Hence, to monitor the stability of the calibration system itself with an iterative method is a faithful calibration approach.

## 4. Calibration

### 4.1. Calibration clusters

In this work the old globular clusters 47 Tuc and M 15 are chosen for the southern, respectively northern hemisphere. 47 Tuc has a distance of about 4.5 kpc and an age of about 11 Gyrs (e.g. McLaughlin et al. [119], Thompson et al. [183], Gratton et al. [69]). The distance of the globular cluster M 15 is about 10 kpc and the age is determined to about 13 Gyrs (e.g. McNamara et al. [120]). Hence, both globular clusters are old and far away.

Fig. 4.1 is a negative image from the core region of 47 Tuc taken with the WFPC<sup>1</sup> of the HST (image from the *ST-ECF Hubble Science Archive*). The field observed in this work is also shown in Fig. 4.1 as a black rectangle. The criteria are a high rate of well distinguishable and detectable point sources within the NACO S13 field of view (FoV).

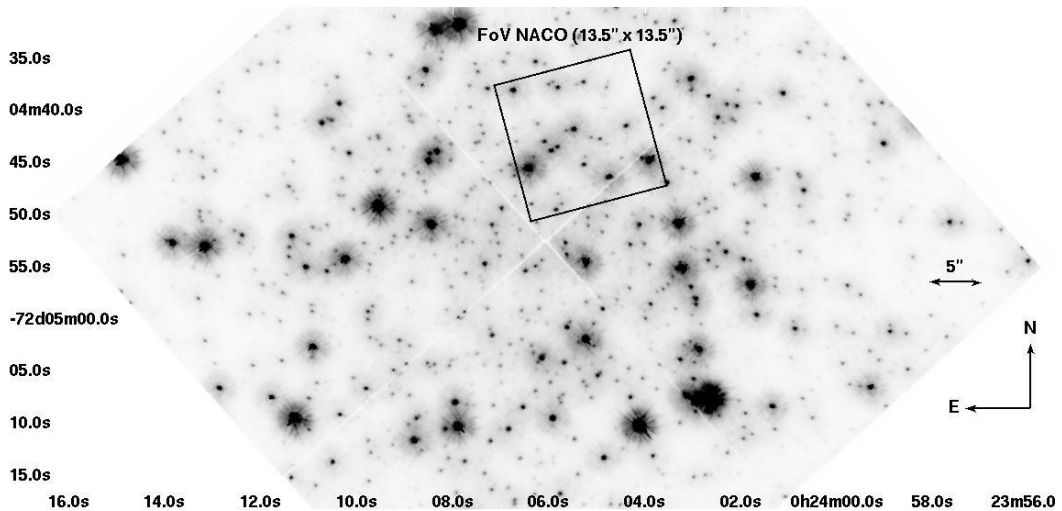


Fig. 4.1.: Negative HST/WFPC image from the core region of the old globular cluster 47 Tuc, taken from the *ST-ECF Hubble Science Archive*. The black rectangle marks the field observed with the NACO S13 camera for the astrometric monitoring in this work.

<sup>1</sup> Wide Field Planetary Camera

The calibration strategy described in this chapter is independent from the cluster itself, thus it is the same for 47 Tuc and M 15. In order to measure deviations at the sub-mas level the calibration cluster has to be promptly observed in the same nights as the scientific target system. Also the clusters have to be observed with the same NIR narrow-band filter and with the same instrument settings as the target systems. In simple terms, the complete optics have to be the same. In contrast to the target systems the exposure time is increased to obtain a sufficient signal to noise ratio for the cluster stars.

The measure, which is used to monitor the instrument's astrometric properties is the mean value of the separations and position angles from each to each star. In other words, the relative alignment of the cluster stars is measured and compared. These values, the mean separation and the mean position angle, are called *Master-Baseline* in this work. Besides the intrinsic instability of the cluster, which is based on the transverse velocity dispersion of the cluster stars, this *Master-Baseline* should be the same for all epoch observations. A measured change of this *Master-Baseline* from one to another epoch observation is interpreted as a change of the astrometric properties of the instrument. The corresponding correction terms are applied to the separation and position angle measurements of the observed target system.

## 4.2. Iterative calibration cycle

An iterative calibration has one disadvantage. The final measurement value and its precision will be known just at the end of the program due to a possible correction obtained by the final iteration (i.e. the

#### 4. Calibration

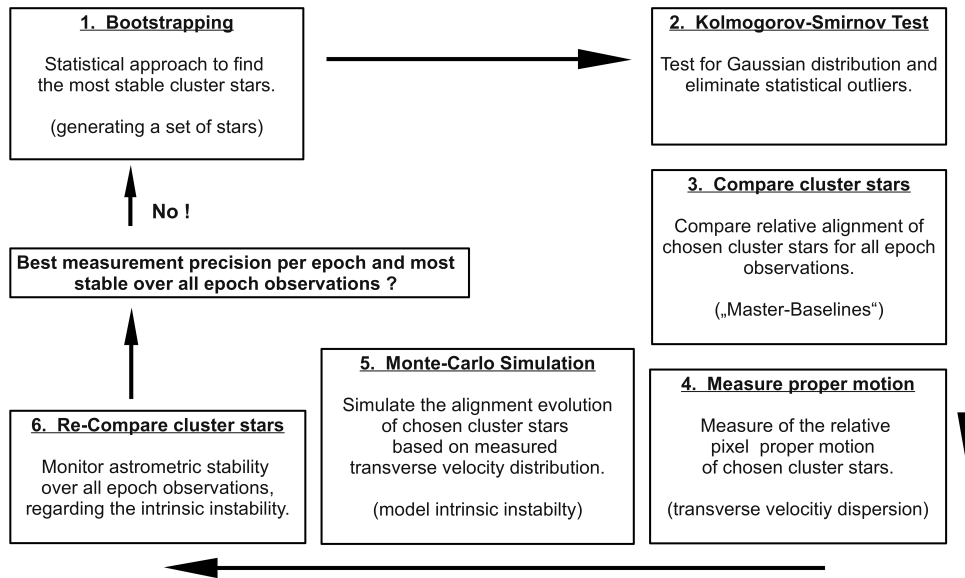


Fig. 4.2.: Sketch of the iterative calibration cycle, which is used in this work to monitor the astrometric stability of the instrument. This calibration cycle will be redone after each new observation for all cluster data obtained so far.

last observation). Furthermore, a sufficient number of observations is needed to analyse the kinematic behaviour of the observed cluster stars. The more observations, the better one can determine the kinematic properties of the cluster stars, thus the intrinsic instability of the calibration cluster. The reason for that is the increasing measurement precision of the proper motions (of the cluster stars) due to an increasing epoch difference.

Fig. 4.2 illustrates the iterative calibration cycle developed in this work. This cycle consists of four major steps. First, a bootstrapping algorithm (Press [151]) statistically generates a set of cluster stars. The measurement precision per epoch and the over-all epoch stability is saved and compared to the next generated set of cluster stars. At the end, the outcome of the bootstrapping algorithm is the set of the most stable stars in the observed cluster field.



The second step is the measurement of the *Master-Baseline* on every frame. Using a Kolmogorov-Smirnov test in combination with a  $2\sigma$  clipping, systematic outliers are identified and excluded. The mean of all *Master-Baselines* measured on all frames of one epoch observation represents the *Master-Baseline* for that epoch (number two and three in Fig. 4.2). As third, the relative proper motions of the cluster stars are measured (using the oldest and newest observations), whereas the proper motions are determined relatively to the mean position of all these stars. Hence, it is not the absolute proper motion of the star, but that portion disturbing the relative alignment of all stars (number four in Fig. 4.2).

The simulation of the temporal behaviour of the *Master-Baseline*, affected by the relative proper motions of the cluster stars is the fourth step of the calibration cycle (number five and six in Fig. 4.2). An offset between the expected (i.e. simulated) and the measured values of the *Master-Baseline* is interpreted as a change of the instrument's astrometric properties.

### 4.3. Geometric field distortions

In the past, the NACOS13 camera was expected to have no measurable geometric field distortions due to its small field of view ( $15'' \times 15''$ ) compared to other instruments. However, no optics system is really perfect. In 2009 the binary HD 19994 was placed in different detector regions on purpose in order to study possible field distortions. Before 2009 all observations were concentrated on the inner part of the detector. Placing the target system always on the same inner detector region, no systematic effects regarding the location on the chip

#### 4. Calibration

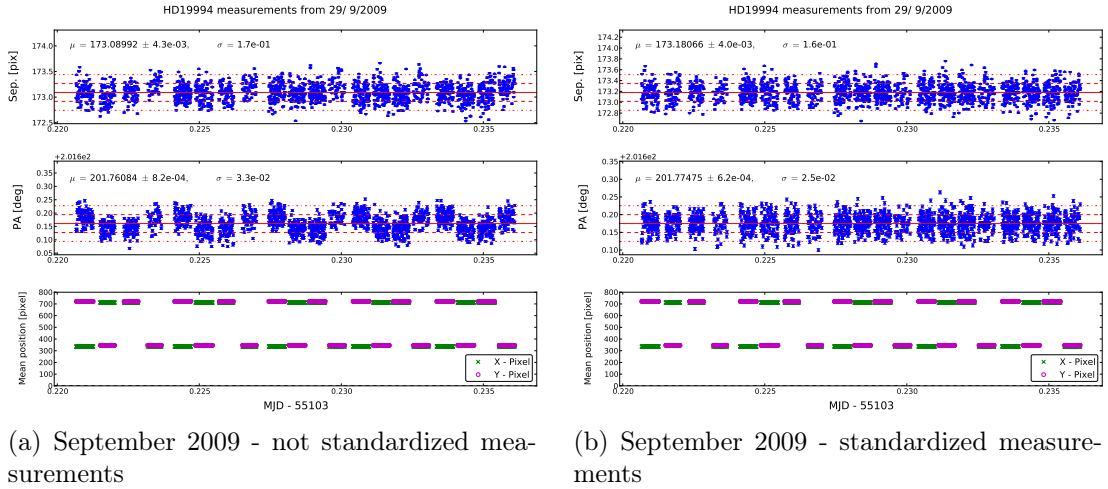


Fig. 4.3.: Binary measurements of HD 19994 observed in 2009. In the left diagram the effects of geometric field distortions are clearly visible. On the right the mean value of each cube is standardized to the mean value of all cubes, where the target system has the closest distance to the center of the detector. The both upper panels are the separation and the position angle measurements of the binary. In the lower panel the binary position (mean position of both stellar components) on the detector is shown.

are found. However, scattering the target system over the whole chip such effects are clearly visible. Fig. 4.3(a) illustrates how the binary separation and position angle depends on the location on the chip for the 2009 measurements.

In addition to HD 19994 also the observations of the calibration cluster 47 Tuc were dithered in 2009. The goal is to measure and model the geometric field distortions on the NACOS13 detector. Typically distortion models are among others two dimensional polynomials or simple radial models. The latter ones only depends on the distance relatively to the center of the distortion. To determine geometric distortions, the number of stars used for the calculation are important. Using just two stars of a binary it is impossible to determine any distortion. In simple terms, the more parameters the distortion

model has the more stars are needed to fit that model. Hence, the observed cluster stars and not the target systems are used to measure and model the geometric distortions.

Until now, no distortion model could be modeled to the dithered observations of 47 Tuc. The distortion models attempt to fit are several simple radial, barrel, and pincushion models as well as multivariate polynomials of different orders and a published distortion model used for the HST (Meurer et al. [121]). Thus, the analysis of the geometric field distortions, which are present, is still in progress.

In 2008, Trippe et al. [187] analyzed the geometric distortions of the NACO camera. The authors used the following radial approach with  $\tilde{r}$  as the true image position and  $\tilde{r}_{\text{dist}}$  as the distorted image position, both relatively to a distortion center.

$$\tilde{r} = \tilde{r}_{\text{dist}} (1 - \beta \times \tilde{r}_{\text{dist}}^2) \quad (4.1)$$

While the chip curvature  $\beta$  could be determined for the S27 camera (FoV  $\simeq 27'' \times 27''$ ), the authors could not find a convergent solution for the S13 camera with classical fitting algorithm. At the end, they used a statistical approach and came up with a chip curvature of  $\beta \simeq (2 \dots 14) \times 10^{-10}/\text{pixel}^2$ . The large spread for this parameter clarifies how difficult it is to measure such relatively small distortions.

The position displacement is  $|\tilde{r} - \tilde{r}_{\text{dist}}| = \beta \times \tilde{r}_{\text{dist}}^3$ , which corresponds for a separation of 530 pixel to  $(2 \dots 14) \times 0.015$  pixel. Looking at Fig. 4.3(a) one can estimate a change of the binary separation of about 0.2 pixel over a range of 530 pixel ( $\simeq 0.04\%$ ). This value is in good agreement with the expected value using the chip curvature from Trippe et al. [187].

#### 4. Calibration

For further analysis of the binary measurements an artificial reference value for the separation and the position angle are defined. In case of a radial distortion, the geometric distortion is weakest at the center of the detector. Assuming such radial distortions, this artificial reference is defined as the mean value of all cubes, where the binary has the closest distance to the center of the detector. The mean value of all other cubes were standardized to this reference value.

## 5. Results

In this chapter the observational results of 47 Tuc and HD 19994 are presented. HD 19994 is one of the target systems on the southern hemisphere observed with VLT/NACO four times so far. The observations were done in November 2006<sup>1</sup>, July 2007<sup>2</sup>, October 2008<sup>3</sup>, and September 2009<sup>4</sup>.

The astrometric precision is the crucial point for astrometric observations and constrains the detectable mass of astrometric companions. The total precision consists of the measurement precision per epoch, the remaining uncertainties of the astrometric corrections as described in chapter 2, and the multi-epoch stability of the instrument's astrometric properties. The latter one is determined by monitor specific stars of the calibration cluster 47 Tuc for all epoch observations as described in chapter 4. It has to be reminiscent, that the calibration strategy used in this work is iterative, thus the calibration results presented in here could change after the next observation. A change of the calibration would also affect the measured astrometric signal. However, with each new observation more information about the intrinsic instability of the cluster stars are gained and the precision of the calibration will increase.

---

<sup>1</sup> 078.C-0249 (PI: R. Neuhäuser) observed by A. Seifahrt

<sup>2</sup> 079.C-0106 (PI: R. Neuhäuser) observed by T. Röhl and A. Seifahrt

<sup>3</sup> 382.C-0329 (PI: R. Neuhäuser) observed by T. Röhl

<sup>4</sup> 083.C-0150 (PI: N. Vogt) observed by M. Mugrauer

## 5.1. Astrometric precision - lower limits

Table 5.1 summarizes the remaining uncertainties of the astrometric corrections (chapter 2), which are in total less than  $150 \mu\text{as}$  for the calibration cluster 47 Tuc and less than  $30 \mu\text{as}$  for the binary HD 19994. These uncertainties have to be added to the detection errors for every star and epoch by splitting them uniformly onto the two dimensions of the detector. For the calibration cluster 47 Tuc, this additional measurement uncertainty is

$$\Delta X = \Delta Y = \frac{1}{\sqrt{2}} \frac{0.15 \text{ mas}}{13.24 \text{ mas/pixel}} = 8 \times 10^{-3} \text{ pixel}, \quad (5.1)$$

while it is  $1.6 \times 10^{-3}$  pixel for the HD 19994 system.

The values listed in table 5.1 also represent the lower limit of the achievable precision for separation measurements ( $\Upsilon_{\text{Sep}}$ ). The lower precision limit for the position angle measurements ( $\Upsilon_{\text{Pa}}$ ) can be determined by assuming a direction of  $\Upsilon_{\text{Sep}}$  perpendicular on the separation of two stars (Sep).

$$\tan \Upsilon_{\text{Pa}} = \Upsilon_{\text{Sep}}/\text{Sep} \quad (5.2)$$

These lower precision limits are listed in table 5.2. In case of the binary HD 19994 (Sep  $\simeq 170$  pixel), the lower precision limits are  $\Upsilon_{\text{Sep}} = 2.27 \times 10^{-3}$  pixel for the separation measurements and  $\Upsilon_{\text{Pa}} = 7.7 \times 10^{-4}$  deg for position angle measurements.

The lower precision limit for the position angle measurements depends on the separation of two stars. For the observations of the calibration cluster 47 Tuc the length of the *Master-Baseline* of about 530

### 5.1. Astrometric precision - lower limits

Effect	47 Tuc	HD 19994
	Uncertainty in $\mu\text{as}$	
Differential atmospheric refraction	< 110	< 15
Differential aberration	< 95	< 5
Differential parallaxe ( $d \geq 3 \text{ pc}$ )	< 10	< 16
Stellar activity ( $d \geq 3 \text{ pc}$ )	< 25	< 10
Differential gravitational light deflection	< 10	< 10
In total	< 150	< 30

Tab. 5.1.: Summary of the remaining uncertainties of the disturbing effects for ground based relative astrometric measurements for a pixel scale of  $13.24 \pm 0.1 \text{ mas/pixel}$ .

pixel is used. That results in  $\Upsilon_{\text{Pa}} = 1.22 \times 10^{-3} \text{ deg}$  for position angle measurements. For the separation measurements, the lower precision limit is  $1.13 \times 10^{-2} \text{ pixel}$ . The lower precision limits as well as the remaining correction uncertainties depend on specific target properties, thus both have to be calculated for each target system separately.

If a measurement error of the cluster 47 Tuc or for the binary HD 19994 is smaller than these lower precision limits listed in table 5.2 the measurement error is set to these lower limits.

	$\Upsilon_{\text{Sep}} [\mu\text{as}]$	$\Upsilon_{\text{Sep}} [\text{pixel}]$	Sep [pixel]	$\Upsilon_{\text{Pa}} [\text{deg}]$
47 Tuc	150	$11.33 \times 10^{-3}$	530	$1.22 \times 10^{-3}$
HD 19994	30	$2.27 \times 10^{-3}$	170	$7.7 \times 10^{-4}$

Tab. 5.2.: Lower precision limits for separation and position angle measurements for the calibration cluster 47 Tuc and the binary HD 19994.

## 5.2. Astrometric calibration cluster - 47 Tuc

As described in chapter 4, the relative alignment of the same certain stars in the observed cluster field is used to monitor the astrometric stability of the instrument. This relative alignment is described by a measure called *Master-Baseline*, which is defined as the mean value of all separations and all position angles measured from each to each star on one frame. The mean value of all *Master-Baselines* measured on all frames from one epoch observation is then the *Master-Baseline* of this epoch.

The number of frames per epoch obtained of the calibration cluster is usually about 150, each with an integration time of 30 seconds. After measuring the *Master-Baseline* on each frame, an Anderson-Darling test (modification of the Kolmogorov-Smirnov test, see chapter 14 in Press [151]) is used to extract the Gaussian core of the measurements. The error of the mean can then be calculated by  $\mu_{\text{err}} = \sigma_{\text{meas}}/\sqrt{N}$ , where N is the number of Gaussian distributed measurements with a standard deviation of  $\sigma_{\text{meas}}$ .

After the first analysis of the 47 Tuc data an image motion within each single epoch observation was detected. More precisely it is a linear motion of the observed cluster field and a slight change of the detector orientation over the time. The reason for that is a different atmospheric refraction of the science target (observed in the near infrared) and the telescope guide star, which is observed in the optical. Because large telescopes have an alt-azimuth mounting a telescope guide star is needed to calculate the tracking velocity for the azimuth and the altitude axis as well as the detector rotation. In case of non considered different atmospheric refraction indices, the tracking



velocity calculated with the telescope guide star can not be adopted for the scientific observations in the near infrared. That results in an image motion and rotation over the time. This effect is also known for spectroscopic observations, where the star can move out of the slit (e.g. Cuby et al. [34]). But it has not to be mixed up with the differential chromatic refraction (DCR) described in section 2.3.2, which regards the effect over the field of view of the NIR detector. The linear image motion itself is not a big deal, but a false rotation velocity of the detector causes a field rotation, which is measurable in the *Master-Baseline* measurements.

The telescope control software of large telescopes can usually correct this effect but the spectral properties of the stars, the atmospheric conditions and the telescope pointing are needed very accurately. However, the spectral types of the cluster stars are not precisely known, thus a slight image motion and field rotation is present in the 47 Tuc data.

For the first image taken after the positioning of the telescope that effect is equal to zero and increases with the tracking time. To correct that effect a simple model is used to shift each of the following frames onto the first one. The model consists of a linear offset in both detector axes ( $x_{\text{off}}, y_{\text{off}}$ ) and a rotation (angle  $\eta$ ) around a certain rotation center ( $\bar{x}_{\text{rot}}, \bar{y}_{\text{rot}}$ ).

$$\begin{aligned} X_{\text{new}} &= x_{\text{off}} + \bar{x}_{\text{rot}} + [(X - \bar{x}_{\text{rot}}) \cos \eta - (Y - \bar{y}_{\text{rot}}) \sin \eta] \\ Y_{\text{new}} &= y_{\text{off}} + \bar{y}_{\text{rot}} + [(Y - \bar{y}_{\text{rot}}) \sin \eta + (X - \bar{x}_{\text{rot}}) \cos \eta] \end{aligned} \quad (5.3)$$

This model has no influence on the relative alignment of the cluster stars, but it removes the trend in the position angle measurements, which is based on a field rotation due to the effect described above.

## 5. Results

Because of the high airmass and the long exposure time of the 47 Tuc observations that image motion is only detected in the cluster observations and not in the measurements of any target system, e.g. HD 19994.

Not all stars in the observed cluster field are used to monitor the astrometric stability of the instrument. Due to a hidden stellar multiplicity (the reflex motion affects the *Master-Baseline*) or a conspicuous proper motion, some stars in the cluster field could falsify the monitoring of the astrometric stability. Such stars have to be identified and rejected.

In this work the identification of the unstable stars is done by determining the most stable ones using a statistical approach. A uniformly distributed set of stars is generated out of all observed cluster stars and the *Master-Baselines* for all epoch observations are measured (see chapter 4, first step in Fig. 4.2). The selection criterion for the chosen set of stars is a combination of the most precise measurements per epoch and the most stable behavior (of the *Master-Baseline*) over all epoch observations.

The cluster stars chosen at the end are shown in Fig. 5.1 and the measurements of their *Master-Baselines* can be found in Fig. 5.2 and are also listed in table 5.3. If the measurement error (as displayed in Fig. 5.2) is smaller than the lower precision limit described in the previous section (table 5.2), the measurement error is set to the lower precision limit.

After measuring the *Master-Baseline* for each epoch observation a change of its separation and position angle over the time can be seen in table 5.3. The reason for this deviation is not only a possible change of the astrometric properties of the instrument, but also

## 5.2. Astrometric calibration cluster - 47 Tuc

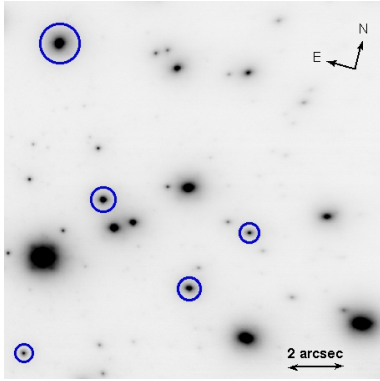


Fig. 5.1: Negative image of the observed 47 Tuc cluster field taken with the NACOS13 camera. The cluster stars determined as the most stable stars by the iterative calibration cycle (Fig. 4.2) are marked by circles.

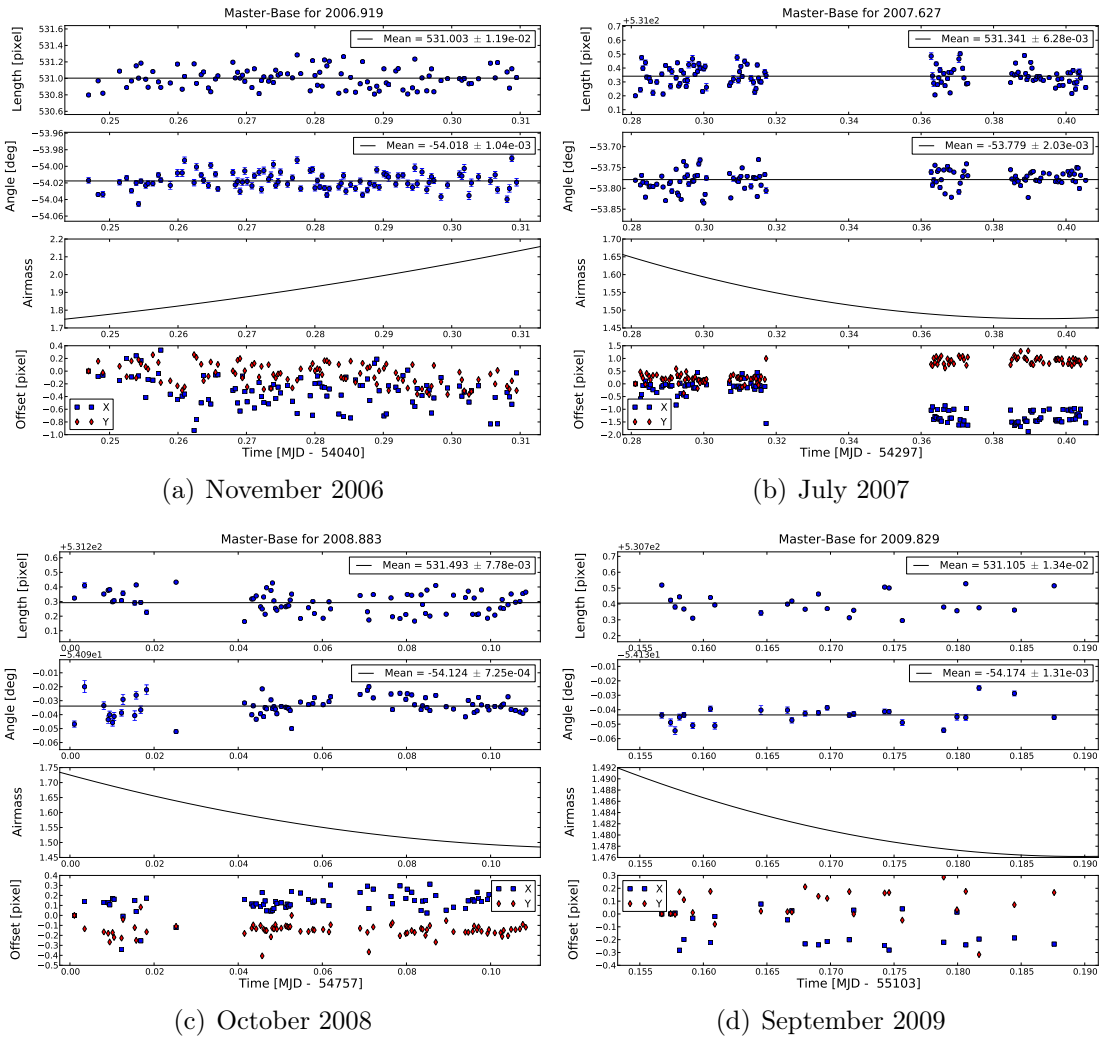


Fig. 5.2.: Measurements of the *Master-Baseline* for all four epoch observations, analyzed with an Anderson-Darling test (Press [151]).

## 5. Results

Date [MJD]	Separation [pixel]	Angle [deg]
54040.279	$531.003 \pm 1.19e-02$	$-54.018 \pm 1.22e-03$
54297.343	$531.341 \pm 1.13e-02$	$-53.779 \pm 2.03e-03$
54757.063	$531.493 \pm 1.13e-02$	$-54.124 \pm 1.22e-03$
55103.169	$531.105 \pm 1.34e-02$	$-54.174 \pm 1.31e-03$

Tab. 5.3.: Measurements of the *Master-Baseline* of the chosen 47 Tuc cluster stars (Fig. 5.2 and 5.1) for all epoch observations. If the measurement error is smaller than the lower precision limit given in table 5.2 this lower limit is taken as measurement precision.

a real change of the relative alignment based on a present transverse velocity dispersion of the stars. This effect is the intrinsic instability of the observed cluster stars and its strength depends on the selected stars. In order to determine the influence of this intrinsic instability a measure, which describes the influence of all selected stars on their *Master-Baseline*, is needed. This measure is the relative proper motion of a star, which is defined as the stellar movement relatively to the center of all chosen stars measured by the oldest and the youngest epoch. Using that relative proper motion the theoretically expected behavior of the *Master-Baseline* can be simulated, which is done by a Monte-Carlo simulation.

The results of this intrinsic instability simulation can be seen in Fig. 5.3 as blue lines. Theoretical the simulation should be conform with the measured values for the first and the last observation because these epoch observations are used to determine the relative proper motion. However, it does not fit perfectly. The reason for that is the different way how these values are obtained. The measurements (red dots in Fig. 5.3) are based on the statistic of all measured *Master-Baselines* on each frame, thus on the measurement of the separations

## 5.2. Astrometric calibration cluster - 47 Tuc

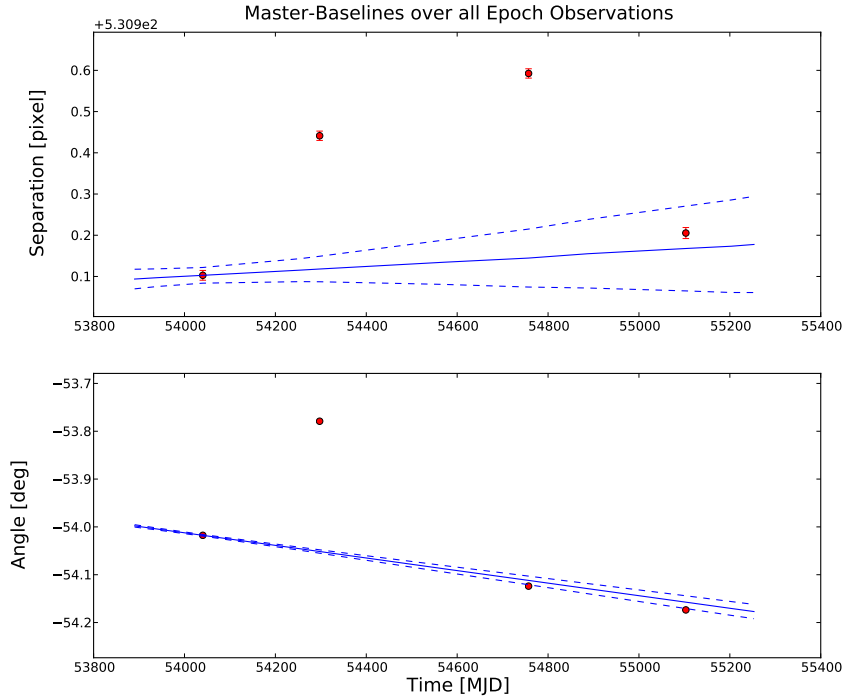


Fig. 5.3.: Measured *Master-Baselines* of the chosen cluster stars. The blue lines represent the expected temporal behavior of the *Master-Baseline* (solid: mean; dashed:  $1\sigma$  uncertainty) simulated with the measured proper motions of the stars.

and position angles. On the other hand, the relative proper motions are based on the statistic of the stellar positions measured on each frame. At the end, the theoretical expected *Master-Baseline* behavior (blue lines in Fig. 5.3) is calculated out of those position statistics.

This is a known effect in relative astrometry. For example, the part of the position uncertainty perpendicular on the separation of two stars has a maximum impact on the position angle, but nearly no influence on the separation measurement of the two stars. In case of a non radial position uncertainty the statistics of the position will slightly differ from the statistics of the separation and position angle measurements.

## 5. Results

Date [MJD]	Separation [pixel]	$\Delta$ Sep [pixel]	$\delta$ Sep [pixel/pixel]
54040.279	531.003 $\pm$ 1.19e-02	0.0 $\pm$ 1.19e-02	0.0 $\pm$ 4.22e-05
54297.343	531.341 $\pm$ 1.13e-02	3.23e-01 $\pm$ 3.09e-02	6.08e-04 $\pm$ 6.19e-05
54757.063	531.493 $\pm$ 1.13e-02	4.48e-01 $\pm$ 7.03e-02	8.43e-04 $\pm$ 1.34e-04
55103.169	531.105 $\pm$ 1.34e-02	3.75e-02 $\pm$ 1.03e-01	7.06e-05 $\pm$ 1.96e-04

Tab. 5.4.: Separation of the *Master-Baseline* for all epoch observations (second column) as given in table 5.3. The third column contains the deviation of the measured value from the theoretical expected value. The last column shows the correction term (relative deviation), which has to be applied on the measurements of scientific target systems (e.g. HD 19994).

Date [MJD]	Position Angle [deg]	$\Delta$ PA = $\delta$ PA [deg]
54040.279	-54.018 $\pm$ 1.22e-03	0.0 $\pm$ 1.65e-03
54297.343	-53.779 $\pm$ 2.03e-03	2.73e-01 $\pm$ 3.57e-03
54757.063	-54.124 $\pm$ 1.22e-03	-1.20e-02 $\pm$ 8.96e-03
55103.169	-54.174 $\pm$ 1.31e-03	-1.62e-02 $\pm$ 1.34e-02

Tab. 5.5.: Position angle of the *Master-Baseline* for all epoch observations (second column), as given in table 5.3. The third column contains the deviation of the measured value from the theoretical expected value. The last column shows the correction term (equal to the deviation), which has to be applied on the measurements of scientific target systems (e.g. HD 19994).

The increase of the  $1\sigma$  uncertainty over the time in Fig. 5.3 is based on the uncertainties of the measured stellar proper motions.

Tables 5.4 and 5.5 listed the astrometric correction terms for every epoch, which are the relative deviation of the *Master-Baseline* for the separation and the absolute deviation for the position angle. These corrections have to be applied to the binary measurements (see next chapter).

### 5.3. Target system - HD 19994

HD 19994<sup>5</sup> ( $\text{RA}_{\text{J2000}} = 03^{\text{h}} 12^{\text{m}} 46.43^{\text{s}}$ ,  $\text{DEC}_{\text{J2000}} = -01^{\circ} 11' 45.96''$ ) is a stellar visual binary located in the constellation Cetus. In 2003, a RV extrasolar planet candidate ( $M \sin i \simeq 1.7 M_{\text{Jup}}$ ,  $P \simeq 536$  days) was detected around the A component and published by Mayor et al. [117] in 2004. The expected astrometric signal of the RV exoplanet candidate varies from 0.15 mas for a planetary edge-on orbit up to more than 1.5 mas for a nearly face-on orbit.

Because of the huge orbital period of more than 1400 years the orbit of HD 19994 AB is just poorly covered with measurements (in fact it is less than one fourth of the complete orbit, see Hartkopf and Mason [74]). Hence, the orbital elements cannot be faithfully determined, but the orbital inclination of the binary is estimated to be about 110 degree. Assuming coplanarity, the mass of the exoplanet candidate would be similar to its minimum mass. The binary has a separation of about 2.5 arcsec and is a high proper motion binary with  $\mu_{\alpha} \simeq 194.6$  mas/yr and  $\mu_{\delta} \simeq -69$  mas/yr (van Leeuwen [197]).

The stellar components of the binary HD 19994 are published as a F8V primary ( $M_{\text{A}} \simeq 1.3 M_{\odot}$ ) and a M3V secondary ( $M_{\text{B}} \simeq 0.4 M_{\odot}$ ) with an age of 3.5...13 Gyrs (see Wright et al. [203], Saffe et al. [164], Duquennoy and Mayor [45], Hale [73], Fuhrmann [64]). The distance of the system was determined by van Leeuwen [197] to about 22.6 pc.

---

<sup>5</sup> alias 94Ceti, GJ128, HIP14954

## 5. Results

### 5.3.1. Relative astrometry

After the standard data reduction procedure the binary measurements are corrected regarding the astrometric effects (differential refraction and differential stellar aberration) as given in chapter 2. Afterwards, the separation and the position angle of the B relatively to the A component are measured for every epoch (Fig. 5.4), including a statistical analysis to extract the Gaussian distributed measurements using a Kolmogorov-Smirnov test.

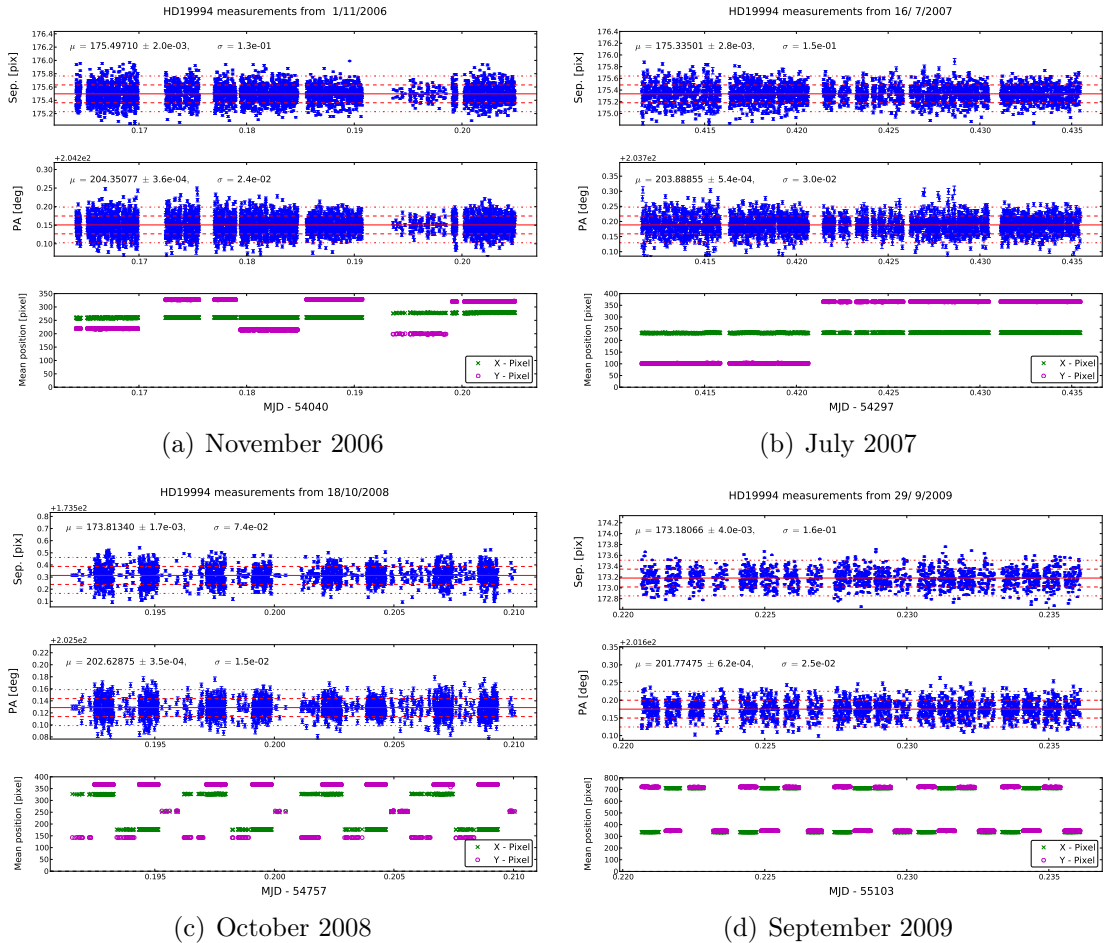


Fig. 5.4.: Binary measurements of HD 19994 A&B for November 2006, July 2007, October 2008, and September 2009.



### 5.3. Target system - HD 19994

Date [MJD]	Separation [pixel]	$\Delta$ Sep [pixel]	Sep <sub>corr</sub> [pixel]
54040.281	175.497±2.3e-3	0.0±7.4e-03	175.497±7.8e-03
54297.344	175.335±2.8e-3	-1.07e-01±1.1e-02	175.228±1.1e-02
54757.069	173.813±2.3e-3	-1.47e-01±2.3e-02	173.666±2.3e-02
55103.172	173.181±4.0e-3	-1.22e-02±3.4e-02	173.169±3.4e-02

Tab. 5.6.: Separation measurements of the binary HD 19994 A&B. The third row is the astrometric correction term derived by the calibration cluster and the last row shows the corrected binary separation. The astrometric correction term for the binary is calculated by the relative deviation ( $\delta$  Sep from table 5.4) multiplied with the binary separation.

The separation and position angle measurements of HD 19994 are listed in the tables 5.6 and 5.7. Both tables show the measured value, the astrometric correction term derived by the calibration cluster (tables 5.4, and 5.5) as well as the final corrected value. The astrometric error includes the respective measurement error of the binary and the calibration uncertainty. If the measurement error is smaller than the lower precision limit given in table 5.2, the measurement error is set to that lower limit. The reason for the increase of the final precision over the time is the simulation of the intrinsic instability of the cluster, which is based on the measured proper motions of the cluster stars. The measurement error of these proper motions will decrease with an increasing epoch difference. Hence, with further epoch observations the final multi-epoch precision will decrease too.

Preliminary analysis of the binary measurements indicates an astrometric signal of more than 10 mas, far too large to be caused by the RV exoplanet candidate around the A component. This leads to the assumption of a further component in the HD 19994 system, which has to be located around HD 19994 B because in the course of the RV

## 5. Results

Date [MJD]	Position Angle [deg]	$\Delta$ PA [deg]	PA <sub>corr</sub> [deg]
54040.281	204.3508 $\pm$ 7.7e-4	0.0 $\pm$ 2.0e-03	204.3508 $\pm$ 2.2e-03
54297.344	203.8886 $\pm$ 7.7e-4	-2.7e-01 $\pm$ 4.1e-03	203.6166 $\pm$ 4.2e-03
54757.069	202.6288 $\pm$ 7.7e-4	1.2e-02 $\pm$ 9.0e-03	202.6408 $\pm$ 9.1e-03
55103.172	201.7747 $\pm$ 7.7e-4	1.6e-02 $\pm$ 1.4e-02	201.7909 $\pm$ 1.4e-03

Tab. 5.7.: Position angle measurements of the binary HD 19994 A&B. The third row is the astrometric correction term derived by the calibration cluster (table 5.5) and the last row shows the corrected position angles of the binary.

exoplanet candidate detection around the A component no hints for a further and heavier companion were found.

### 5.3.2. Speckle Interferometry

To check the assumption of a new component around HD 19994 B the obtained cube-mode data are analyzed with speckle interferometry using a program written and kindly provided by Rainer Köhler (Köhler et al. [89]). Because the RV observations, which detected the exoplanet candidate, would have detected any further and brighter object around HD 19994 A the primary is chosen as the PSF reference.

In addition to own data previous observations of HD 19994 obtained with the NACO S13 camera from 2004<sup>6</sup> are taken from the *ESO Science Archive*<sup>7</sup>. Because that data from 2004 were taken without observations of the calibration cluster 47 Tuc, they can not be used for an astrometric analysis, but are suitable for speckle interferometry. The speckle interferometric analysis yields evidence for an additional

<sup>6</sup> 074.C-0628 (PI: R. Neuhäuser) observed by A. Bedalov

<sup>7</sup> <http://archive.eso.org/cms/>

### 5.3. Target system - HD 19994

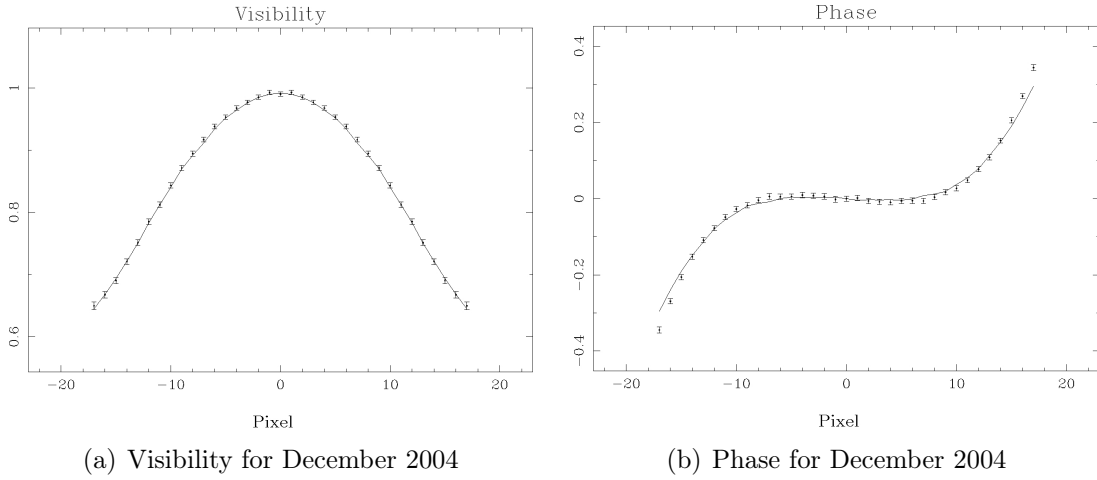


Fig. 5.5.: Visibility and phase of the HD 19994 BC component for the 2004 measurements. The visibility of a single star would be just a horizontal line, thus this is a clear signal of a bright and close companion.

companion around the B component (Fig. 5.5 and Fig. 5.7) with a non-negligible brightness. Thus, the brightness ratio of HD1994 B and the new component (called HD 19994 C) has to be considered for the orbital fit. However, the separation of the B and C component is too small to obtain the position angle, the separation, and the brightness ratio independently. As one can see in appendix C, the visibility for each observation epoch just consists of the mean maximum without any detectable minimum.

In 2004, HD 19994 B&C reaches the largest separation and their visibility and phase could be fitted very well. The best fit for the brightness ratio of  $F_C/F_B = 0.25$  obtained for the 2004 data is set as a fixed value for all other epoch observations. Because the parameters for the speckle interferometry are not independently the fit where done by eye. All speckle measurements are listed in table 5.8 as well as the measurement errors, which are chosen very conservatively. Actually, the astrometric correction terms (section 5.2) also have to be applied

## 5. Results

Date [MJD]	Sep [pixel]	Sep [mas]	PA [deg]
53355.126	$3.1 \pm 0.35$	$41.0 \pm 5$	$10 \pm 50$
54040.281	$1.5 \pm 0.35$	$19.9 \pm 5$	$114 \pm 50$
54297.344	$2.0 \pm 0.35$	$26.5 \pm 5$	$239 \pm 50$
54757.069	$2.2 \pm 0.35$	$29.1 \pm 5$	$194 \pm 50$
55103.172	$1.5 \pm 0.35$	$19.9 \pm 5$	$184 \pm 50$

Tab. 5.8.: HD 19994 B&C speckle measurements for a fixed brightness ratio of  $F_C/F_B = 0.25$  with conservative errors (see text for further information).

on the speckle measurements but these terms are much smaller than the speckle measurement error itself and thus can be neglected. A plot of these speckle measurements including the fitted orbital model for HD 19994 B&C will be presented in section 5.3.4.

### 5.3.3. Radial velocity

HD 19994 was included in a new NIR RV search campaign for extra-solar planets under the Large Program 182.C-0748 led by Jacob Bean (Bean et al. [7]) using the near infrared, high resolution spectrograph CRIRES<sup>8</sup> at the ESO/VLT on Paranal in Chile. This program uses an ammonia gas absorption cell as a spectral fiducial, and achieves long-term RV precisions of 5 m/s for mid- to late-M type stars (Bean et al. [10]). This technique is equivalent to the Iodine-cell technique used in the optical (Marcy and Butler [108]) but includes a sophisticated model of the telluric absorption features present in the NIR (Seifahrt et al. [174]). The data for HD 19994 B were obtained by Jacob Bean and Andreas Seifahrt, while the reduction and analysis of the spectra was performed by Andreas Seifahrt.

<sup>8</sup> CRyogenic high-resolution InfraRed Echelle Spectrograph

Date [MJD]	RV <sub>B</sub> [km/s]	RV <sub>C</sub> [km/s]
54882.018	26.15 ± 0.1	15.65 ± 0.2
55051.393	24.70 ± 0.1	16.90 ± 0.2
55141.148	8.66 ± 0.1	43.16 ± 0.2
55143.161	8.92 ± 0.1	42.52 ± 0.2
55429.365	24.60 ± 0.1	16.90 ± 0.2

Tab. 5.9.: Radial velocities of HD 19994 B&C, measured with CRILES (by Andreas Seifahrt and Jacob Bean) at the ESO/VLT in Chile.

Because HD 19994 B turned out to be a spectral binary itself, two synthetic stellar model spectra have to be fitted to the CRILES spectra. Using a synthetic spectrum of the telluric lines, a precise wavelength solution at the 50 m/s level is achieved. The telluric lines used in this case are mostly methane lines (see section 4.1.3 in Seifahrt et al. [174]) coinciding with a rich system of carbon monoxide (CO) overtone transitions in the stellar spectrum. A model grid of Drift-PHOENIX models (Witte et al. [202]), kindly provided by Soeren Witte, was used for the fit. In the context of stellar spectra (i.e. above the dust formation temperature) Drift-PHOENIX spectra represent an improved version of the widely used PHOENIX models (Hauschildt and Baron [78]). The use of synthetic model spectra compromises the achievable RV precision, since the spectral models do not fit perfectly the measured spectra. However, since empirical reference spectra of the two stellar components present in the spectrum of HD 19994 BC can not be obtained individually for obvious reasons, synthetic templates had to be used to fit the measured spectra. The fit included the effective temperatures and surface gravities of the two models, their absolute RV shifts under consideration of the barycentric RV at the time of observations, the wavelength solution, and the total flux level.

## 5. Results

Once RVs were measured, the ratio of the RV signals of the two components could be used to infer a preliminary mass ratio of the two components of about 0.63 from the ratio of the RV amplitudes. Using the mass-radius relationship for low-mass stars given in Demory et al. [38], the ratio of radii, and thus the ratio of the surface areas of the two components, was determined and fixed to 0.4 for a final and refined fit of the data. The effective temperatures of the two models together with the ratio of the surface areas of both components yield a flux ratio of  $F_C/F_B \simeq 0.29$ , which compares well with the value obtained from speckle interferometry.

It should be noted that the parameter values for the stellar models are poorly constrained to  $T_{\text{eff}}^B \simeq 4300$  K and  $T_{\text{eff}}^C \simeq 3600$  K with an uncertainty of several hundred Kelvin. The surface gravity are  $\log g_B \simeq 5.0 \pm 0.5$  and  $\log g_C \simeq 5.5 \pm 0.5$ . The final error of the RVs are conservatively adopted to  $\pm 100$  m/s for the B component and  $\pm 200$  m/s for the new C component. A plot of these radial velocities including the fitted orbital model can be found in the next section.

### 5.3.4. Companion HD 19994 C

At the end, the results from all three techniques (astrometry, speckle interferometry, and radial velocity) are combined in order to determine the orbital elements of the HD 19994 B&C system by minimize an error weighted  $\chi^2$ . That one is defined as

$$\chi^2 = \sum_i \frac{(O_i - C_i)^2}{\sigma_i^2}, \quad (5.4)$$

where O-C is the deviation between the observed and the calculated values and  $\sigma$  is the individual measurement error. For the  $\chi^2$  mini-

Date [MJD]	<u>Measurements</u>		<u>Deviations</u>	
	Sep [pixel]	Pa [deg]	Sep [mas]	Pa [deg]
54040.185	175.497±7.8e-03	204.351±2.2e-03	-1.25±0.10	0.062±2.2e-03
54297.425	175.228±1.1e-02	203.617±4.2e-03	3.32±0.15	-0.064±4.2e-03
54757.200	173.666±2.3e-02	202.641±9.1e-03	-4.79±0.31	0.037±9.1e-03
55103.225	173.169±3.4e-02	201.791±1.4e-02	-3.57±0.45	-0.012±1.4e-02

Tab. 5.10.: HD 19994 corrected measurements and deviations to a binary orbital motion, which is fitted as a second order polynomial. The used pixel scale has a value of  $(13.24 \pm 0.1)$  mas/pixel.

mization the *SciPy*<sup>9</sup> package (Jones et al. [84]), a collection of scientific algorithm for the programming language *Python*<sup>10</sup>, was used.

Fig. 5.6 shows the astrometric measurements of the HD 19994 A&BC system (upper panel), the deviation to a binary orbital motion (middle panel), and the residuals of the astrometric companion model (lower panel). The orbital motion of a real binary is fitted as a second order polynomial (dotted line), while the model including an astrometric companion around the B component is shown as the solid red line. The astrometric signal of the new detected astrometric companion is about 15 mas.

The orbital elements, derived by the  $\chi^2$  minimization, are listed in table 5.11 including the  $1\sigma$  and  $3\sigma$  uncertainty levels. These uncertainties are defined as the parameter values, where the  $\chi^2$  increases to  $\chi_{min}^2 + 1$  and  $\chi_{min}^2 + 9$  and correspond to the confidential levels of about 68 % and 95 % (see Press [151] for further information). The one and two dimensional  $\chi^2$  maps can be found in appendix E. The value  $\chi_{red}^2$  is defined as the  $\chi^2$  divided by the number of free param-

<sup>9</sup> Scientific Python

<sup>10</sup> <http://www.python.org/>

## 5. Results

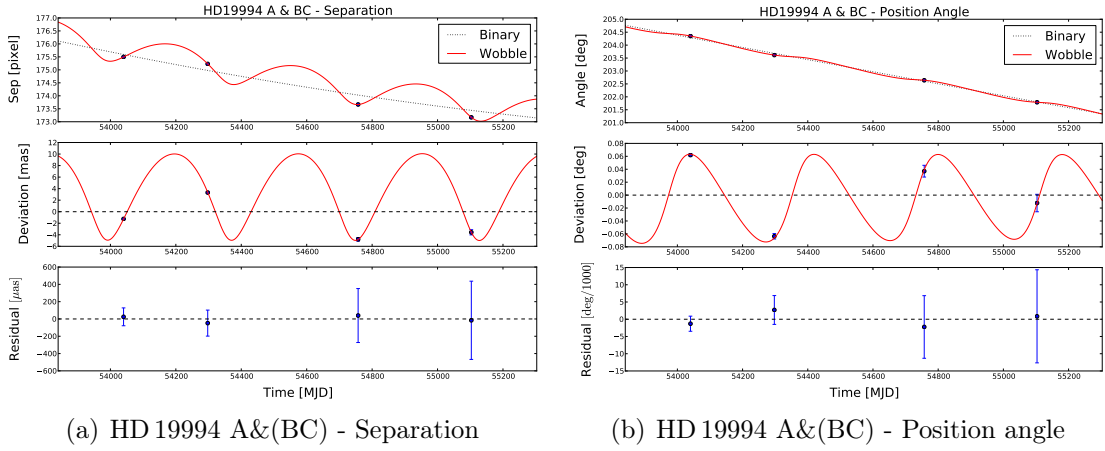


Fig. 5.6.: Astrometric measurements and orbital solution of the HD 19994 A&BC system. The dotted line is the fitted binary orbital motion and the solid red line is the binary orbital motion disturbed by an astrometric companion around HD 19994 B. The reason for the increase of the final precision is the simulation of the intrinsic instability of the astrometric calibration cluster 47 Tuc. With further observations the final precision will decrease to about 0.1 mas, which is the final precision of the first epoch observation in November 2006.

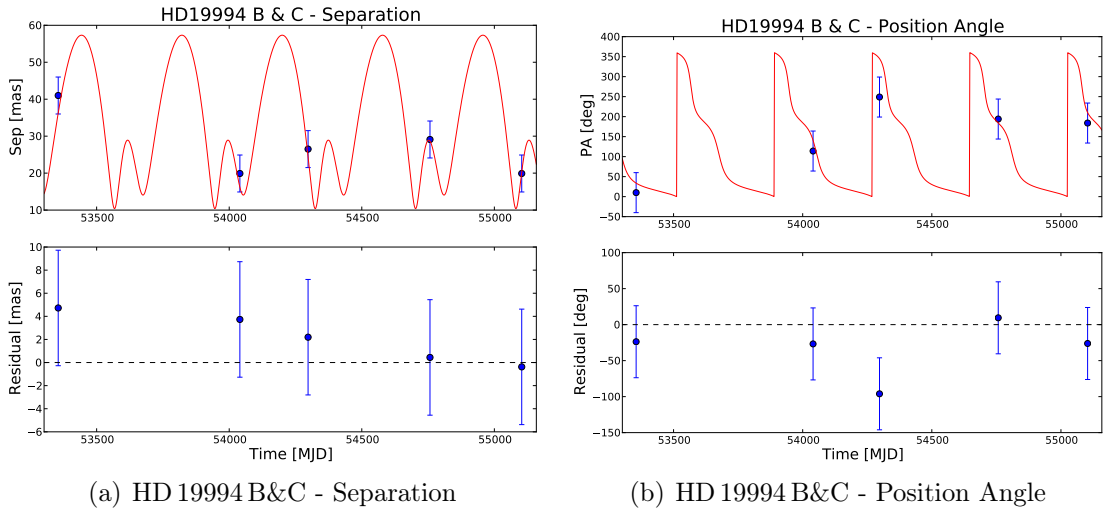


Fig. 5.7.: Speckle measurements and orbital solution (solid red line) of the HD 19994 B&C system.



### 5.3. Target system - HD 19994

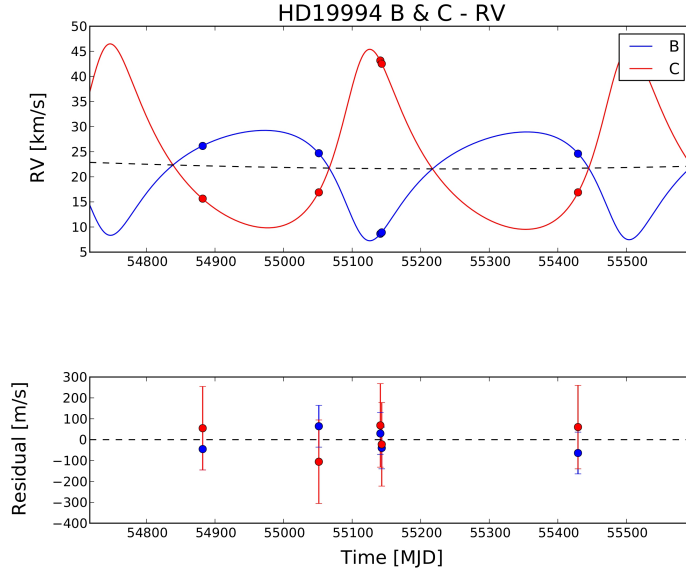


Fig. 5.8.: Orbital fit for the radial velocity measurements of HD 19994 B&C. The radial velocity of the HD 19994 BC system itself (dashed line in the upper panel) is fitted as a second order polynomial.

Parameter	$1\sigma$ – Uncertainty	$3\sigma$ – Uncertainty
P [days]	$378.35^{+0.36}_{-0.34}$	$378.35 \pm 1.06$
$M_{\star}$ [ $M_{\odot}$ ]	$0.554 \pm 0.006$	$0.554 \pm 0.018$
$m_{\text{comp}} / M_{\star}$	$0.604 \pm 0.006$	$0.604 \pm 0.017$
$\omega$ [deg]	$334.895 \pm 0.240$	$334.895 \pm 0.721$
$\Omega$ [deg]	$191.496^{+1.602}_{-1.562}$	$191.496^{+4.765}_{-4.725}$
Eccentricity	$0.360 \pm 0.005$	$0.360 \pm 0.014$
Inclination [deg]	$108.323^{+0.581}_{-0.561}$	$108.323^{+1.762}_{-1.642}$
$m_{\text{comp}}$ [ $M_{\odot}$ ]	$0.335 \pm 0.009$	$0.335 \pm 0.017$
$a_{\text{total}}$ [AU]	$0.984 \pm 0.007$	$0.984 \pm 0.013$

Tab. 5.11.: Orbital elements of the new detected companion HD 19994 C, derived by a  $\chi^2$  minimization. The latter two parameters are calculated with the fitted values above. A table with all orbital elements can be found in appendix D.

## 5. Results

eters, which is the number of observations subtracted by the number of free parameters minus one.

The orbital fitting results presented in table 5.11 have a  $\chi_{\text{red}}^2$  of about 0.5, thus the fitting result is some kind of “too good”. The reason for that is the binary influence fitted to the astrometric and the radial velocity measurements. By using the respective residuals to fit this binary influence, the resulting residuals at the end of the fitting procedure are “pushed” towards smaller values. That effect is amplified by the low number of measurements, especially for the astrometric data. With an increasing number of observations the  $\chi_{\text{red}}^2$  will also increase to about one.

The new detected companion HD 19994 C is a low mass star with a mass of  $m_{\text{comp}} = (0.335 \pm 0.017) M_{\odot}$  in a 378 days orbit. The mass of the B component, which is previously published as  $0.4 M_{\odot}$ , is slightly different, namely  $(0.554 \pm 0.018) M_{\odot}$ .

### 5.3.5. Comparison with theoretical models

Taking a look at NIR (near infrared) catalogues, the HD 19994 ABC system has a combined Ks brightness of  $3.75^{\text{m}} \pm 0.24^{\text{m}}$  in 2MASS<sup>11</sup> (Skrutskie et al. [177]) and  $3.68^{\text{m}} \pm 0.1^{\text{m}}$  in DENIS<sup>12</sup> (Borsenberger et al. [17]). Furthermore, the brightness ratio between the A and the BC component, measured in the Br $\gamma$  narrow band filter, is known from own data observed for this astrometric search program.

2MASS, DENIS, and ESO using similar Ks filters and the measurement error in the catalogues is much larger than any systematic difference between these three Ks filters. But the brightness ratio of

---

<sup>11</sup> Two Micron All Sky Survey, see <http://www.ipac.caltech.edu/2mass/>

<sup>12</sup> Deep Near Infrared Survey of the Southern Sky, see <http://cdsweb.u-strasbg.fr/denis.html>

the A and the BC component is measured with the Br $\gamma$  narrow band filter, which is located within the Ks filter curve. However, it is a different filter and one has to check if photometric measurements of both filters can be combined.

This is shown in Fig. 5.9, where the brightness ratio of the transmitted flux of two blackbodies with given effective temperatures and radii are simulated for both filters and compared to each other. The resulting difference in the  $\Delta$  mag measurements is less than 5 mmag<sup>13</sup>. Considering the measurement error from the near infrared catalogues (0.25<sup>m</sup>), this effect is negligible. The values for the effective temperature and the radius are chosen to be similar to those ones of HD 19994 A and HD 19994 BC.

Hence, the brightness ratio measured in the Br $\gamma$  narrow band filter can be applied on the Ks brightness of the whole HD 19994 system given in the NIR catalogues. Including the distance of the system that results in an absolute Ks band brightness for the HD 19994 BC component of  $4.78^m \pm 0.26^m$ . Using the fixed brightness ratio of  $F_C/F_B = 0.25$  (derived by speckle interferometry, see section 3.4), one can calculate the absolute brightness of each component by

$$m_{B,C} = m_{B+C} + 2.5 \log_{10} \left( 1 + \frac{F_{C,B}}{F_{B,C}} \right). \quad (5.5)$$

In addition to the combined Ks band brightness of the BC component, the mass ratio of both components is known. These values are plotted in Fig. 5.10(a) together with theoretical evolutionary tracks by Baraffe et al. [6]. The lines represent certain masses for the heavy component (HD 19994 B) and the markers illustrate different

---

<sup>13</sup> 1 mmag = 1/1000 mag

## 5. Results

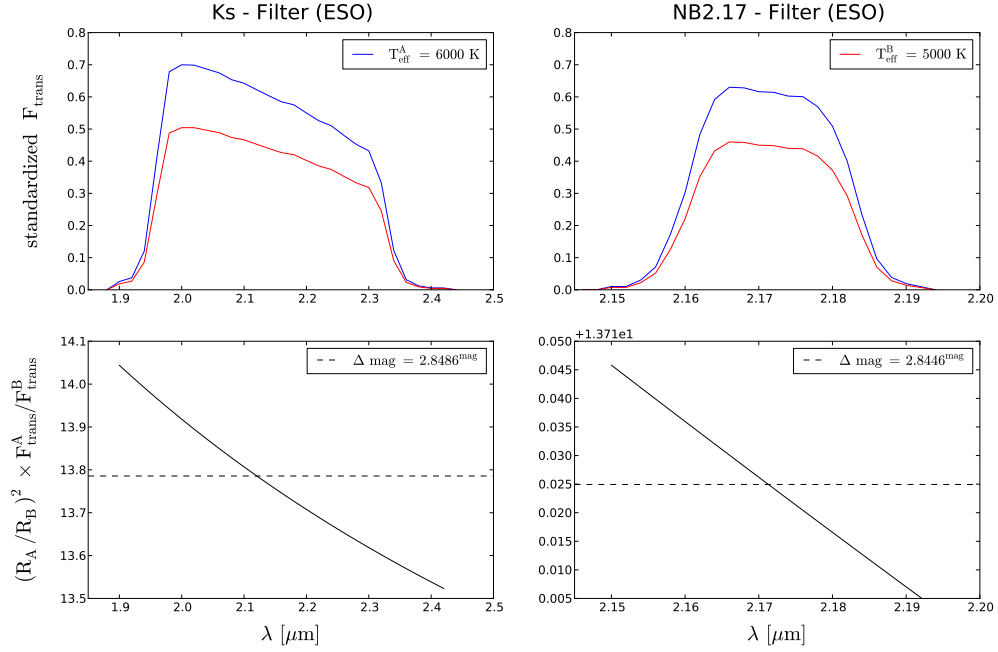


Fig. 5.9.: Comparison of the brightness ratio measurements of two different blackbodies for the  $\text{Br}\gamma$  narrow band (right) and Ks broad band filter (left). The upper panel shows the standardized flux density folded with the respective filter curve. The solid line in the lower panel is the measured brightness ratio (dashed line: mean value) of these two blackbodies.

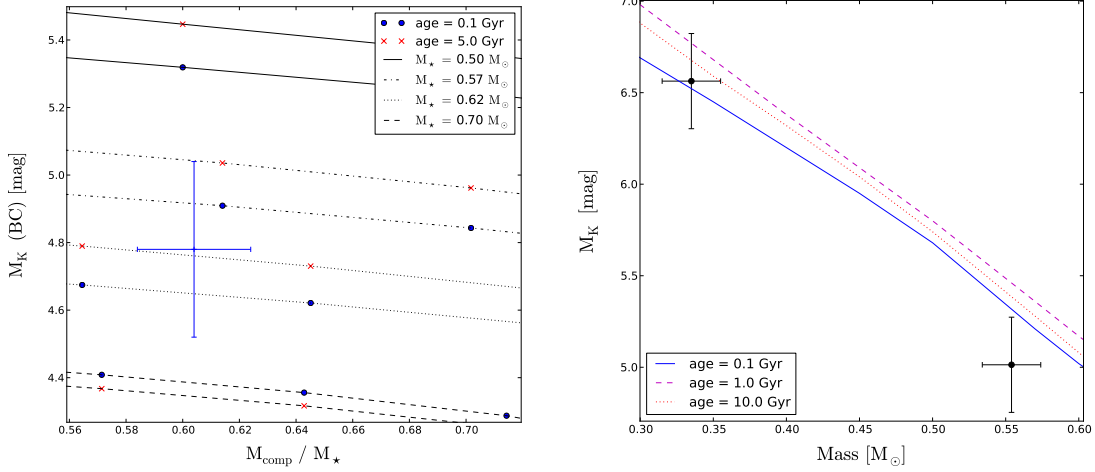
$K_{\text{ABC}}$ [mag]	$K_{\text{BC}} - K_{\text{A}}$ [mag]	Distance Module [mag]
$3.7 \pm 0.25$	$2.85 \pm 0.05$	$1.77 \pm 0.02$

$M_{\text{K}}(\text{BC})$ [mag]	$M_{\text{K}}(\text{B})$ [mag]	$M_{\text{K}}(\text{C})$ [mag]
$4.78 \pm 0.26$	$5.01 \pm 0.26$	$6.56 \pm 0.26$

Tab. 5.12.: Ks band magnitudes of the HD 19994 system for the parallax of  $44.29 \pm 0.28$  mas from van Leeuwen [197] and a brightness ratio of 0.25 determined with speckle interferometry.

### 5.3. Target system - HD 19994



(a) Model data (Baraffe et al. [6]) of the combined Ks band brightness over the mass ratio of two stars. The data point is the HD 19994 BC component, thus it is independent from their brightness ratio.

(b) Model data (Baraffe et al. [6]) of the Ks band brightness over the stellar mass. The data points are HD 19994 B&C individually, thus they depend on their brightness ratio.

Fig. 5.10.: Theoretical evolutionary tracks by Baraffe et al. [6]. The data points are the derived properties of HD 19994 B&C obtained by the orbital fit.

stellar ages. Hence, from theoretical evolutionary models, a mass of about  $(0.5 \dots 0.7) M_{\odot}$  for HD 19994 B is expected, which is in good agreement with the mass of  $M_B = (0.554 \pm 0.018) M_{\odot}$  obtained by the orbital fit.

Fig. 5.10(b) shows the Ks band brightness over the mass of B and C component individually. Also, evolutionary tracks by Baraffe et al. [6] are plotted, which fits not very well the data point of HD 19994 B. The mass as well as the Ks band brightness are determined using the fixed brightness ratio of the B and C component. This was fixed to 0.25 determined by speckle interferometric analysis, but analyzing the CRIFRES spectra, a ratio of 0.29 was obtained. The brightness ratio can be constrained to  $0.2 \dots 0.3$ , but the exact value is still vague. The reason that HD 19994 B&C does not fit the evolutionary tracks

## 5. Results

perfectly is most likely the remaining uncertainty of their brightness ratio, which has impact on their mass and their Ks brightness.

Another explanation are systematic effects of the theoretical models itself. Hillenbrand and White [80] did an extensive work comparing the dynamically measured mass of stars with their theoretically expected mass from different evolutionary models. For main-sequence stars with a mass lower than  $1.2 M_{\odot}$ , all masses predicted by theory differ from the dynamically measured mass. For masses between  $(0.2 \dots 0.5) M_{\odot}$ , this discrepancies are dominant.

There are still some inconsistencies in the HD 19994 system. The radius of HD 19994 A was measured to be about  $1.8 \dots 1.9 R_{\odot}$  (with optical interferometry using the CHARA<sup>14</sup> Array by Baines et al. [3] and with spectroscopy by Fuhrmann [64]), which is too large for an F8 dwarf. One explanation could be a wrong system age, which is supported by the large spread of published age determinations of about 3 to 13 Gyrs. But the age determination of dwarf stars is complicated (the isochrones are very similar) and not a part of this work.

---

<sup>14</sup> Center for High Angular Resolution Astronomy

## 6. Summary and outlook

The first part of this work is an extensive study of exoplanets in stellar multiple systems (presented in chapter 1.5). Searching the literature and by matching the host stars of exoplanets (detected by the transit or radial velocity technique) with the CCDM<sup>1</sup>, 79 exoplanets in stellar multiple system were found. These systems are listed in the tables 1.1, 1.2, and 1.3. The resulting multiplicity rate of about 17% is in good agreement with previous published values of about 20%, where the host star multiplicity of exoplanets detected by the radial velocity technique was studied. Compared to the multiplicity rate of solar like stars, which is about 50%, the multiplicity of exoplanet host stars is quite low.

Using a two dimensional Kolmogorov-Smirnov test (Fig. 1.3), a difference in the mass-period and the eccentricity-period relation between exoplanets around single stars and in stellar multiple systems was found. Furthermore, as one can see in Fig. 1.5, the mass and the number of exoplanets in stellar multiple systems depend on the separation of their host-star and the nearest stellar companion. This could be a direct hint for a gravitational interaction of the stellar companion with the protoplanetary disk of an exoplanet host star, which is predict by theory.

---

<sup>1</sup> Catalogue of Components of Double and Multiple Stars by Dommanget and Nys [44]

## 6. *Summary and outlook*

In very close stellar systems with an apparent separation of less than 10 AU, no exoplanet is found so far. For apparent separations of about 10...100 AU, called close stellar systems in this work, all detected exoplanets have a mass of more than one Jupiter mass. The mass of exoplanets in intermediate systems decreases with an increasing apparent separation from 100 AU up to about 1000 AU. Furthermore, multi-planet systems are only present in stellar systems with an apparent separation of more than 500 AU. In wide stellar systems, with a semi-major axis of more than 1000 AU, no influence of the stellar multiplicity on the formation and evolution of exoplanets was found.

In order to enlarge the observational data of exoplanets in stellar multiple systems, an observation method to search for exoplanets in especially close binaries is developed and tested in the second part of this work. That method can be described as ground based and AO assisted astrometric (lucky) imaging with large apertures. In contrast to other techniques like RV or transit observations, AO assisted astrometric imaging is a suitable and efficient method to search for exoplanets in close binaries because of its high spatial resolution.

Ground based astrometric observations have to account for disturbing effects, like atmospheric, stellar, and relativistic effects. These effects were discussed in detail and their influence on relative astrometric measurements were analyzed (chapter 2). Considering these disturbing effects and using old globular clusters for an iterative calibration procedure (chapter 4), a final multi-epoch precision down to  $100 \mu\text{as}$  is achieved. Hence, the astrometric detection of Jovian exoplanets around solar like stars and even less mass exoplanets around nearby low-mass stars is possible. By increasing the amount of ob-



servational data, the influence of a close stellar companion on the planetary formation and evolution can be studied in more detail by comparing these observational results with current planet formation theories.

After developing the observation, the analysis, and the calibration strategies (chapter 2, 3 and 4), the feasibility of this ground based astrometric search program was tested on the HD 19994 system. HD 19994 is a formerly known stellar binary with a RV exoplanet candidate around its primary. After four epoch observations a signal of about 15 mas was detected, which is larger than the expected planetary astrometric signal of about 0.15...1.5 mas depending on the planetary inclination. The origin of this larger signal is an unseen further component around HD 19994 B. That astrometric detection of an additionally body in the HD 19994 system was confirmed in this work by speckle interferometry as well as by RV follow-up observations (chapter 5).

The detected astrometric companion HD 19994 C has a mass of  $0.335 \pm 0.017 M_{\odot}$ , an orbital period of  $378.35 \pm 1.06$  days, and an inclination of  $108.3 \pm 1.8$  degree. That inclination is equal to the expected inclination for HD 19994 A&B of about 110 degree. Assuming coplanarity, the true mass of the RV planet candidate would be about  $1.8 M_{\text{Jup}}$ . The existence of a further component around HD 19994 B does not obviate the existence of the RV planet candidate around HD 19994 A. The orbital periods of both objects are different and with further observations, one can search for the astrometric signal of HD 19994 Ab, superposed on that signal of the new C component.

## 6. Summary and outlook

Looking at the residuals in Fig. 5.6, an additional astrometric signal of more than 1 mas can be excluded, which results in a planetary inclination angle larger than eight degrees and an upper mass limit of  $12 M_{\text{Jup}}$  for the RV planet candidate. Hence, HD 19994 Ab is a planet.

In addition to HD 19994, ten further stellar systems are already observed in one or two epoch (section 2.5.2). Because of the special analysis strategy, at least four observations are needed to search for an astrometric signal. Hence, this astrometric search program has just started. With just a few more observations, the search for an astrometric signal in the other target systems can be done. Furthermore, an extended target list of more than 150 suitable stellar systems is build by matching the *Gliese catalogue of nearby stars*<sup>2</sup> with the CCDM (appendix F).

As mentioned by Kley and Nelson [87], the formation of planets in close binaries is still a challenge for current planet formation theories. With continuous observations, the astrometric search program presented in this work will improve our knowledge of exoplanets in stellar multiple systems. Especially the observational data of very close systems will be enlarged and thus the understanding of the influence of a close stellar companion on the planetary formation and evolution will be improved.

---

<sup>2</sup> Gliese and Jahreiss [68]

# A. Calculation of ephemerides

For further information about the orbits of double stars and the calculation of ephemerides, please take a look at Aitken [2] or Montenbruck [123] and references therein.

To determine the position and velocity of a celestial body in an elliptical orbit seven parameters are needed in total, which define the position of the body within the orbit as well as the position of the orbital plane within the space. These parameters are called orbital elements.

$$\begin{aligned} P & \dots \text{orbital period} \\ T & \dots \text{time of periastron passage} \\ a & \dots \text{semimajor axis} \\ \omega & \dots \text{argument of periastron} \\ \Omega & \dots \text{longitude of ascending node} \\ i & \dots \text{inclination} \\ e & \dots \text{eccentricity} \end{aligned} \tag{A.1}$$

The argument of periastron is the orbit position where the secondary has the smallest separation to its primary. The corresponding counterpart is the apastron, which is the orbit position with the largest distance. To calculate the exact position of an celestial body within the orbit three angles (also called anomaly) are needed, which

## A. Calculation of ephemerides

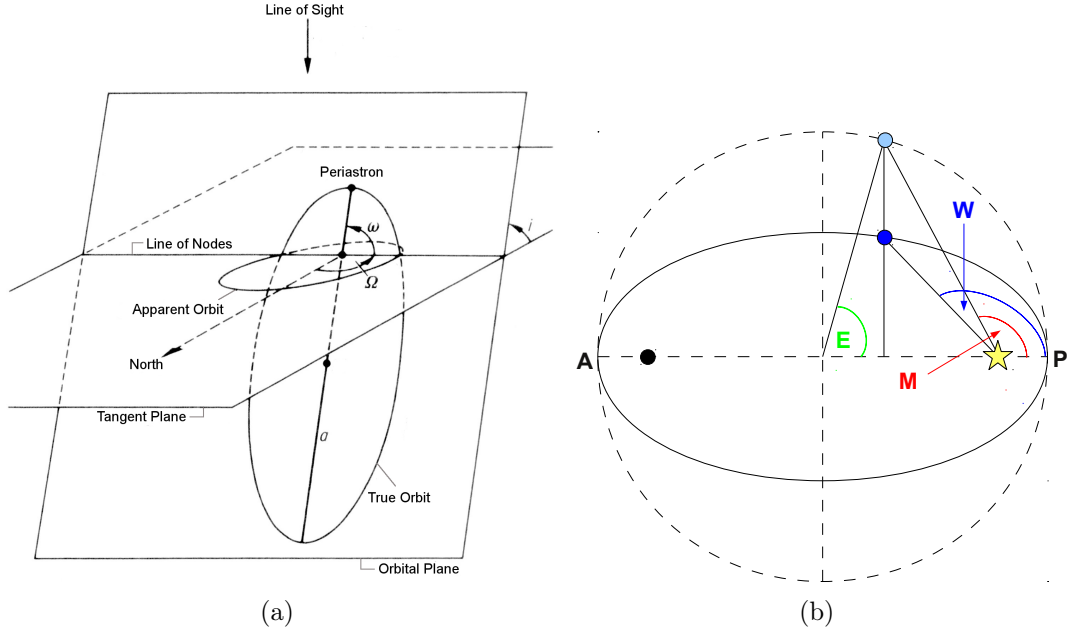


Fig. A.1.: (a) Location of the orbit relative to the observer [204] and (b) the different angle definitions of an elliptical orbit.

can be calculated with the period  $P$ , the time of periastron passage  $T$ , and the eccentricity for any given date  $t$ .

$$\begin{aligned}
 E & \dots \text{eccentric anomaly} \\
 M & \dots \text{mean anomaly} \\
 W & \dots \text{true anomaly}
 \end{aligned}
 \tag{A.2}$$

The mean anomaly  $M$  has a uniform angular velocity and can be calculated for any date  $t$  by

$$M = \frac{2\pi}{P} (t - T).
 \tag{A.3}$$

The “Kepler equation” (Equ. A.4) yields the relation between the mean and the eccentric anomaly.

$$M = E - e \sin(E)
 \tag{A.4}$$

That equation cannot be solved analytically but with numerical methods like the “Newton method”, which is defined by

$$x_{n+1} = x_n - \frac{f(x)}{f'(x)}. \quad (\text{A.5})$$

As first approach for the eccentric anomaly, the mean anomaly can be used.

$$E_{n+1} = E_n - \frac{M + e \sin(E_n) - E_n}{e \cos(E_n) - 1}, \quad E_0 = M \quad (\text{A.6})$$

The angle between periastron and the position of the celestial body in the orbit, the true anomaly, is the result of the following relation.

$$\tan\left(\frac{W}{2}\right) = \sqrt{\frac{1+e}{1-e}} \tan\left(\frac{E}{2}\right) \quad (\text{A.7})$$

The true position of the celestial body can now be determined by:

$$\begin{aligned} R &= a [1 - e \cos(E)] \\ X = R \cos(W) &= a [\cos(E) - e] \\ Y = R \sin(W) &= a \sqrt{1 - e^2} \sin(E) \end{aligned} \quad (\text{A.8})$$

However, the measurable apparent position and the shape of the orbit are affected by projection effects due to the orientation of the orbital plane in the space. That orientation is described by the inclination angle  $i$ , the argument of periastron  $\omega$ , and the longitude of the ascending node  $\Omega$ . The position of the celestial body in the apparent orbit (as seen by the observer) is the projection of the true orbit and position onto the plane of reference, which is the tangent plane relatively to the observer.

A. Calculation of ephemerides

The vectors  $\mathbf{P}$  and  $\mathbf{Q}$  are called ‘‘Gaußsche Vectors’’ and are comparable with the widely used ‘‘Thiele-Innes-elements’’.

$$\begin{pmatrix} x \\ y \\ z \end{pmatrix} = X \begin{pmatrix} P_x \\ P_y \\ P_z \end{pmatrix} + Y \begin{pmatrix} Q_x \\ Q_y \\ Q_z \end{pmatrix} \quad (\text{A.9})$$

$$\mathbf{P} = \begin{pmatrix} \cos(\omega) \cos(\Omega) - \sin(\omega) \cos(i) \sin(\Omega) \\ \cos(\omega) \sin(\Omega) + \sin(\omega) \cos(i) \cos(\Omega) \\ \sin(\omega) \sin(\Omega) \end{pmatrix} \quad (\text{A.10})$$

$$\mathbf{Q} = \begin{pmatrix} -\sin(\omega) \cos(\Omega) - \cos(\omega) \cos(i) \sin(\Omega) \\ -\sin(\omega) \sin(\Omega) + \cos(\omega) \cos(i) \cos(\Omega) \\ \cos(\omega) \sin(\Omega) \end{pmatrix} \quad (\text{A.11})$$

The orbital velocity of a celestial body can be determined by the following formulas, whereas  $\dot{x}$  and  $\dot{y}$  stand for the tangential proper motion and  $\dot{z}$  for the radial velocity.

$$\begin{pmatrix} \dot{x} \\ \dot{y} \\ \dot{z} \end{pmatrix} = \sqrt{\frac{4\pi^2 a^2}{P^2(1-e^2)}} \{-\sin(W) \mathbf{P} + [e + \cos(W)] \mathbf{Q}\} \quad (\text{A.12})$$

## B. Calculation of atmospheric refraction index

Stone [180] published accurate formulas to calculate the atmospheric refraction index, which only require the knowledge of the relative humidity  $H$  in percent, the air pressure  $p_{\text{air}}$  in mm, and the air temperature  $t_{\text{air}}$  in  $^{\circ}\text{C}$ . Using the relation  $x = \ln(H/100)$ , the dew point  $t_{\text{dp}}$  can be calculated as

$$t_{\text{dp}} [^{\circ}\text{C}] = 238.3 \left[ \frac{(t_{\text{air}} + 238.3)x + 17.2694t_{\text{air}}}{(t_{\text{air}} + 238.3)(17.2694 - x) - 17.2694t_{\text{air}}} \right]. \quad (\text{B.1})$$

According to Owens [146], the water vapor pressure  $p_{\text{wv}}$  is

$$\begin{aligned} p_{\text{wv}} [\text{mm}] = & 4.50874 + 0.341724 t_{\text{dp}} \\ & + 1.06778 \times 10^{-4} t_{\text{dp}}^2 + 1.84889 \times 10^{-4} t_{\text{dp}}^3 \\ & + 2.38294 \times 10^{-6} t_{\text{dp}}^4 + 2.03447 \times 10^{-8} t_{\text{dp}}^5 \end{aligned} \quad (\text{B.2})$$

$$P_{\text{wv}} [\text{mbar}] = 1.333224 p_{\text{wv}}.$$

The air pressure for dry air  $P_{\text{air}}^{\text{dry}}$ , which is the air pressure  $p_{\text{air}}$  corrected for water vapor, is given by

$$P_{\text{air}}^{\text{dry}} [\text{mbar}] = 1.333224 (p_{\text{air}} - p_{\text{wv}}). \quad (\text{B.3})$$

*B. Calculation of atmospheric refraction index*

At the end, the refraction index  $n$  for a given wave number  $\sigma = 10^4/\lambda$  of a monochromatic wavelength  $\lambda$  in  $\mu\text{m}$  can be calculated as

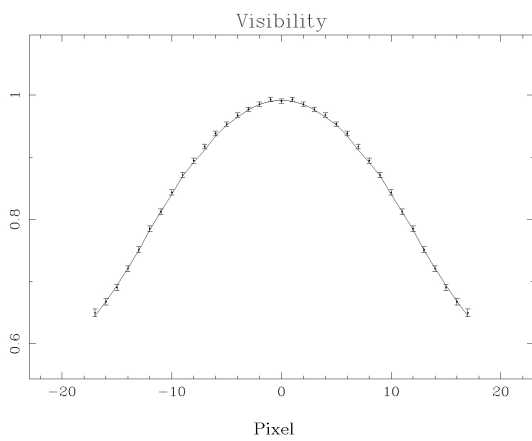
$$\begin{aligned}
 (n - 1) \times 10^{-8} = & A \left[ 2371.34 + \frac{683939.7}{130 - \sigma^2} + \frac{4547.3}{38.9 - \sigma^2} \right] \\
 & + B (6487.31 + 58.058 \sigma^2 \\
 & - 0.7115 \sigma^4 + 0.08851 \sigma^6)
 \end{aligned} \tag{B.4}$$

with the constants A and B, where  $T_{\text{air}}$  is the air tempertaure in Kelvin ( $T_{\text{air}} = 273.15 + t_{\text{air}}$ ).

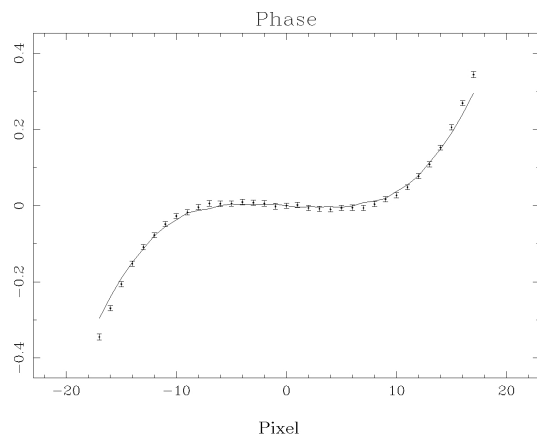
$$\begin{aligned}
 A = & \frac{P_{\text{air}}^{\text{dry}}}{T_{\text{air}}} \left[ 1 + P_{\text{air}}^{\text{dry}} \left( 57.9 \times 10^{-8} - \frac{9.325 \times 10^{-4}}{T_{\text{air}}} + \frac{0.25844}{T_{\text{air}}^2} \right) \right] \\
 B = & \left( -2.37321 \times 10^{-3} + \frac{2.23366}{T_{\text{air}}} - \frac{710.792}{T_{\text{air}}^2} + \frac{7.75141 \times 10^4}{T_{\text{air}}^3} \right) \\
 & \times \frac{P_{\text{wv}}}{T_{\text{air}}} (1 + P_{\text{wv}} + 3.7 \times 10^{-4} P_{\text{wv}}^2)
 \end{aligned} \tag{B.5}$$



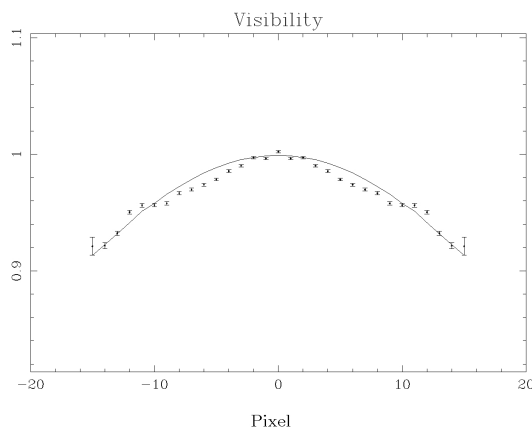
## C. HD 1994 BC - Complex visibilities



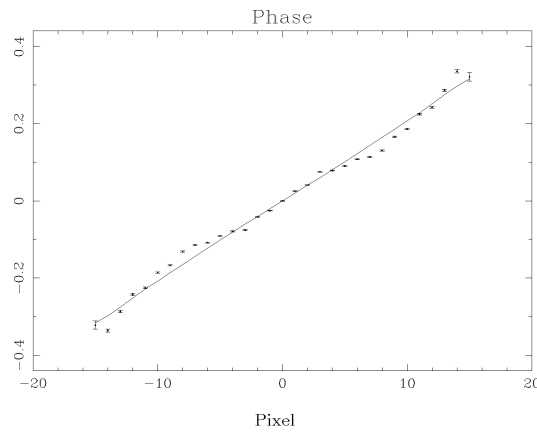
(a) Visibility for December 2004



(b) Phase for December 2004



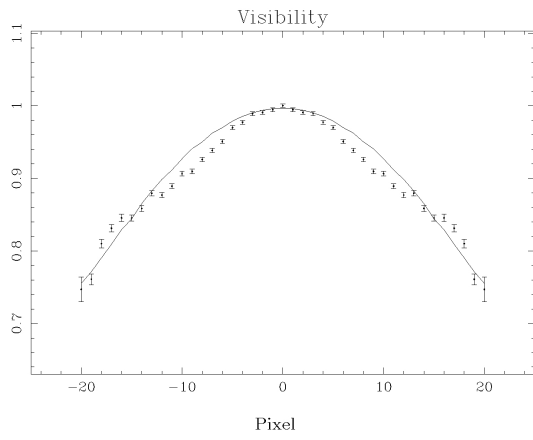
(c) Visibility for November 2006



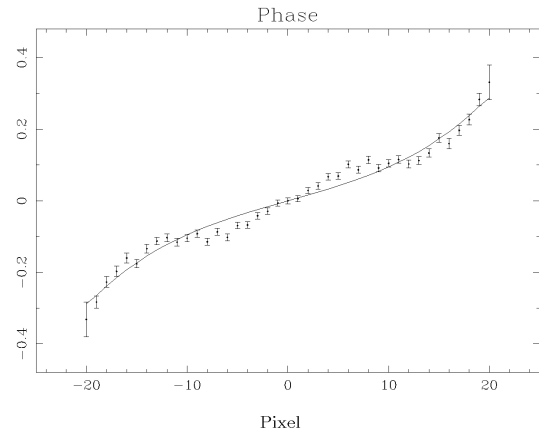
(d) Phase for November 2006

Fig. C.1.: Visibilities of the HD 1994 BC component. The A component is used as PSF reference.

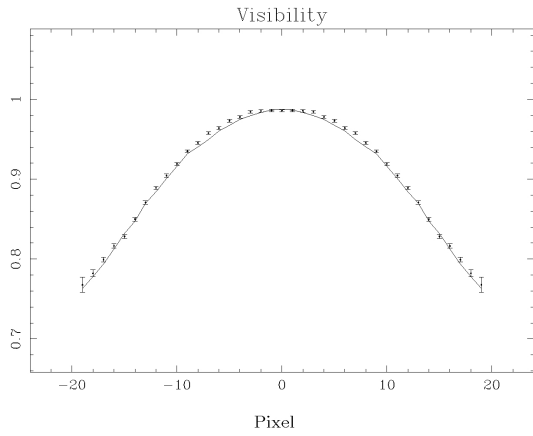
C. HD 1994 BC - Complex visibilities



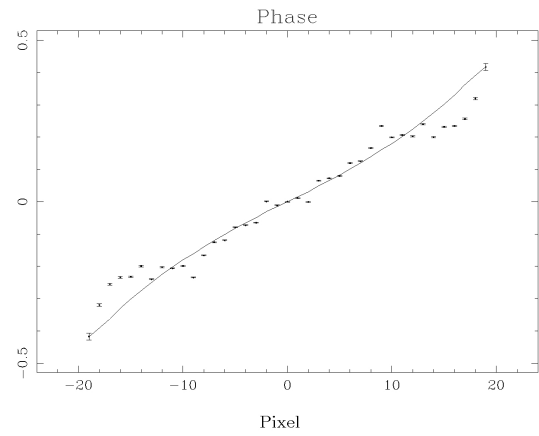
(a) Visibility for July 2007



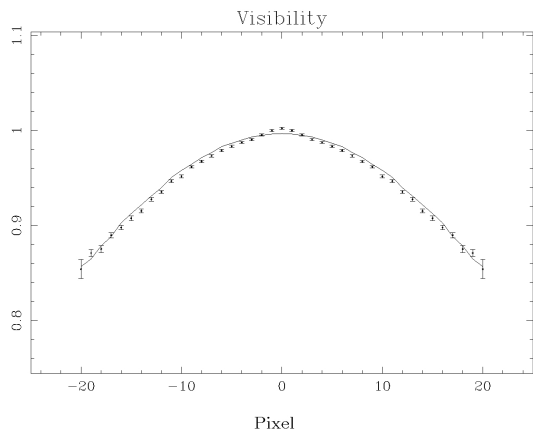
(b) Phase for July 2007



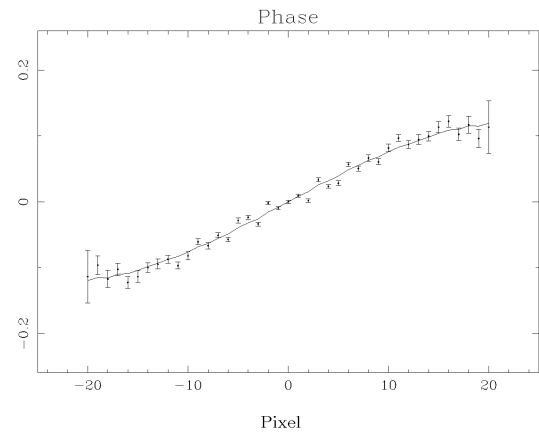
(c) Visibility for October 2008



(d) Phase for October 2008



(e) Visibility for September 2009



(f) Phase for September 2009

Fig. C.2.: Visibilities of the HD 1994 BC component (cont). The A component is used as PSF reference.

## D. HD 19994 C - Orbital solution

Parameter	$1\sigma$ - Uncertainty	$3\sigma$ - Uncertainty
P [days]	$378.353^{+0.360}_{-0.340}$	$378.353 \pm 1.061$
T [MJD]	$55113.904 \pm 0.220$	$55113.904^{+0.641}_{-0.681}$
$M_{\star} [M_{\odot}]$	$0.554 \pm 0.006$	$0.554 \pm 0.018$
$m_{\text{comp}} / M_{\star}$	$0.604 \pm 0.006$	$0.604 \pm 0.017$
$\omega$ [deg]	$334.895 \pm 0.240$	$334.895 \pm 0.721$
$\Omega$ [deg]	$191.496^{+1.602}_{-1.562}$	$191.496^{+4.765}_{-4.725}$
Eccentricity	$0.360 \pm 0.005$	$0.360 \pm 0.014$
Inclination [deg]	$108.323^{+0.581}_{-0.561}$	$108.323^{+1.762}_{-1.642}$
$m_{\text{comp}} [M_{\odot}]$	$0.335 \pm 0.009$	$0.335 \pm 0.017$
$M_{\text{total}} [M_{\odot}]$	$0.889 \pm 0.017$	$0.889 \pm 0.034$
$a_{\text{total}} [\text{AU}]$	$0.984 \pm 0.007$	$0.984 \pm 0.013$

Tab. D.1.: Orbital elements of HD 19994 C, derived by  $\chi^2$  minimization. The latter three parameters are calculated with the fitted values above.

D. HD 1994 C - Orbital solution

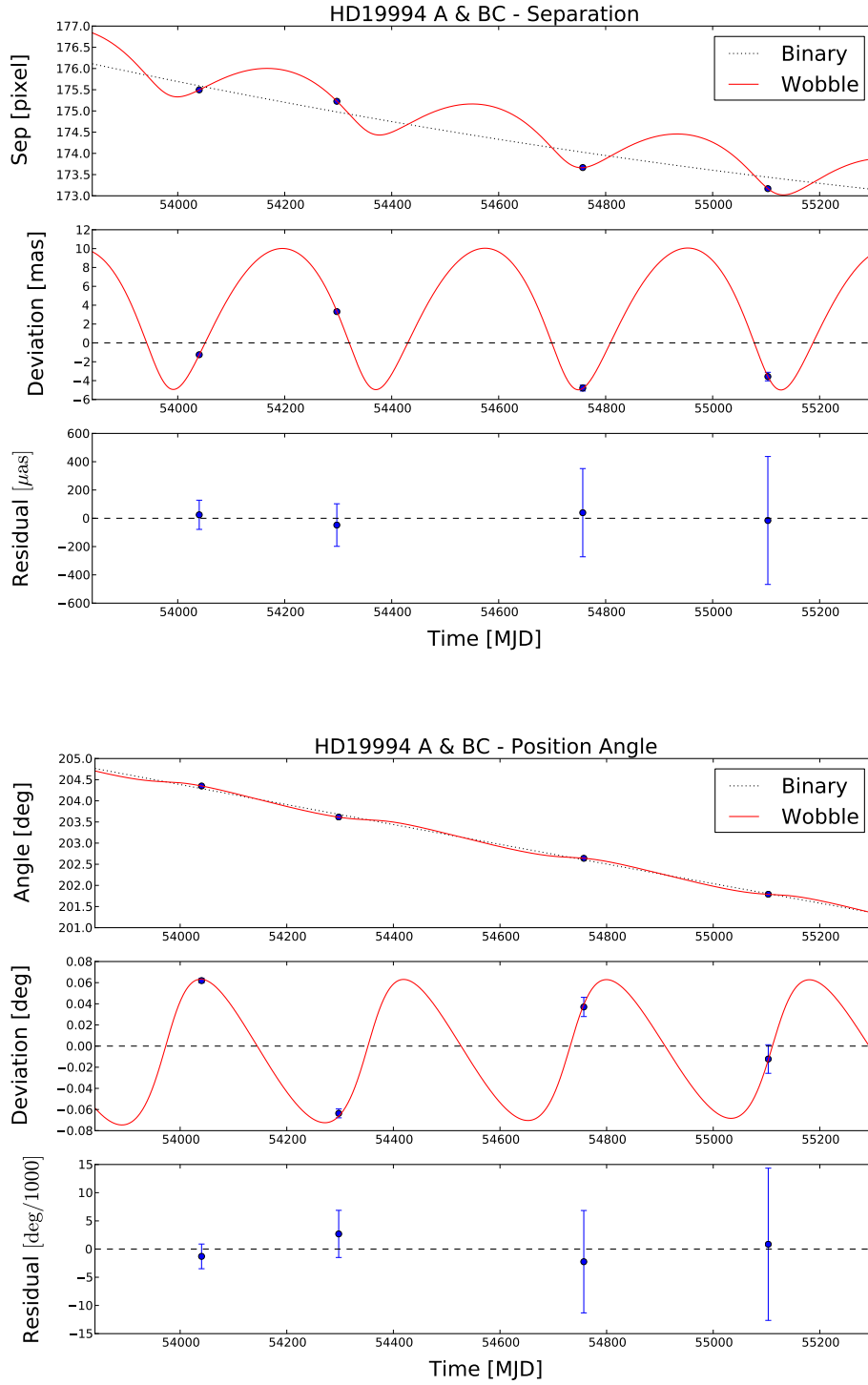


Fig. D.1.: Measurements and orbital solution of the HD 1994 A&BC system. The dotted line is the binary orbital motion. The solid line is the binary orbital motion disturbed by the Wobble orbit of the B component, which is induced by the astrometric companion HD 1994 C.

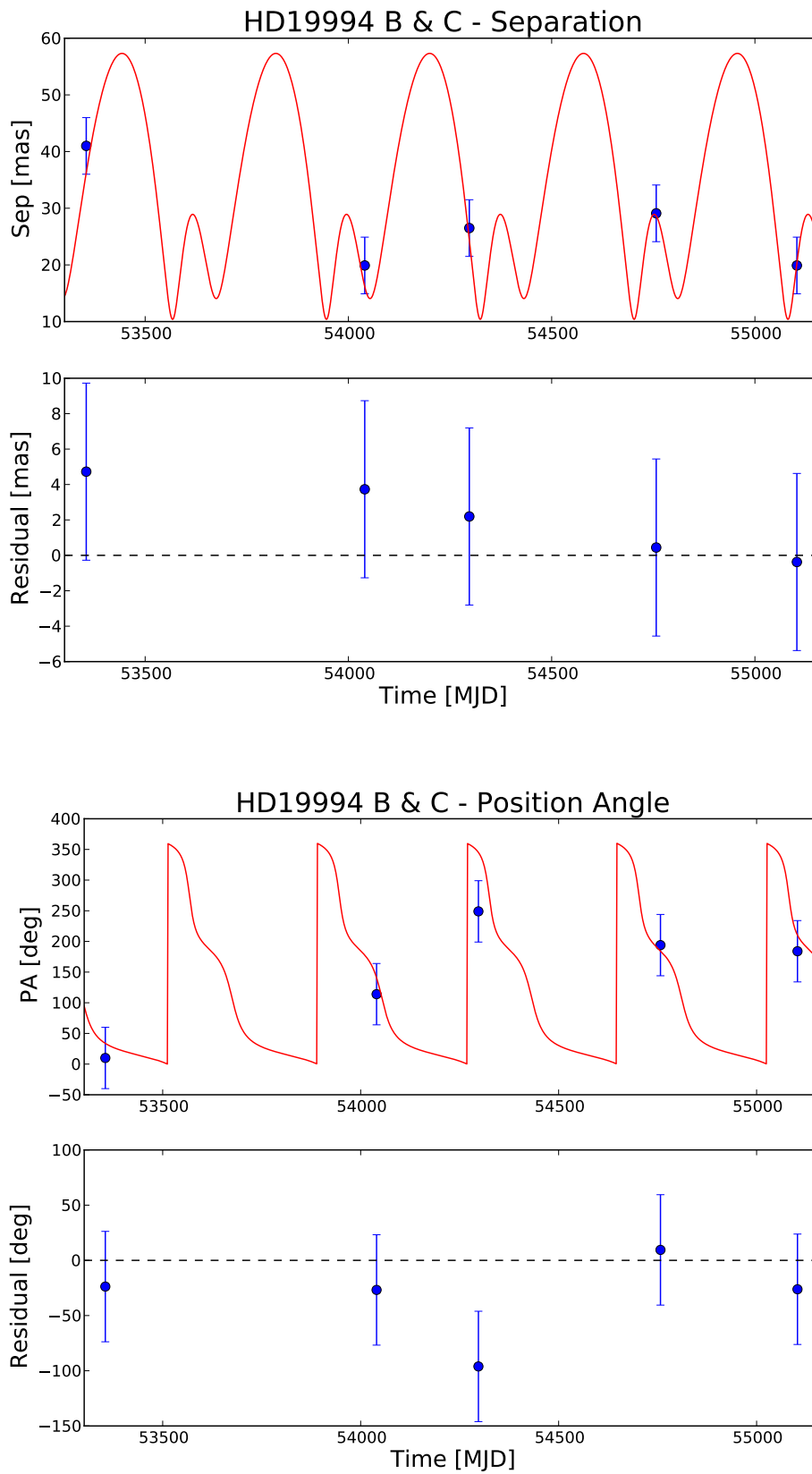


Fig. D.2.: Orbital solution (solid line) and speckle measurements of HD 19994 B&C

D. HD 19994 C - Orbital solution

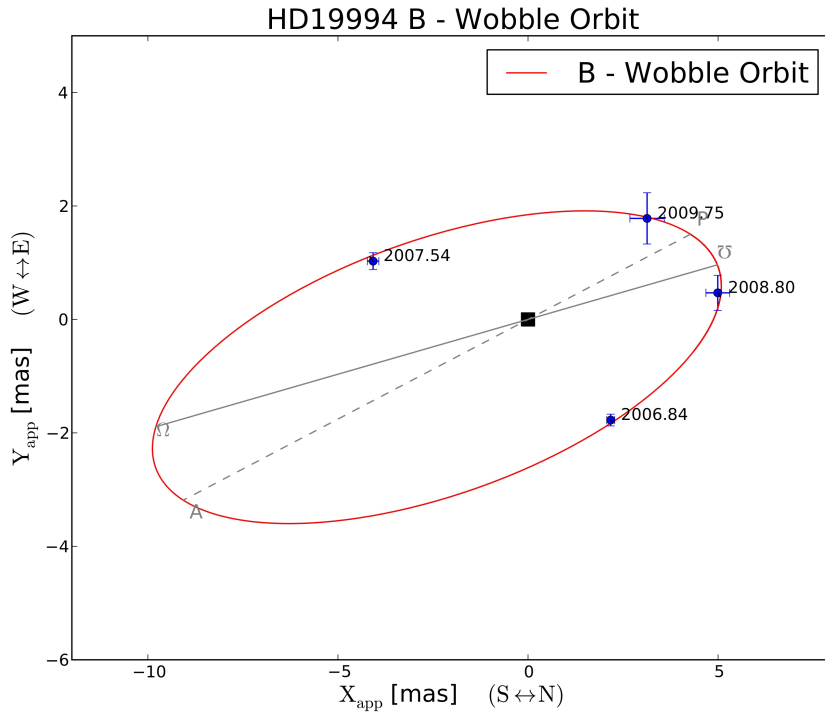


Fig. D.3.: Reflex orbit (solid line) of the flux center of HD 19994 B&C around their common center of mass. The data shown are reconstructed from the astrometric binary measurements.

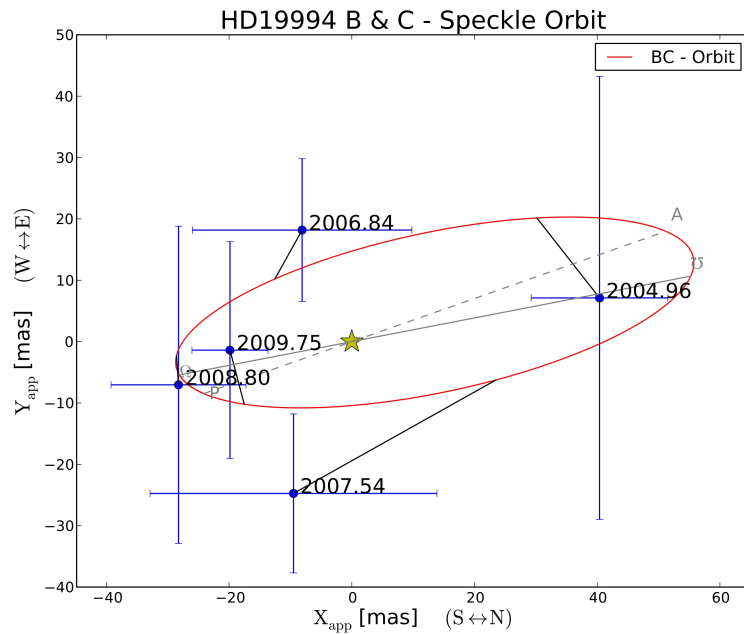


Fig. D.4.: Orbit (solid line) of HD 19994 C around HD 19994 B. The data shown are the speckle measurements.

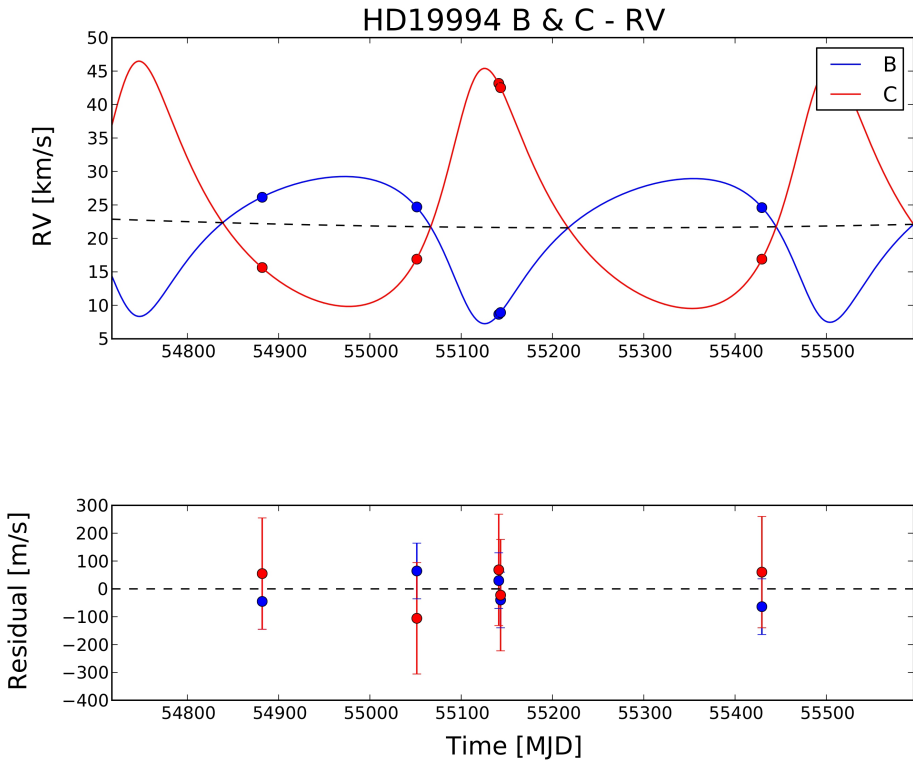


Fig. D.5.: Orbital fit of the radial velocity measurements of HD 19994 B&C. The radial velocity of the HD 19994 system itself was fitted as a third order polynomial.





## E. HD 19994 C - $\chi^2$ Maps

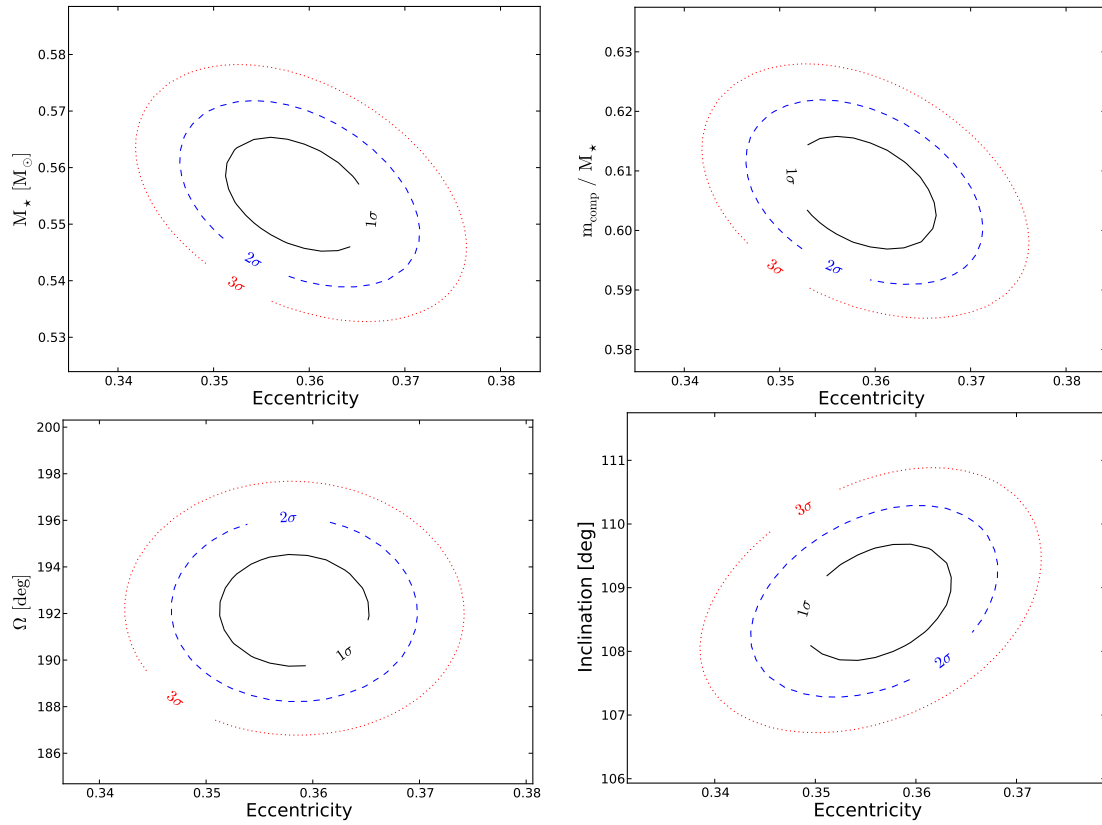


Fig. E.1.: Two dimensional  $\chi^2$  maps for the orbital elements of the new detected HD 19994 C component around HD 19994 B. The additional  $\Delta\chi^2$  terms for the  $1\sigma$ ,  $2\sigma$ , and  $3\sigma$  uncertainties are 2.3, 6.2, and 11.8 (see Press [151, page 815] for further information).

E. HD 19994 C -  $\chi^2$  Maps

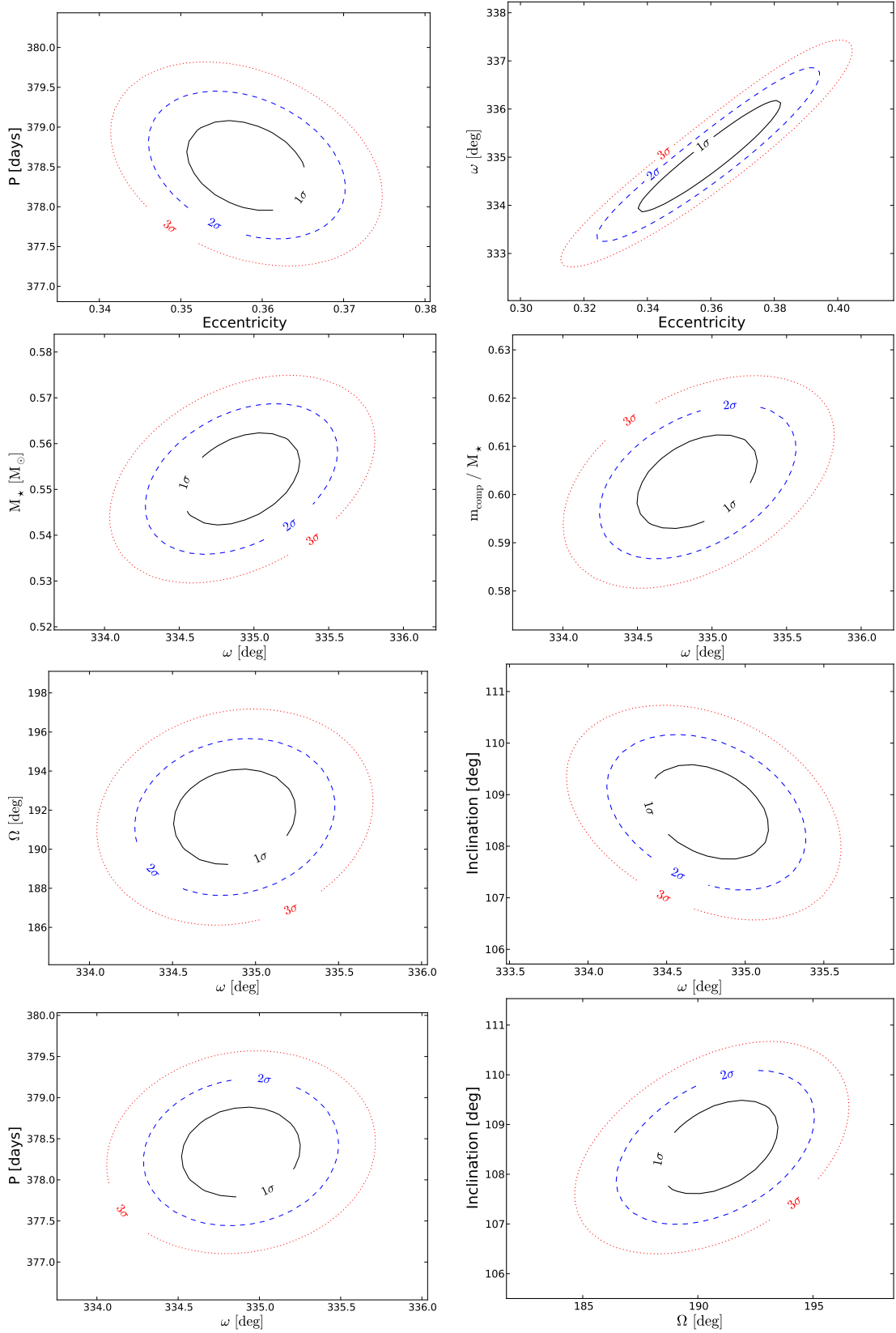


Fig. E.2.: Two dimensional  $\chi^2$  maps for the orbital elements of the new detected HD 19994 C component around HD 19994 B (continuation). XVI

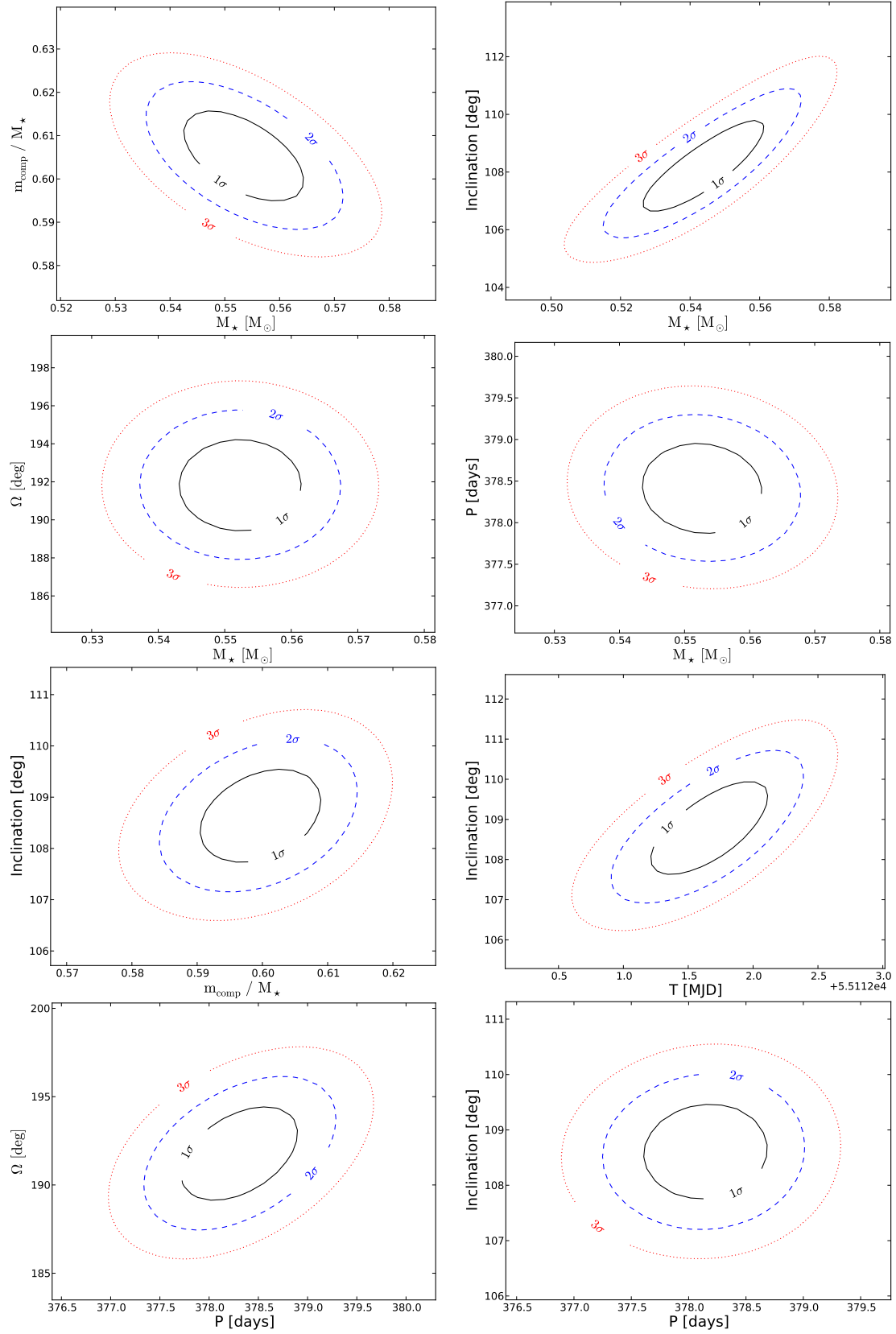


Fig. E.3.: Two dimensional  $\chi^2$  maps for the orbital elements of the new detected HD 19994 C component around HD 19994 B (continuation). XVII

### E. HD 19994 C - $\chi^2$ Maps

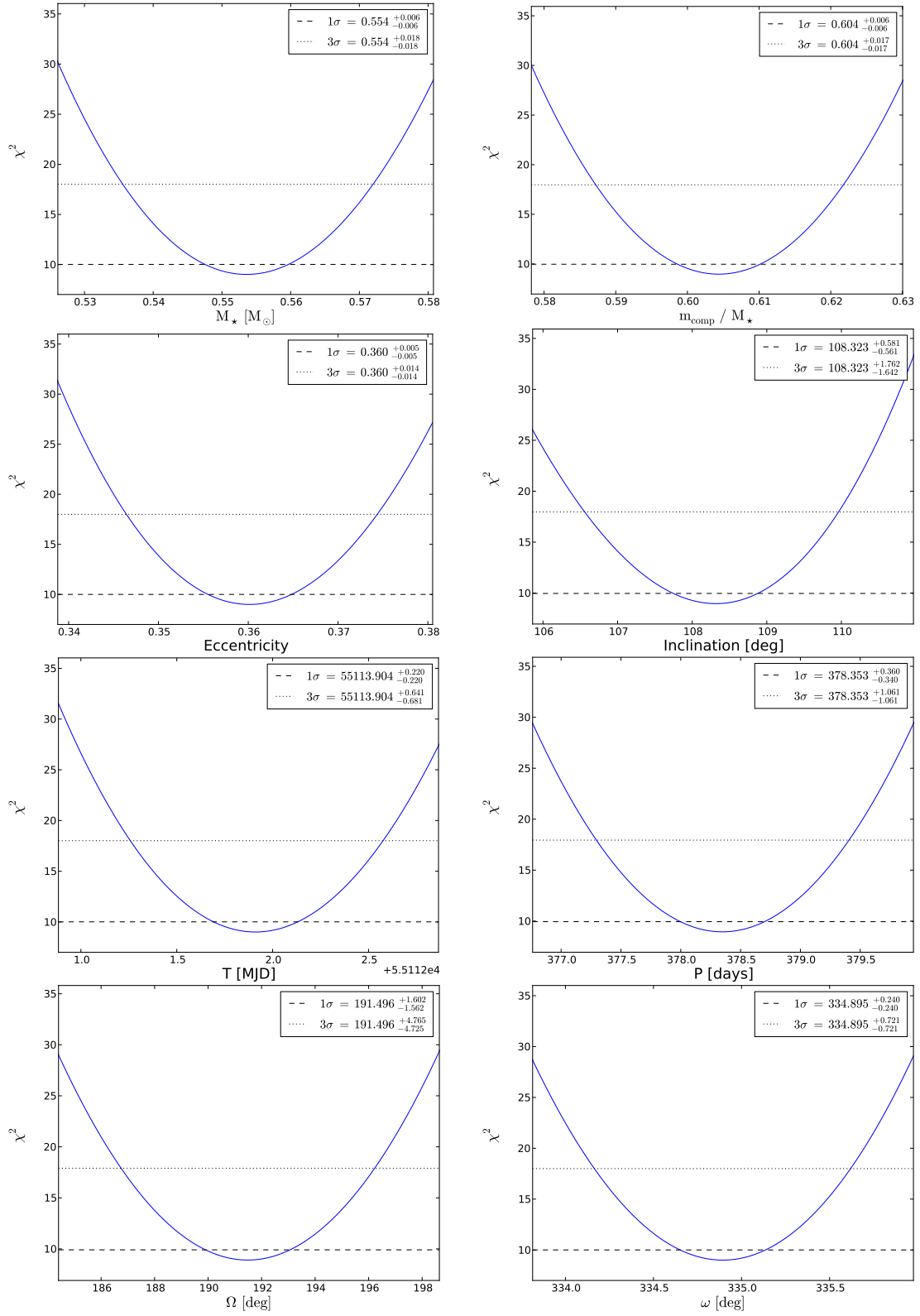


Fig. E.4.: One dimensional  $\chi^2$  maps for the orbital elements of the new detected HD 19994 C component around HD 19994 B. The additional  $\Delta\chi^2$  terms for the  $1\sigma$ ,  $2\sigma$ , and  $3\sigma$  uncertainties are 1, 4, and 9 (see Press [151]).

## F. Extended target list

More than 150 suitable systems were found by matching the *Gliese catalogue of nearby stars* (Gliese and Jahreiss [68]) with the *Catalogue of Components of Double and Multiple Stars* (Dommagnet and Nys [44]). The following table listed these systems sorted by name with the spectraltype of the primary, the distance of the system as well as the separation and the position angle of the companions. The selection criteria are dwarf stars with a spectral type later or equal than G0, a distance of less than 60 parsec, and at least one companion with a stellar separation of 0.1 arcsec up to about 15 arcsec. All data shown in the table are taken from these both catalogs.

*F. Extended target list*

Name	Spectraltype	Distance [pc]	Companion	Separation [arcsec]	Position Angle [degree]
BD+01 2684	M0 V	15.9	A		
BD+01 2684 B			B	1.30	66.00
BD+01 3942	K4	21.8	A		
BD+01 3942 B			B	9.20	180.00
BD+05 3409	M1 V	10.0	A		
BD+05 3409 B			B	10.10	286.00
BD+10 1857	M0	15.0	A		
BD+10 1857 B			B	2.20	169.00
BD+10 1857 C			C	115.00	96.00
BD+21 1764	K5	16.9	A		
BD+21 1764 B			B	10.40	151.00
BD+27 1311	M0 Ve	16.8	A		
BD+27 1311 B			B	12.10	299.00
BD+27 4120	M0	12.4	A		
BD+27 4120 B			B	5.00	220.00
BD+27 4120 C			C	0.20	109.00
BD+32 3326	M3.5	8.2	A		
BD+32 3326 B			B	3.40	300.00
BD+32 3326 C			C	48.00	50.00
BD+38 4818	M2	14.1	A		
BD+38 4818 B			B	0.10	355.00
BD+39 0710	K5	25.0	A		
BD+39 0710 B			B	3.00	214.00
BD+76 614	K7	34.5	A		
BD+76 614 B			B	3.70	164.00
BD- 3 3952	K5	22.7	A		
BD- 3 3952 B			B	7.00	299.00

*continued on next page*

Name	Spectraltype	Distance [pc]	Companion	Separation [arcsec]	Position Angle [degree]
BD-12 2918	M3	9.3	A		
BD-12 2918 B			B	0.50	109.00
BD-18 3019	M1	12.9	A		
BD-18 3019 B			B	7.50	352.00
BD-20 958	M0 V	25.0	A		
BD-20 958 B			B	0.20	341.00
BD-20 3198	K7 V	23.3	A		
BD-20 3198 B			B	0.60	328.00
BD-20 3198 C			C	5.60	189.00
BD-20 6558	K7 V	22.7	A		
BD-20 6558 B			B	7.50	202.00
BD-21 1074	M2	12.0	A		
BD-21 1074 B			B	8.30	319.00
BD-21 1074 C			C	1.30	5.00
CD-31 7745	M0 V	20.0	A		
CD-31 7745 B			B	8.00	270.00
CD-36 6589	M0 V	13.3	A		
CD-36 6589 B			B	1.10	166.00
CD-37 10765	M3	7.7	A		
CD-37 10765 B			B	7.60	50.00
CD-44 3045	M3	8.6	A		
CD-44 3045 B			B	3.20	50.00
CD-58 538	M0 Ve	13.0	A		
CD-58 538 B			B	0.20	300.00
CD-72 1700	M2 Ve	10.2	A		
CD-72 1700 B			B	1.30	5.00
CP-49 990	K0	14.3	A		
CP-49 990 B			B	1.30	257.00

*continued on next page*

*F. Extended target list*

Name	Spectraltype	Distance [pc]	Companion	Separation [arcsec]	Position Angle [degree]
G009-008	M5 e	8.8	A		
G009-008 B			B	12.00	348.00
G123-013	M2 V	20.0	A		
G123-013 B			B	0.50	340.00
G140-009	M2	15.6	A		
G140-009 B			B	0.40	122.00
G145-031	M3	20.4	A		
G145-031 B			B	3.80	347.00
G164-042	M4	16.9	A		
G164-042 B			B	0.40	286.00
G188-014	M3	18.9	A		
G188-014 B			B	0.30	135.00
GJ 2036	M2 Ve	10.5	A		
GJ 2036 B			B	9.00	315.00
Gl 236	M0	14.9	A		
Gl 236 B			B	8.10	236.00
HD 101177	G0 V	25.0	A		
HD 101177 B			B	9.70	253.00
HD 10307	G1.5 V	13.7	A		
HD 10307 B			B	0.50	35.00
HD 103493	G5 V	30.3	A		
HD 103493 B			B	3.20	180.00
HD 104471	G0 V	37.0	A		
HD 104471 B			B	0.60	121.00
HD 105590	G2 V	22.7	A		
HD 105590 B			B	10.00	89.00
HD 105590 C			C	19.10	75.00

---

*continued on next page*



Name	Spectraltype	Distance [pc]	Companion	Separation [arcsec]	Position Angle [degree]
HD 105963	K2	22.7	A		
HD 105963 B			B	12.70	221.00
HD 106116	G4 V	21.5	A		
HD 106116 B			B	2.00	5.00
HD 106783	K4 V	22.7	A		
HD 106783 B			B	0.30	237.00
HD 108421	K3 V	23.8	A		
HD 108421 B			B	2.30	18.00
HD 109358	G0 V	8.7	A		
HD 109358 B			B	0.10	43.00
HD 109358 C			C	76.20	220.00
HD 109524	K4 V	16.1	A		
HD 109524 B			B	97.00	135.00
HD 109952	K5 V	20.4	A		
HD 109952 B			B	0.80	209.00
HD 111261	K4/5 V	20.8	A		
HD 111261 B			B	12.50	311.00
HD 111312	K2 V	20.0	A		
HD 111312 B			B	2.70	63.00
HD 112758	K0 V	23.8	A		
HD 112758 B			B	1.60	300.00
HD 113693	K3 V	25.0	A		
HD 113693 B			B	0.20	163.00
HD 115404	K1 V	11.9	A		
HD 115404 B			B	6.40	108.00
HD 115404 C			C	92.50	3.00
HD 117635	G9 V	21.3	A		
HD 117635 B			B	0.20	122.00

*continued on next page*

*F. Extended target list*

Name	Spectraltype	Distance [pc]	Companion	Separation [arcsec]	Position Angle [degree]
HD 120036	K5 V	14.5	A		
HD 120036 B			B	8.00	86.00
HD 120237	K4	29.4	A		
HD 120237 B			B	11.60	355.00
HD 120780	K1 V	16.7	A		
HD 120780 B			B	6.00	70.00
HD 121271	K7 V	14.1	A		
HD 121271 B			B	1.20	34.00
HD 124498	K4 V	25.0	A		
HD 124498 B			B	1.70	279.00
HD 125354	K5	23.9	A		
HD 125354 B			B	0.30	94.00
HD 127356	G5 V	43.5	A		
HD 127356 B			B	2.10	84.00
HD 12759	G3 V	27.0	A		
HD 12759 B			B	1.00	178.00
HD 135204	K0 V	17.0	A		
HD 135204 B			B	0.10	231.00
HD 136466	G5 V	17.8	A		
HD 136466 B			B	0.70	77.00
HD 140538	G5 V	19.8	A		
HD 140538 B			B	4.20	61.00
HD 140901	G6 V	13.6	A		
HD 140901 B			B	14.90	133.00
HD 140901 C			C	8.10	135.00
HD 145958	G8 V	19.3	A		
HD 145958 B			B	4.20	344.00

---

*continued on next page*

Name	Spectraltype	Distance [pc]	Companion	Separation [arcsec]	Position Angle [degree]
HD 148704	K0 V	17.8	A		
HD 148704 B			B	11.00	238.00
HD 148704 C			C	4.10	221.00
HD 153026	K5 V	13.7	A		
HD 153026 B			B	4.00	8.00
HD 15468	K4 V	20.4	A		
HD 15468 B			B	0.60	312.00
HD 154712	K4 V	23.3	A		
HD 154712 B			B	12.10	47.00
HD 155121	G5	20.8	A		
HD 155121 B			B	0.60	20.00
HD 159462	G2 V	25.4	A		
HD 159462 B			B	6.00	336.00
HD 159704	G8 V	18.5	A		
HD 159704 B			B	1.40	106.00
HD 163545	K0	27.8	A		
HD 163545 B			B	0.60	291.00
HD 163840	G2 V	20.0	A		
HD 163840 B			B	0.10	160.00
HD 174564	K3 V	25.0	A		
HD 174564 B			B	11.20	4.00
HD 175224	K7 V	13.7	A		
HD 175224 B			B	3.60	319.00
HD 178076	K0 V	25.6	A		
HD 178076 B			B	9.00	210.00
HD 179930	K9 V	13.8	A		
HD 179930 B			B	0.20	43.00

*continued on next page*

*F. Extended target list*

Name	Spectraltype	Distance [pc]	Companion	Separation [arcsec]	Position Angle [degree]
HD 179958	G6 V	23.0	A		
HD 179958 B			B	8.20	212.00
HD 179958 C			C	47.10	13.00
HD 183783	K5 V	20.0	A		
HD 183783 B			B	11.20	244.00
HD 184467	K1 V	20.6	A		
HD 184467 B			B	0.10	74.00
HD 18455	K1/2 V	22.7	A		
HD 18455 B			B	0.90	333.00
HD 18455 C			C	28.60	224.00
HD 18455 D			D	5.10	172.00
HD 184860	K2 V	19.0	A		
HD 184860 B			B	5.00	328.00
HD 185454	G5 V	27.8	A		
HD 185454 B			B	1.70	163.00
HD 18757	G4 V	22.2	A		
HD 18757 B			B	12.70	132.00
HD 189484	K5 V	19.6	A		
HD 189484 B			B	14.20	48.00
HD 191408	K3 V	5.6	A		
HD 191408 B			B	7.10	123.00
HD 196850	G2 V	25.0	A		
HD 196850 B			B	34.20	327.00
HD 196850 C			C	16.90	14.00
HD 196850 D			D	113.50	219.00
HD 200968	K1 Ve	14.7	A		
HD 200968 B			B	4.90	167.00
HD 200968 C			C	11.70	301.00

*continued on next page*

Name	Spectraltype	Distance [pc]	Companion	Separation [arcsec]	Position Angle [degree]
HD 202940	G5 V	17.7	A		
HD 202940 B			B	3.20	255.00
HD 207496	K3/4 V	20.4	A		
HD 207496 B			B	2.10	118.00
HD 207966	G8	27.8	A		
HD 207966 B			B	10.50	87.00
HD 207966 C			C	55.00	50.00
HD 21019	G2 V	18.2	A		
HD 21019 B			B	3.90	48.00
HD 210460	G0 V	17.2	A		
HD 210460 B			B	0.50	9.00
HD 211415	G1 V	12.1	A		
HD 211415 B			B	3.40	32.00
HD 211472	K1 V	21.3	A		
HD 211472 B			B	59.10	65.00
HD 211472 C			C	5.90	300.00
HD 211472 P			P	31.90	116.00
HD 211472 Q			Q	37.40	263.00
HD 211472 R			R	40.10	261.00
HD 211472 S			S	57.80	358.00
HD 211472 T			T	78.00	106.00
HD 21175	K0 V	14.5	A		
HD 21175 B			B	2.10	221.00
HD 211998	G0 V	14.3	A		
HD 211998 B			B	0.10	
HD 21209	K5 V	22.7	A		
HD 21209 B			B	14.70	234.00

*continued on next page*

F. Extended target list

Name	Spectraltype	Distance [pc]	Companion	Separation [arcsec]	Position Angle [degree]
HD 212698	G3 V	16.4	A		
HD 212698 B			B	4.40	324.00
HD 212698 C			C	46.70	339.00
HD 212698 D			D	1.80	101.00
HD 212989	K0 V	16.1	A		
HD 212989 B			B	0.90	227.00
HD 212989 C			C	119.20	129.00
HD 21411	G8 V	31.2	A		
HD 21411 B			B	10.00	135.00
HD 214615	G8/K0 V	37.0	A		
HD 214615 B			B	3.60	298.00
HD 214615 C			C	98.20	245.00
HD 214953	G1 V	20.4	A		
HD 214953 B			B	7.80	129.00
HD 218572	K4 V	22.7	A		
HD 218572 B			B	13.10	107.00
HD 218640	G2 V	47.6	A		
HD 218640 B			B	0.40	7.00
HD 218738	G5	34.8	A		
HD 218738 B			B	15.40	254.00
HD 221613	G0	32.3	A		
HD 221613 B			B	0.20	341.00
HD 222474	K2	17.9	A		
HD 222474 B			B	0.70	236.00
HD 222474 C			C	101.90	3.00
HD 223515	K1 V	25.0	A		
HD 223515 B			B	2.50	9.00
HD 223778	K3 V	10.4	A		
HD 223778 B			B	4.60	95.00

*continued on next page*

Name	Spectraltype	Distance [pc]	Companion	Separation [arcsec]	Position Angle [degree]
HD 224953	M0 V	16.7	A		
HD 224953 B			B	3.70	120.00
HD 23189	K7	19.3	A		
HD 23189 B			B	17.00	16.00
HD 23189 C			C	0.70	234.00
HD 23189 D			D	43.60	
HD 23439	K1 V	20.4	A		
HD 23439 B			B	8.00	50.00
HD 23439 C			C	77.90	327.00
HD 23439 D			D	4.40	142.00
HD 23588	K5 V	20.8	A		
HD 23588 B			B	1.80	78.00
HD 238224	M0 V	20.4	A		
HD 238224 B			B	0.20	193.00
HD 24409	G0	21.3	A		
HD 24409 D			D	6.80	216.00
HD 24409 Q			Q	33.40	67.00
HD 24496	G5	21.3	A		
HD 24496 B			B	2.60	255.00
HD 24916	K4 V	14.7	A		
HD 24916 B			B	11.10	22.00
HD 28255	G4 V	25.0	A		
HD 28255 B			B	5.90	242.00
HD 286955	K3 V	20.2	A		
HD 286955 B			B	36.00	164.00
HD 286955 C			C	0.80	172.00
HD 30090	G0	19.2	A		
HD 30090 B			B	0.10	148.00
HD 30973	K5 V	23.3	A		

*continued on next page*

*F. Extended target list*

Name	Spectraltype	Distance [pc]	Companion	Separation [arcsec]	Position Angle [degree]
HD 30973 B			B	4.40	201.00
HD 32450	M0 V	7.7	A		
HD 32450 B			B		
HD 32450 C			C	10.40	28.00
HD 331161	M0.5	13.5	A		
HD 331161 B			B	3.70	132.00
HD 34673	K3 V	12.5	A		
HD 34673 B			B	2.70	29.00
HD 34721	G0 V	20.4	A		
HD 34721 B			B	46.00	234.00
HD 34721 C			C	15.80	101.00
HD 34751	K3/5 V	16.4	A		
HD 34751 B			B	5.00	75.00
HD 37706	G5 V	25.0	A		
HD 37706 B			B	5.00	67.00
HD 40397	G0	25.0	A		
HD 40397 B			B	4.10	359.00
HD 40865	G5 V	21.3	A		
HD 40865 B			B	10.80	328.00
HD 40865 C			C	4.10	265.00
HD 40887	K5 V	15.2	A		
HD 40887 B			B		
HD 40887 C			C	1.70	42.00
HD 40887 D			D	11.90	191.00
HD 4378	K5 V	12.3	A		
HD 4378 B			B	5.70	91.00
HD 45088	K2 V e	15.0	A		
HD 45088 B			B	1.30	162.00

*continued on next page*



Name	Spectraltype	Distance [pc]	Companion	Separation [arcsec]	Position Angle [degree]
HD 48189	G0 V	21.7	A		
HD 48189 B			B	2.40	270.00
HD 5109	G0	18.8	A		
HD 5109 B			B	6.50	71.00
HD 51849	K4 V	21.3	A		
HD 51849 B			B	0.40	49.00
HD 5425	K5 V	25.0	A		
HD 5425 B			B	1.00	84.00
HD 5857	G5	19.7	A		
HD 5857 B			B	4.20	249.00
HD 6101	K0	23.3	A		
HD 6101 B			B	0.70	62.00
HD 64606	G8 V	23.3	A		
HD 64606 B			B	4.90	99.00
HD 65277	K5 V	18.9	A		
HD 65277 B			B	4.10	69.00
HD 65277 C			C	4.50	230.00
HD 65907	G2 V	15.9	A		
HD 65907 B			B	60.00	90.00
HD 65907 C			C	2.30	270.00
HD 6660	K4 V	21.3	A		
HD 6660 B			B	10.00	74.00
HD 69565	G8/K0 V	14.1	A		
HD 69565 B			B	11.80	195.00
HD 73350	G0	22.2	A		
HD 73350 B			B	61.00	202.00
HD 73350 C			C	9.80	211.00

*continued on next page*

F. Extended target list

Name	Spectraltype	Distance [pc]	Companion	Separation [arcsec]	Position Angle [degree]
HD 75632	K5 V	11.3	A		
HD 75632 B			B	1.20	138.00
HD 77175	K5	18.2	A		
HD 77175 B			B	5.20	189.00
HD 78643	G1 V	29.4	A		
HD 78643 B			B	1.60	345.00
HD 79096	K0 V	21.9	A		
HD 79096 B			B	35.40	118.00
HD 79096 P			P	0.20	127.00
HD 79170	K0 V	22.1	A		
HD 79170 B			B	9.00	281.00
HD 81809	G2 V	18.5	A		
HD 81809 B			B	0.40	153.00
HD 82342	K3 V	22.2	A		
HD 82342 B			B	5.40	267.00
HD 82885	G8 V	11.5	A		
HD 82885 B			B	2.00	31.00
HD 85228	K1 V	22.2	A		
HD 85228 B			B	1.40	277.00
HD 86590	K0 V	20.8	A		
HD 86590 B			B	0.20	38.00
HD 88746	G8 V	34.5	A		
HD 88746 B			B	5.30	127.00
HD 8997	K2 V	18.2	A		
HD 8997 B			B	79.80	73.00
HD 8997 C			C	2.70	93.00
HD 8997 D			D	80.40	189.00

*continued on next page*

Name	Spectraltype	Distance [pc]	Companion	Separation [arcsec]	Position Angle [degree]
HD 9619	K0/1 V	23.8	A		
HD 9619 B			B	0.10	185.00
HD 97782	K4 V	19.6	A		
HD 97782 B			B	2.80	217.00
HD 98712	K4/5 V	15.7	A		
HD 98712 B			B	5.10	329.00
HD 98736	K0	25.0	A		
HD 98736 B			B	5.20	321.00
HD 98800	K4 V	14.7	A		
HD 98800 B			B	0.20	
LHS 1047	M4	5.3	A		
LHS 1047 B			B	0.30	149.00
LHS 1180	M1.5	17.1	A		
LHS 1180 B			B	3.00	23.00
LHS 1522	M1.5	14.2	A		
LHS 1522 B			B	4.70	23.00
LHS 1731	M3	11.8	A		
LHS 1731 B			B	10.90	347.00
LHS 1771	K5 V	25.0	A		
LHS 1771 B			B	5.00	67.00
LHS 2069	M6	14.6	A		
LHS 2069 B			B	2.40	77.00
LHS 221	M3.5	10.9	A		
LHS 221 B			B	0.30	265.00
LHS 2253	M3	18.2	A		
LHS 2253 B			B	12.00	45.00
LHS 2368	M3	16.4	A		
LHS 2368 B			B	4.00	70.00

*continued on next page*

*F. Extended target list*

Name	Spectraltype	Distance [pc]	Companion	Separation [arcsec]	Position Angle [degree]
LHS 247	M0 V	29.4	A		
LHS 247 B			B	0.60	214.00
LHS 2470	M3	12.2	A		
LHS 2470 B			B	9.00	110.00
LHS 2789	M3	24.3	A		
LHS 2789 B			B	1.30	33.00
LHS 2997	M3.5	10.6	A		
LHS 2997 B			B	0.30	104.00
LHS 3269	M3.5	11.7	A		
LHS 3269 B			B	0.50	100.00
LHS 3602	M3	15.7	A		
LHS 3602 B			B	14.00	312.00

## G. Acknowledgment

Extrasolar planets are a fascinating and fast evolving field of science. Hence, I would like to thank my supervisor Prof. Dr. Ralph Neuhäuser for gave me the possibility working in that area. Ground based astrometric imaging as a method to find extrasolar planets is still a hard task. Prof. Neuhäuser always supported me with scientific advice, suggestions, and comments.

Furthermore, I like to thank Andreas Seifahrt and Jacob Bean for the radial velocity follow-up observations of HD 19994 B. The atmosphere models for the analysis of the HD 19994 spectra, which is done by Andreas Seifahrt, are kindly provided by Soeren Witte.

Since I was a diploma student, Andreas Seifahrt always listen my questions and problems. Our discussions are a great pleasure for me and his answers always help me solving scientific problems. I am glad to call him a friend.

Science is not a one man show. I thank all my colleagues at the AIU Jena, especially Thomas Eisenbeiß, Tobias Schmidt, and Christian Adam. A discussion with other scientist (also an aggressive ones) is the first step to get the right answers to scientific problems.

This work would not be finished without the support of my family (especially my mother) and my friends. In 2009, I got the luck to get my own older brother. Lorenz, I like to welcome you in my family. This work is dedicated to our father, Siegmund Meisch.

Last but not least, the person who is perhaps luckier than me, that this thesis is finally finished. Nadine, thank you for everything! You know how important you are to me.

## *G. Acknowledgment*

At the end, I would like to summarize some excellent services, which was used in this work.

- The Extrasolar Planets Encyclopaedia, operated by Jean Schneider  
(<http://exoplanet.eu/>)
- SIMBAD database, operated at CDS in Strasbourg, France  
(<http://simbad.u-strasbg.fr/simbad/>)
- ST-ECF Hubble Science Data Archive  
(<http://archive.eso.org/cms/hubble-space-telescope-data>)
- ESO Science Archive Facility  
(<http://archive.eso.org/cms/eso-data>)

## H. Ehrenwörtliche Erklärung

Ich erkläre hiermit ehrenwörtlich, dass ich die vorliegende Arbeit, ohne unzulässige Hilfe Dritter und ohne Benutzung anderer als der angegebenen Hilfsmittel und Literatur angefertigt habe. Die aus anderen Quellen direkt oder indirekt übernommenen Daten und Konzepte sind unter Angabe der Quelle in dieser Arbeit gekennzeichnet. Nachstehend aufgeführte Personen haben mir in der jeweils beschriebenen Weise unentgeltlich geholfen:

- Die Spektren von HD 19994 B&C wurden von Dr. Jacob Bean und Dr. Andreas Seifahrt mit dem Spektrographen CRIRES am ESO/VLT aufgenommen. Die Auswertung der Spektren wurde von Dr. Andreas Seifahrt durchgeführt.
- Das Programm, welches für die Speckle Interferometrie benutzt wurde, stammt von Dr. Rainer Köhler.
- Einige Beobachtungen für diese Arbeit wurden von Ana Bedalov, Dr. Andreas Seifahrt, Dr. Markus Mugrauer und Tobias Schmidt durchgeführt.

Weitere Personen waren an der inhaltlichen-materiellen Erstellung der vorliegenden Arbeit nicht beteiligt. Insbesondere habe ich hierfür nicht die entgeltliche Hilfe von Vermittlungs- bzw. Beratungsdiensten (Promotionsberater oder andere Personen) in Anspruch genommen. Niemand hat von mir unmittelbar oder mittelbar geldwerte Leistungen für Arbeiten erhalten, die im Zusammenhang mit dem Inhalt der vorgelegten Dissertation stehen.

Die Arbeit wurde bisher weder im In- noch im Ausland in gleicher oder ähnlicher Form einer anderen Prüfungsbehörde vorgelegt. Die geltende Promotionsordnung der Physikalisch-Astronomischen Fakultät ist mir bekannt. Ich versichere ehrenwörtlich, dass ich nach bestem Wissen die reine Wahrheit gesagt und nichts verschwiegen habe.

Jena, 08. Juni 2011





# Bibliography

- [1] H. A. Abt and S. G. Levy. Multiplicity among solar-type stars. *ApJS*, 30:273–306, March 1976. doi: 10.1086/190363.
- [2] R. G. Aitken. *The binary stars*. 1935.
- [3] E. K. Baines, H. A. McAlister, T. A. ten Brummelaar, N. H. Turner, J. Sturmann, L. Sturmann, P. J. Goldfinger, and S. T. Ridgway. CHARA Array Measurements of the Angular Diameters of Exoplanet Host Stars. *ApJ*, 680:728–733, June 2008. doi: 10.1086/588009.
- [4] G. Á. Bakos, R. W. Noyes, G. Kovács, D. W. Latham, D. D. Sasselov, G. Torres, D. A. Fischer, R. P. Stefanik, B. Sato, J. A. Johnson, A. Pál, G. W. Marcy, R. P. Butler, G. A. Esquerdo, K. Z. Stanek, J. Lázár, I. Papp, P. Sári, and B. Sipőcz. HAT-P-1b: A Large-Radius, Low-Density Exoplanet Transiting One Member of a Stellar Binary. *ApJ*, 656:552–559, February 2007. doi: 10.1086/509874.
- [5] J. E. Baldwin, P. J. Warner, and C. D. Mackay. The point spread function in Lucky Imaging and variations in seeing on short timescales. *A&A*, 480:589–597, March 2008. doi: 10.1051/0004-6361:20079214.
- [6] I. Baraffe, G. Chabrier, F. Allard, and P. H. Hauschildt. Evolutionary models for solar metallicity low-mass stars: mass-magnitude relationships and color-magnitude diagrams. *A&A*, 337:403–412, September 1998.
- [7] J. Bean, A. Seifahrt, H. Hartman, H. Nilsson, G. Wiedemann, A. Reiners, S. Dreizler, and T. Henry. The CRIFRES Search for Planets at the Bottom of the Main Sequence. *The Messenger*, 140:41–45, June 2010.
- [8] J. L. Bean, B. E. McArthur, G. F. Benedict, T. E. Harrison, D. Bizyaev, E. Nelan, and V. V. Smith. The Mass of the Candidate Exoplanet Companion to HD 33636 from Hubble Space Telescope Astrometry and High-Precision Radial Velocities. *AJ*, 134:749–758, August 2007. doi: 10.1086/519956.
- [9] J. L. Bean, A. Seifahrt, H. Hartman, H. Nilsson, A. Reiners, S. Dreizler, T. J. Henry, and G. Wiedemann. The Proposed Giant Planet Orbiting VB 10 Does Not Exist. *ApJ*, 711:L19–L23, March 2010. doi: 10.1088/2041-8205/711/1/L19.
- [10] J. L. Bean, A. Seifahrt, H. Hartman, H. Nilsson, G. Wiedemann, A. Reiners, S. Dreizler, and T. J. Henry. The CRIFRES Search for Planets Around the Lowest-mass Stars. I. High-precision Near-infrared Radial Velocities with an Ammonia Gas Cell. *ApJ*, 713:410–422, April 2010. doi: 10.1088/0004-637X/713/1/410.

## Bibliography

- [11] G. F. Benedict, B. E. McArthur, T. Forveille, X. Delfosse, E. Nelan, R. P. Butler, W. Spiesman, G. Marcy, B. Goldman, C. Perrier, W. H. Jefferys, and M. Mayor. A Mass for the Extrasolar Planet Gliese 876b Determined from Hubble Space Telescope Fine Guidance Sensor 3 Astrometry and High-Precision Radial Velocities. *ApJ*, 581:L115–L118, December 2002. doi: 10.1086/346073.
- [12] G. F. Benedict, B. E. McArthur, G. Gatewood, E. Nelan, W. D. Cochran, A. Hatzes, M. Endl, R. Wittenmyer, S. L. Baliunas, G. A. H. Walker, S. Yang, M. Kürster, S. Els, and D. B. Paulson. The Extrasolar Planet  $\epsilon$  Eridani b: Orbit and Mass. *AJ*, 132:2206–2218, November 2006. doi: 10.1086/508323.
- [13] F. W. Bessel. Über Veränderlichkeit der eigenen Bewegungen der Fixsterne. Von Herrn Geh. Rath Bessel. *Astronomische Nachrichten*, 22:169–+, September 1844. doi: 10.1002/asna.18450221202.
- [14] K. Beuermann, F. V. Hessman, S. Dreizler, T. R. Marsh, S. G. Parsons, D. E. Winget, G. F. Miller, M. R. Schreiber, W. Kley, V. S. Dhillon, S. P. Littlefair, C. M. Copperwheat, and J. J. Hermes. Two planets orbiting the recently formed post-common envelope binary NN Serpentis. *A&A*, 521:L60+, October 2010. doi: 10.1051/0004-6361/201015472.
- [15] M. Bonavita and S. Desidera. The frequency of planets in multiple systems. *A&A*, 468:721–729, June 2007. doi: 10.1051/0004-6361:20066671.
- [16] P. Bordé, D. Rouan, and A. Léger. Exoplanet detection capability of the COROT space mission. *A&A*, 405:1137–1144, July 2003. doi: 10.1051/0004-6361:20030675.
- [17] J. Borsenberger, B. de Batz, S. Derriere, G. Mamon, A. Omont, G. Patrel, G. Simon, and I. Vaughin. DENIS, a European DEep Near Infrared Survey of the Southern Sky. In V. Coudé du Foresto, D. Rouan, & G. Rousset, editor, *Visions for Infrared Astronomy, Instrumentation, Mesure, Métrologie*, pages 135–138, 2006.
- [18] W. J. Borucki, D. Koch, G. Basri, N. Batalha, T. Brown, D. Caldwell, J. Caldwell, J. Christensen-Dalsgaard, W. D. Cochran, E. DeVore, E. W. Dunham, A. K. Dupree, T. N. Gautier, J. C. Geary, R. Gilliland, A. Gould, S. B. Howell, J. M. Jenkins, Y. Kondo, D. W. Latham, G. W. Marcy, S. Meibom, H. Kjeldsen, J. J. Lissauer, D. G. Monet, D. Morrison, D. Sasselov, J. Tarter, A. Boss, D. Brownlee, T. Owen, D. Buzasi, D. Charbonneau, L. Doyle, J. Fortney, E. B. Ford, M. J. Holman, S. Seager, J. H. Steffen, W. F. Welsh, J. Rowe, H. Anderson, L. Buchhave, D. Ciardi, L. Walkowicz, W. Sherry, E. Horch, H. Isaacson, M. E. Everett, D. Fischer, G. Torres, J. A. Johnson, M. Endl, P. MacQueen, S. T. Bryson, J. Dotson, M. Haas, J. Kolodziejczak, J. Van Cleve, H. Chandrasekaran, J. D. Twicken, E. V. Quintana, B. D. Clarke, C. Allen, J. Li, H. Wu, P. Tenenbaum, E. Verner, F. Bruhweiler, J. Barnes, and A. Prsa. Kepler Planet-Detection Mission: Introduction and First Results. *Science*, 327:977–, February 2010. doi: 10.1126/science.1185402.

- [19] F. Bouchy, S. Udry, M. Mayor, C. Moutou, F. Pont, N. Iribarne, R. da Silva, S. Illovaisky, D. Queloz, N. C. Santos, D. Ségransan, and S. Zucker. ELODIE metallicity-biased search for transiting Hot Jupiters. II. A very hot Jupiter transiting the bright K star HD 189733. *A&A*, 444:L15–L19, December 2005. doi: 10.1051/0004-6361:200500201.
- [20] F. Bouchy, G. Hébrard, S. Udry, X. Delfosse, I. Boisse, M. Desort, X. Bonfils, A. Eggenberger, D. Ehrenreich, T. Forveille, A. M. Lagrange, H. Le Coroller, C. Lovis, C. Moutou, F. Pepe, C. Perrier, F. Pont, D. Queloz, N. C. Santos, D. Ségransan, and A. Vidal-Madjar. The SOPHIE search for northern extrasolar planets . I. A companion around HD 16760 with mass close to the planet/brown-dwarf transition. *A&A*, 505:853–858, October 2009. doi: 10.1051/0004-6361/200912427.
- [21] R. P. Butler, G. W. Marcy, E. Williams, H. Hauser, and P. Shirts. Three New “51 Pegasi–Type” Planets. *ApJ*, 474:L115+, January 1997. doi: 10.1086/310444.
- [22] R. P. Butler, G. W. Marcy, D. A. Fischer, T. M. Brown, A. R. Contos, S. G. Korzennik, P. Nisenson, and R. W. Noyes. Evidence for Multiple Companions to  $\nu$  Andromedae. *ApJ*, 526:916–927, December 1999. doi: 10.1086/308035.
- [23] R. P. Butler, C. G. Tinney, G. W. Marcy, H. R. A. Jones, A. J. Penny, and K. Apps. Two New Planets from the Anglo-Australian Planet Search. *ApJ*, 555: 410–417, July 2001. doi: 10.1086/321467.
- [24] R. P. Butler, G. W. Marcy, S. S. Vogt, D. A. Fischer, G. W. Henry, G. Laughlin, and J. T. Wright. Seven New Keck Planets Orbiting G and K Dwarfs. *ApJ*, 582: 455–466, January 2003. doi: 10.1086/344570.
- [25] R. P. Butler, J. T. Wright, G. W. Marcy, D. A. Fischer, S. S. Vogt, C. G. Tinney, H. R. A. Jones, B. D. Carter, J. A. Johnson, C. McCarthy, and A. J. Penny. Catalog of Nearby Exoplanets. *ApJ*, 646:505–522, July 2006. doi: 10.1086/504701.
- [26] M. R. Calabretta and E. W. Greisen. Representations of celestial coordinates in FITS. *A&A*, 395:1077–1122, December 2002. doi: 10.1051/0004-6361:20021327.
- [27] A. C. Cameron, F. Bouchy, G. Hébrard, P. Maxted, D. Pollacco, F. Pont, I. Skillen, B. Smalley, R. A. Street, R. G. West, D. M. Wilson, S. Aigrain, D. J. Christian, W. I. Clarkson, B. Enoch, A. Evans, A. Fitzsimmons, M. Fleenor, M. Gillon, C. A. Haswell, L. Hebb, C. Hellier, S. T. Hodgkin, K. Horne, J. Irwin, S. R. Kane, F. P. Keenan, B. Loeillet, T. A. Lister, M. Mayor, C. Moutou, A. J. Norton, J. Osborne, N. Parley, D. Queloz, R. Ryans, A. H. M. J. Triaud, S. Udry, and P. J. Wheatley. WASP-1b and WASP-2b: two new transiting exoplanets detected with SuperWASP and SOPHIE. *MNRAS*, 375:951–957, March 2007. doi: 10.1111/j.1365-2966.2006.11350.x.
- [28] B. Campbell, G. A. H. Walker, and S. Yang. A search for substellar companions to solar-type stars. *ApJ*, 331:902–921, August 1988. doi: 10.1086/166608.

## Bibliography

- [29] G. Chauvin, A.-M. Lagrange, S. Udry, and M. Mayor. Characterization of the long-period companions of the exoplanet host stars: HD 196885, HD 1237 and HD 27442. VLT/NACO and SINFONI near-infrared, follow-up imaging and spectroscopy. *A&A*, 475:723–727, November 2007. doi: 10.1051/0004-6361:20067046.
- [30] Chauvin, G., Beust, H., Lagrange, A.-M., and Eggenberger, A. Planetary systems in close binary stars: the case of hd 196885 - combined astrometric and radial velocity study. *A&A*, 528:A8, 2011. doi: 10.1051/0004-6361/201015433. URL <http://dx.doi.org/10.1051/0004-6361/201015433>.
- [31] W. D. Cochran, A. P. Hatzes, R. P. Butler, and G. W. Marcy. The Discovery of a Planetary Companion to 16 Cygni B. *ApJ*, 483:457–+, July 1997. doi: 10.1086/304245.
- [32] A. C. M. Correia, S. Udry, M. Mayor, A. Eggenberger, D. Naef, J.-L. Beuzit, C. Perrier, D. Queloz, J.-P. Sivan, F. Pepe, N. C. Santos, and D. Ségransan. The ELODIE survey for northern extra-solar planets. IV. HD 196885, a close binary star with a 3.7-year planet. *A&A*, 479:271–275, February 2008. doi: 10.1051/0004-6361:20078908.
- [33] S. Correia, H. Zinnecker, T. Ratzka, and M. F. Sterzik. A VLT/NACO survey for triple and quadruple systems among visual pre-main sequence binaries. *A&A*, 459:909–926, December 2006. doi: 10.1051/0004-6361:20065545.
- [34] J. G. Cuby, D. Bottini, and J. P. Picat. Handling atmospheric dispersion and differential refraction effects in large-field multiobject spectroscopic observations. In S. D’Odorico, editor, *Society of Photo-Optical Instrumentation Engineers (SPIE) Conference Series*, volume 3355 of *Presented at the Society of Photo-Optical Instrumentation Engineers (SPIE) Conference*, pages 36–47, July 1998.
- [35] S. Daemgen, F. Hormuth, W. Brandner, C. Bergfors, M. Janson, S. Hippler, and T. Henning. Binarity of transit host stars. Implications for planetary parameters. *A&A*, 498:567–574, May 2009. doi: 10.1051/0004-6361/200810988.
- [36] J. R. de Medeiros, J. Setiawan, A. P. Hatzes, L. Pasquini, L. Girardi, S. Udry, M. P. Döllinger, and L. da Silva. A planet around the evolved intermediate-mass star HD 110014. *A&A*, 504:617–623, September 2009. doi: 10.1051/0004-6361/200911658.
- [37] F. Delplancke. The PRIMA facility phase-referenced imaging and micro-arcsecond astrometry. *New Astronomy Review*, 52:199–207, June 2008. doi: 10.1016/j.newar.2008.04.016.
- [38] B.-O. Demory, D. Ségransan, T. Forveille, D. Queloz, J.-L. Beuzit, X. Delfosse, E. di Folco, P. Kervella, J.-B. Le Bouquin, C. Perrier, M. Benisty, G. Duvert, K.-H. Hofmann, B. Lopez, and R. Petrov. Mass-radius relation of low and very low-mass stars revisited with the VLTI. *A&A*, 505:205–215, October 2009. doi: 10.1051/0004-6361/200911976.

- [39] S. Desidera and M. Barbieri. Properties of planets in binary systems. The role of binary separation. *A&A*, 462:345–353, January 2007. doi: 10.1051/0004-6361:20066319.
- [40] S. Desidera, R. G. Gratton, S. Scuderi, R. U. Claudi, R. Cosentino, M. Barbieri, G. Bonanno, E. Carretta, M. Endl, S. Lucatello, A. F. Martinez Fiorenzano, and F. Marzari. Abundance difference between components of wide binaries. *A&A*, 420:683–697, June 2004. doi: 10.1051/0004-6361:20041242.
- [41] S. Desidera, R. Gratton, M. Endl, A. F. Martinez Fiorenzano, M. Barbieri, R. Claudi, R. Cosentino, S. Scuderi, and M. Bonavita. The SARG Planet Search. *ArXiv e-prints*, May 2007.
- [42] E. Diolaiti, O. Bendinelli, D. Bonaccini, L. Close, D. Currie, and G. Parmeggiani. Analysis of isoplanatic high resolution stellar fields by the StarFinder code. *A&AS*, 147:335–346, December 2000. doi: 10.1051/aas:2000305.
- [43] J. A. Docobo, V. S. Tamazian, Y. Y. Balega, M. Andrade, D. Schertl, G. Weigelt, P. Campo, and M. Palacios. A methodology for studying physical and dynamical properties of multiple stars. Application to the system of red dwarfs Gl 22. *A&A*, 478:187–191, January 2008. doi: 10.1051/0004-6361:20078594.
- [44] J. Dommagnet and O. Nys. The visual double stars observed by the Hipparcos satellite. *A&A*, 363:991–994, November 2000.
- [45] A. Duquennoy and M. Mayor. Multiplicity among solar-type stars in the solar neighbourhood. II - Distribution of the orbital elements in an unbiased sample. *A&A*, 248:485–524, August 1991.
- [46] A. Duquennoy and M. Mayor. Multiplicity among solar-type stars in the solar neighbourhood. II - Distribution of the orbital elements in an unbiased sample. *A&A*, 248:485–524, August 1991.
- [47] A. Eggenberger, S. Udry, and M. Mayor. Planets in Binaries. In D. Deming & S. Seager, editor, *Scientific Frontiers in Research on Extrasolar Planets*, volume 294 of *Astronomical Society of the Pacific Conference Series*, pages 43–46, 2003.
- [48] A. Eggenberger, S. Udry, and M. Mayor. Statistical properties of exoplanets. III. Planet properties and stellar multiplicity. *A&A*, 417:353–360, April 2004. doi: 10.1051/0004-6361:20034164.
- [49] A. Eggenberger, M. Mayor, D. Naef, F. Pepe, D. Queloz, N. C. Santos, S. Udry, and C. Lovis. The CORALIE survey for southern extrasolar planets. XIV. HD 142022 b: a long-period planetary companion in a wide binary. *A&A*, 447:1159–1163, March 2006. doi: 10.1051/0004-6361:20053720.
- [50] A. Eggenberger, S. Udry, G. Chauvin, J.-L. Beuzit, A.-M. Lagrange, D. Ségransan, and M. Mayor. The impact of stellar duplicity on planet occurrence and

## Bibliography

- properties. I. Observational results of a VLT/NACO search for stellar companions to 130 nearby stars with and without planets. *A&A*, 474:273–291, October 2007. doi: 10.1051/0004-6361:20077447.
- [51] N. M. Elias, R. N. Tubbs, R. Köhler, S. Reffert, I. Stiliz, R. Launhardt, J. de Jong, A. Quirrenbach, F. Delplancke, T. Henning, and D. Queloz. The astrometric data reduction software (ADRS) and error budget for PRIMA. In Y.-S. Sun, S. Ferraz-Mello, & J.-L. Zhou, editor, *IAU Symposium*, volume 249 of *IAU Symposium*, pages 119–122, May 2008. doi: 10.1017/S1743921308016499.
- [52] U. Eriksson and L. Lindgren. Limits of ultra-high-precision optical astrometry. Stellar surface structures. *A&A*, 476:1389–1400, December 2007. doi: 10.1051/0004-6361:20078031.
- [53] D. Fischer, P. Driscoll, H. Isaacson, M. Giguere, G. W. Marcy, J. Valenti, J. T. Wright, G. W. Henry, J. A. Johnson, A. Howard, K. Peek, and C. McCarthy. Five Planets and an Independent Confirmation of HD 196885Ab from Lick Observatory. *ApJ*, 703:1545–1556, October 2009. doi: 10.1088/0004-637X/703/2/1545.
- [54] D. A. Fischer and G. W. Marcy. Multiplicity among M dwarfs. *ApJ*, 396:178–194, September 1992. doi: 10.1086/171708.
- [55] D. A. Fischer, G. W. Marcy, R. P. Butler, S. S. Vogt, and K. Apps. Planetary Companions around Two Solar-Type Stars: HD 195019 and HD 217107. *PASP*, 111:50–56, January 1999. doi: 10.1086/316304.
- [56] D. A. Fischer, G. W. Marcy, R. P. Butler, S. S. Vogt, S. Frink, and K. Apps. Planetary Companions to HD 12661, HD 92788, and HD 38529 and Variations in Keplerian Residuals of Extrasolar Planets. *ApJ*, 551:1107–1118, April 2001. doi: 10.1086/320224.
- [57] D. A. Fischer, R. P. Butler, G. W. Marcy, S. S. Vogt, and G. W. Henry. A Sub-Saturn Mass Planet Orbiting HD 3651. *ApJ*, 590:1081–1087, June 2003. doi: 10.1086/375027.
- [58] D. A. Fischer, G. W. Marcy, R. P. Butler, S. S. Vogt, G. W. Henry, D. Pourbaix, B. Walp, A. A. Misch, and J. T. Wright. A Planetary Companion to HD 40979 and Additional Planets Orbiting HD 12661 and HD 38529. *ApJ*, 586:1394–1408, April 2003. doi: 10.1086/367889.
- [59] D. A. Fischer, G. Laughlin, G. W. Marcy, R. P. Butler, S. S. Vogt, J. A. Johnson, G. W. Henry, C. McCarthy, M. Ammons, S. Robinson, J. Strader, J. A. Valenti, P. R. McCullough, D. Charbonneau, J. Haislip, H. A. Knutson, D. E. Reichart, P. McGee, B. Monard, J. T. Wright, S. Ida, B. Sato, and D. Minniti. The N2K Consortium. III. Short-Period Planets Orbiting HD 149143 and HD 109749. *ApJ*, 637:1094–1101, February 2006. doi: 10.1086/498557.

- [60] D. A. Fischer, S. S. Vogt, G. W. Marcy, R. P. Butler, B. Sato, G. W. Henry, S. Robinson, G. Laughlin, S. Ida, E. Toyota, M. Omiya, P. Driscoll, G. Takeda, J. T. Wright, and J. A. Johnson. Five Intermediate-Period Planets from the N2K Sample. *ApJ*, 669:1336–1344, November 2007. doi: 10.1086/521869.
- [61] D. L. Fried. Statistics of a Geometric Representation of Wavefront Distortion. *Journal of the Optical Society of America (1917-1983)*, 55:1427–+, November 1965.
- [62] D. L. Fried. Probability of getting a lucky short-exposure image through turbulence. *Journal of the Optical Society of America (1917-1983)*, 68:1651–1658, December 1978.
- [63] S. Frink, D. S. Mitchell, A. Quirrenbach, D. A. Fischer, G. W. Marcy, and R. P. Butler. Discovery of a Substellar Companion to the K2 III Giant  $\iota$  Draconis. *ApJ*, 576:478–484, September 2002. doi: 10.1086/341629.
- [64] K. Fuhrmann. Nearby stars of the Galactic disc and halo - IV. *MNRAS*, 384: 173–224, February 2008. doi: 10.1111/j.1365-2966.2007.12671.x.
- [65] F. Galland, A.-M. Lagrange, S. Udry, A. Chelli, F. Pepe, J.-L. Beuzit, and M. Mayor. Extrasolar planets and brown dwarfs around A-F type stars. II. A planet found with ELODIE around the F6V star HD 33564. *A&A*, 444:L21–L24, December 2005. doi: 10.1051/0004-6361:200500176.
- [66] G. Gatewood and H. Eichhorn. An unsuccessful search for a planetary companion of Barnard’s star BD +4 3561. *AJ*, 78:769–776, October 1973. doi: 10.1086/111480.
- [67] M. Giersz and D. C. Heggie. Monte Carlo simulations of star clusters - VII. The globular cluster 47 Tuc. *MNRAS*, pages 1747–+, November 2010. doi: 10.1111/j.1365-2966.2010.17648.x.
- [68] W. Gliese and H. Jahreiss. Nearby Stars, Preliminary 3rd Version (Gliese+ 1991). *VizieR Online Data Catalog*, 5070:0–+, November 1995.
- [69] R. G. Gratton, A. Bragaglia, E. Carretta, G. Clementini, S. Desidera, F. Grundahl, and S. Lucatello. Distances and ages of NGC 6397, NGC 6752 and 47 Tuc. *A&A*, 408:529–543, September 2003. doi: 10.1051/0004-6361:20031003.
- [70] E. W. Guenther, M. Hartmann, M. Esposito, A. P. Hatzes, F. Cusano, and D. Gandolfi. A substellar component orbiting the F-star 30 Arietis B. *A&A*, 507:1659–1665, December 2009. doi: 10.1051/0004-6361/200912112.
- [71] N. Haghighipour and S. N. Raymond. Habitable Planet Formation in Binary Planetary Systems. *ApJ*, 666:436–446, September 2007. doi: 10.1086/520501.
- [72] J. L. Halbwachs, M. Mayor, and S. Udry. Statistical properties of exoplanets. IV. The period-eccentricity relations of exoplanets and of binary stars. *A&A*, 431: 1129–1137, March 2005. doi: 10.1051/0004-6361:20041219.

## Bibliography

- [73] A. Hale. Orbital coplanarity in solar-type binary systems: Implications for planetary system formation and detection. *AJ*, 107:306–332, January 1994. doi: 10.1086/116855.
- [74] W. Hartkopf and B. Mason. Sixth catalog of orbits of visual binary stars. Website, 2001. <http://ad.usno.navy.mil/wds/orb6.html>, October 2010.
- [75] A. P. Hatzes and W. D. Cochran. Long-period radial velocity variations in three K giants. *ApJ*, 413:339–348, August 1993. doi: 10.1086/173002.
- [76] A. P. Hatzes, W. D. Cochran, M. Endl, B. McArthur, D. B. Paulson, G. A. H. Walker, B. Campbell, and S. Yang. A Planetary Companion to  $\gamma$  Cephei A. *ApJ*, 599:1383–1394, December 2003. doi: 10.1086/379281.
- [77] A. P. Hatzes, W. D. Cochran, M. Endl, E. W. Guenther, S. H. Saar, G. A. H. Walker, S. Yang, M. Hartmann, M. Esposito, D. B. Paulson, and M. P. Döllinger. Confirmation of the planet hypothesis for the long-period radial velocity variations of  $\beta$  Geminorum. *A&A*, 457:335–341, October 2006. doi: 10.1051/0004-6361:20065445.
- [78] P. H. Hauschildt and E. Baron. Numerical solution of the expanding stellar atmosphere problem. *Journal of Computational and Applied Mathematics*, 109: 41–63, September 1999.
- [79] J. L. Hershey. Astrometric analysis of the field of AC +65 6955 from plates taken with the Sproul 24-inch refractor. *AJ*, 78:421–425, June 1973. doi: 10.1086/111436.
- [80] L. A. Hillenbrand and R. J. White. An Assessment of Dynamical Mass Constraints on Pre-Main-Sequence Evolutionary Tracks. *ApJ*, 604:741–757, April 2004. doi: 10.1086/382021.
- [81] M. J. Holman and P. A. Wiegert. Long-Term Stability of Planets in Binary Systems. *AJ*, 117:621–628, January 1999. doi: 10.1086/300695.
- [82] J. Holmberg, B. Nordström, and J. Andersen. The Geneva-Copenhagen survey of the solar neighbourhood. III. Improved distances, ages, and kinematics. *A&A*, 501:941–947, July 2009. doi: 10.1051/0004-6361/200811191.
- [83] J. A. Johnson, G. W. Marcy, D. A. Fischer, J. T. Wright, S. Reffert, J. M. Kregenow, P. K. G. Williams, and K. M. G. Peek. Retired A Stars and Their Companions. II. Jovian planets orbiting  $\kappa$  CrB and HD 167042. *ApJ*, 675:784–789, March 2008. doi: 10.1086/526453.
- [84] Eric Jones, Travis Oliphant, Pearu Peterson, et al. SciPy: Open source scientific tools for Python, 2001. URL <http://www.scipy.org/>.



- [85] H. R. A. Jones, R. Paul Butler, G. W. Marcy, C. G. Tinney, A. J. Penny, C. McCarthy, and B. D. Carter. Extrasolar planets around HD 196050, HD 216437 and HD 160691. *MNRAS*, 337:1170–1178, December 2002. doi: 10.1046/j.1365-8711.2002.05787.x.
- [86] H. R. A. Jones, R. P. Butler, C. G. Tinney, G. W. Marcy, B. D. Carter, A. J. Penny, C. McCarthy, and J. Bailey. High-eccentricity planets from the Anglo-Australian Planet Search. *MNRAS*, 369:249–256, June 2006. doi: 10.1111/j.1365-2966.2006.10298.x.
- [87] W. Kley and R. P. Nelson. Planet formation in binary stars: the case of  $\gamma$  Cephei. *A&A*, 486:617–628, August 2008. doi: 10.1051/0004-6361:20079324.
- [88] W. Kley, J. C. B. Papaloizou, and G. I. Ogilvie. Simulations of eccentric disks in close binary systems. *A&A*, 487:671–687, August 2008. doi: 10.1051/0004-6361:200809953.
- [89] R. Köhler, M. Kunkel, C. Leinert, and H. Zinnecker. Multiplicity of X-ray selected T Tauri stars in the Scorpius-Centaurus OB association. *A&A*, 356:541–558, April 2000.
- [90] S. G. Korzennik, T. M. Brown, D. A. Fischer, P. Nisenson, and R. W. Noyes. A High-Eccentricity Low-Mass Companion to HD 89744. *ApJ*, 533:L147–L150, April 2000. doi: 10.1086/312611.
- [91] H. Lammer, R. Dvorak, M. Deleuil, P. Barge, H. J. Deeg, C. Moutou, A. Erikson, S. Csizmadia, B. Tingley, H. Bruntt, M. Havel, S. Aigrain, J. M. Almenara, R. Alonso, M. Auvergne, A. Baglin, M. Barbieri, W. Benz, A. S. Bonomo, P. Bordé, F. Bouchy, J. Cabrera, L. Carone, S. Carpano, D. Ciardi, S. Ferraz-Mello, M. Fridlund, D. Gandolfi, J.-C. Gazzano, M. Gillon, P. Gondoin, E. Guenther, T. Guillot, R. den Hartog, J. Hasiba, A. Hatzes, M. Hidas, G. Hébrard, L. Jorda, P. Kabath, A. Léger, T. Lister, A. Llebaria, C. Lovis, M. Mayor, T. Mazeh, A. Mura, M. Ollivier, H. Ottacher, M. Pätzold, F. Pepe, F. Pont, D. Queloz, M. Rabus, H. Rauer, D. Rouan, B. Samuel, J. Schneider, A. Shporer, B. Stecklum, M. Steller, R. Street, S. Udry, J. Weingrill, and G. Wuchterl. Exoplanet discoveries with the CoRoT space observatory. *Solar System Research*, 44: 520–526, December 2010. doi: 10.1134/S0038094610060055.
- [92] U. Lammers, L. Lindegren, W. O’Mullane, and D. Hobbs. To Boldly Go Where No Man has Gone Before: Seeking Gaia’s Astrometric Solution with AGIS. In D. A. Bohlender, D. Durand, & P. Dowler, editor, *Astronomical Society of the Pacific Conference Series*, volume 411 of *Astronomical Society of the Pacific Conference Series*, pages 55–+, September 2009.
- [93] D. W. Latham, R. P. Stefanik, T. Mazeh, M. Mayor, and G. Burki. The unseen companion of HD114762 - A probable brown dwarf. *Nature*, 339:38–40, May 1989. doi: 10.1038/339038a0.

## Bibliography

- [94] R. Launhardt. Exoplanet search with astrometry. *ArXiv e-prints*, April 2009.
- [95] N. M. Law, C. D. Mackay, and J. E. Baldwin. Lucky imaging: high angular resolution imaging in the visible from the ground. *A&A*, 446:739–745, February 2006. doi: 10.1051/0004-6361:20053695.
- [96] P. F. Lazorenko, M. Mayor, M. Dominik, F. Pepe, D. Segransan, and S. Udry. Precision multi-epoch astrometry with VLT cameras FORS1/2. *A&A*, 505:903–918, October 2009. doi: 10.1051/0004-6361/200912026.
- [97] P. F. Lazorenko, J. Sahlmann, D. Segransan, P. Figueira, C. Lovis, E. Martin, M. Mayor, F. Pepe, D. Queloz, F. Rodler, N. Santos, and S. Udry. Astrometric search for a planet around VB 10. *ArXiv e-prints*, November 2010.
- [98] J. W. Lee, S.-L. Kim, C.-H. Kim, R. H. Koch, C.-U. Lee, H.-I. Kim, and J.-H. Park. The sdB+M Eclipsing System HW Virginis and its Circumbinary Planets. *AJ*, 137:3181–3190, February 2009. doi: 10.1088/0004-6256/137/2/3181.
- [99] R. Lenzen, M. Hartung, W. Brandner, G. Finger, N. N. Hubin, F. Lacombe, A.-M. Lagrange, M. D. Lehnert, A. F. M. Moorwood, and D. Mouillet. NAOS-CONICA first on sky results in a variety of observing modes. In M. Iye & A. F. M. Moorwood, editor, *Society of Photo-Optical Instrumentation Engineers (SPIE) Conference Series*, volume 4841 of *Presented at the Society of Photo-Optical Instrumentation Engineers (SPIE) Conference*, pages 944–952, March 2003. doi: 10.1117/12.460044.
- [100] L. Lindegren. The Astrometric Instrument of Gaia: Principles. In C. Turon, K. S. O’Flaherty, & M. A. C. Perryman, editor, *The Three-Dimensional Universe with Gaia*, volume 576 of *ESA Special Publication*, pages 29–+, January 2005.
- [101] S. L. Lippincott. Astrometric search for unseen stellar and sub-stellar companions to nearby stars and the possibility of their detection. *Space Science Reviews*, 22: 153–189, July 1978. doi: 10.1007/BF00212072.
- [102] G. Lo Curto, M. Mayor, J. V. Clausen, W. Benz, F. Bouchy, C. Lovis, C. Moutou, D. Naef, F. Pepe, D. Queloz, N. C. Santos, J.-P. Sivan, S. Udry, X. Bonfils, X. Delfosse, C. Mordasini, P. Fouqué, E. H. Olsen, and J. D. Pritchard. The HARPS search for southern extra-solar planets. VII. A very hot Jupiter orbiting HD 212301. *A&A*, 451:345–350, May 2006. doi: 10.1051/0004-6361:20054083.
- [103] G. Lo Curto, M. Mayor, W. Benz, F. Bouchy, C. Lovis, C. Moutou, D. Naef, F. Pepe, D. Queloz, N. C. Santos, D. Segransan, and S. Udry. The HARPS search for southern extra-solar planets . XXII. Multiple planet systems from the HARPS volume limited sample. *A&A*, 512:A48+, March 2010. doi: 10.1051/0004-6361/200913523.
- [104] C. Lovis, M. Mayor, F. Bouchy, F. Pepe, D. Queloz, N. C. Santos, S. Udry, W. Benz, J.-L. Bertaux, C. Mordasini, and J.-P. Sivan. The HARPS search for

- southern extra-solar planets. III. Three Saturn-mass planets around HD 93083, HD 101930 and HD 102117. *A&A*, 437:1121–1126, July 2005. doi: 10.1051/0004-6361:20052864.
- [105] V. V. Makarov, N. Zacharias, and G. S. Hennessy. Common Proper Motion Companions to Nearby Stars: Ages and Evolution. *ApJ*, 687:566–578, November 2008. doi: 10.1086/591638.
- [106] G. Mandushev, F. T. O’Donovan, D. Charbonneau, G. Torres, D. W. Latham, G. Á. Bakos, E. W. Dunham, A. Sozzetti, J. M. Fernández, G. A. Esquerdo, M. E. Everett, T. M. Brown, M. Rabus, J. A. Belmonte, and L. A. Hillenbrand. TrES-4: A Transiting Hot Jupiter of Very Low Density. *ApJ*, 667:L195–L198, October 2007. doi: 10.1086/522115.
- [107] G. Marcy, R. P. Butler, D. Fischer, S. Vogt, J. T. Wright, C. G. Tinney, and H. R. A. Jones. Observed Properties of Exoplanets: Masses, Orbits, and Metallicities. *Progress of Theoretical Physics Supplement*, 158:24–42, 2005. doi: 10.1143/PTPS.158.24.
- [108] G. W. Marcy and R. P. Butler. Precision radial velocities with an iodine absorption cell. *PASP*, 104:270–277, April 1992. doi: 10.1086/132989.
- [109] G. W. Marcy and R. P. Butler. A Planetary Companion to 70 Virginis. *ApJ*, 464:L147+, June 1996. doi: 10.1086/310096.
- [110] G. W. Marcy, R. P. Butler, S. S. Vogt, D. Fischer, and J. J. Lissauer. A Planetary Companion to a Nearby M4 Dwarf, Gliese 876. *ApJ*, 505:L147–L149, October 1998. doi: 10.1086/311623.
- [111] G. W. Marcy, R. P. Butler, and S. S. Vogt. Sub-Saturn Planetary Candidates of HD 16141 and HD 46375. *ApJ*, 536:L43–L46, June 2000. doi: 10.1086/312723.
- [112] G. W. Marcy, R. P. Butler, D. A. Fischer, G. Laughlin, S. S. Vogt, G. W. Henry, and D. Pourbaix. A Planet at 5 AU around 55 Cancri. *ApJ*, 581:1375–1388, December 2002. doi: 10.1086/344298.
- [113] G. W. Marcy, R. P. Butler, S. S. Vogt, D. A. Fischer, G. W. Henry, G. Laughlin, J. T. Wright, and J. A. Johnson. Five New Extrasolar Planets. *ApJ*, 619:570–584, January 2005. doi: 10.1086/426384.
- [114] A. F. Martínez Fiorenzano, R. G. Gratton, S. Desidera, R. Cosentino, and M. Endl. Line bisectors and radial velocity jitter from SARG spectra. *A&A*, 442:775–784, November 2005. doi: 10.1051/0004-6361:20052888.
- [115] B. D. Mason, W. I. Hartkopf, G. L. Wycoff, and G. Wieder. Speckle Interferometry at the US Naval Observatory. XIII. *AJ*, 134:1671–1678, October 2007. doi: 10.1086/521555.

## Bibliography

- [116] M. Mayor and D. Queloz. A Jupiter-mass companion to a solar-type star. *Nature*, 378:355–359, November 1995. doi: 10.1038/378355a0.
- [117] M. Mayor, S. Udry, D. Naef, F. Pepe, D. Queloz, N. C. Santos, and M. Burnet. The CORALIE survey for southern extra-solar planets. XII. Orbital solutions for 16 extra-solar planets discovered with CORALIE. *A&A*, 415:391–402, February 2004. doi: 10.1051/0004-6361:20034250.
- [118] B. E. McArthur, M. Endl, W. D. Cochran, G. F. Benedict, D. A. Fischer, G. W. Marcy, R. P. Butler, D. Naef, M. Mayor, D. Queloz, S. Udry, and T. E. Harrison. Detection of a Neptune-Mass Planet in the  $\rho^1$  Cancri System Using the Hobby-Eberly Telescope. *ApJ*, 614:L81–L84, October 2004. doi: 10.1086/425561.
- [119] D. E. McLaughlin, J. Anderson, G. Meylan, K. Gebhardt, C. Pryor, D. Minniti, and S. Phinney. Hubble Space Telescope Proper Motions and Stellar Dynamics in the Core of the Globular Cluster 47 Tucanae. *ApJS*, 166:249–297, September 2006. doi: 10.1086/505692.
- [120] B. J. McNamara, T. E. Harrison, and H. Baumgardt. The Dynamical Distance to M15: Estimates of the Cluster’s Age and Mass and of the Absolute Magnitude of Its RR Lyrae Stars. *ApJ*, 602:264–270, February 2004. doi: 10.1086/380905.
- [121] G. R. Meurer, D. J. Lindler, J. Blakeslee, C. R. Cox, A. Martel, H. D. Tran, R. Bouwens, H. C. Ford, M. Clampin, G. F. Hartig, M. Sirianni, and G. De Marchi. Calibration of geometric distortion in the ACS detectors. In J. C. Blades & O. H. W. Siegmund, editor, *Society of Photo-Optical Instrumentation Engineers (SPIE) Conference Series*, volume 4854 of *Society of Photo-Optical Instrumentation Engineers (SPIE) Conference Series*, pages 507–514, February 2003. doi: 10.1117/12.460259.
- [122] D. S. Mitchell, S. Frink, A. Quirrenbach, D. A. Fischer, G. W. Marcy, and R. P. Butler. Four Substellar Companions Found Around K Giant Stars. In *Bulletin of the American Astronomical Society*, volume 35 of *Bulletin of the American Astronomical Society*, pages 1234–+, December 2003.
- [123] O. Montenbruck. *Grundlagen der Ephemeridenrechnung*. 2005. doi: 10.1007/978-3-8274-2292-7.
- [124] D. Montes, J. López-Santiago, M. C. Gálvez, M. J. Fernández-Figueroa, E. De Castro, and M. Cornide. Late-type members of young stellar kinematic groups - I. Single stars. *MNRAS*, 328:45–63, November 2001. doi: 10.1046/j.1365-8711.2001.04781.x.
- [125] C. Mordasini, Y. Alibert, W. Benz, and D. Naef. Extrasolar planet population synthesis. II. Statistical comparison with observations. *A&A*, 501:1161–1184, July 2009. doi: 10.1051/0004-6361/200810697.

- [126] G. Morlet, M. Salaman, and R. Gili. Nice Observatory CCD measurements of visual double stars (4th series). *A&A*, 396:933–935, December 2002. doi: 10.1051/0004-6361:20021459.
- [127] M. Mugrauer and R. Neuhauser. Gl86B: a white dwarf orbits an exoplanet host star. *MNRAS*, 361:L15–L19, July 2005. doi: 10.1111/j.1745-3933.2005.00055.x.
- [128] M. Mugrauer and R. Neuhauser. The multiplicity of exoplanet host stars. New low-mass stellar companions of the exoplanet host stars HD 125612 and HD 212301. *A&A*, 494:373–378, January 2009. doi: 10.1051/0004-6361:200810639.
- [129] M. Mugrauer, R. Neuhauser, T. Mazeh, J. Alves, and E. Guenther. A low-mass stellar companion of the planet host star HD 75289. *A&A*, 425:249–253, October 2004. doi: 10.1051/0004-6361:20041009.
- [130] M. Mugrauer, R. Neuhauser, T. Mazeh, E. Guenther, and M. Fernández. Astrometric confirmation of a wide low-mass companion to the planet host star HD 89744. *Astronomische Nachrichten*, 325:718–722, December 2004. doi: 10.1002/ansa.200410252.
- [131] M. Mugrauer, R. Neuhauser, A. Seifahrt, T. Mazeh, and E. Guenther. Four new wide binaries among exoplanet host stars. *A&A*, 440:1051–1060, September 2005. doi: 10.1051/0004-6361:20042297.
- [132] M. Mugrauer, A. Seifahrt, R. Neuhauser, and T. Mazeh. HD3651B: the first directly imaged brown dwarf companion of an exoplanet host star. *MNRAS*, 373:L31–L35, November 2006. doi: 10.1111/j.1745-3933.2006.00237.x.
- [133] M. Mugrauer, R. Neuhauser, and T. Mazeh. The multiplicity of exoplanet host stars. Spectroscopic confirmation of the companions GJ 3021 B and HD 27442 B, one new planet host triple-star system, and global statistics. *A&A*, 469:755–770, July 2007. doi: 10.1051/0004-6361:20065883.
- [134] M. Mugrauer, A. Seifahrt, and R. Neuhauser. The multiplicity of planet host stars - new low-mass companions to planet host stars. *MNRAS*, 378:1328–1334, July 2007. doi: 10.1111/j.1365-2966.2007.11858.x.
- [135] M. Mugrauer, N. Vogt, R. Neuhauser, and T. O. B. Schmidt. Direct detection of a substellar companion to the young nearby star PZ Telescopii. *A&A*, 523:L1+, November 2010. doi: 10.1051/0004-6361/201015523.
- [136] K. Murakawa, H. Suto, M. Tamura, N. Kaifu, H. Takami, N. Takato, S. Oya, Y. Hayano, W. Gaessler, and Y. Kamata. CIAO: Coronagraphic Imager with Adaptive Optics on the Subaru Telescope. *PASJ*, 56:509–519, June 2004.
- [137] M. W. Muterspaugh, B. F. Lane, S. R. Kulkarni, M. Konacki, B. F. Burke, M. M. Colavita, M. Shao, W. I. Hartkopf, A. P. Boss, and M. Williamson. The Phases Differential Astrometry Data Archive. V. Candidate Substellar Companions to

## Bibliography

- Binary Systems. *AJ*, 140:1657–1671, December 2010. doi: 10.1088/0004-6256/140/6/1657.
- [138] NACO Instrument Team. Eso instruments: Naco. Website, 2008. <http://www.eso.org/sci/facilities/paranal/instruments/naco/inst/>, October 2010.
- [139] D. Naef, M. Mayor, F. Pepe, D. Queloz, N. C. Santos, S. Udry, and M. Burnet. The CORALIE survey for southern extrasolar planets. V. 3 new extrasolar planets. *A&A*, 375:205–218, August 2001. doi: 10.1051/0004-6361:20010841.
- [140] D. Naef, M. Mayor, S. G. Korzennik, D. Queloz, S. Udry, P. Nisenson, R. W. Noyes, T. M. Brown, J. L. Beuzit, C. Perrier, and J. P. Sivan. The ELODIE survey for northern extra-solar planets. II. A Jovian planet on a long-period orbit around GJ 777 A. *A&A*, 410:1051–1054, November 2003. doi: 10.1051/0004-6361:20031341.
- [141] R. Neuhauser, M. Mugrauer, M. Fukagawa, G. Torres, and T. Schmidt. Direct detection of exoplanet host star companion  $\gamma$  Cep B and revised masses for both stars and the sub-stellar object. *A&A*, 462:777–780, February 2007. doi: 10.1051/0004-6361:20066581.
- [142] R. Neuhauser, M. Mugrauer, A. Seifahrt, T. O. B. Schmidt, and N. Vogt. Astrometric and photometric monitoring of GQ Lupi and its sub-stellar companion. *A&A*, 484:281–291, June 2008. doi: 10.1051/0004-6361:20078493.
- [143] R. W. Noyes, S. Jha, S. G. Korzennik, M. Krockenberger, P. Nisenson, T. M. Brown, E. J. Kennelly, and S. D. Horner. A Planet Orbiting the Star Rho Coronae Borealis. *ApJ*, 483:L111+, July 1997. doi: 10.1086/310754.
- [144] R. W. Noyes, S. Jha, S. G. Korzennik, M. Krockenberger, P. Nisenson, T. M. Brown, E. J. Kennelly, and S. D. Horner. A Planet Orbiting the Star Rho Coronae Borealis: Erratum. *ApJ*, 487:L195+, October 1997. doi: 10.1086/310905.
- [145] F. T. O’Donovan, D. Charbonneau, G. Mandushev, E. W. Dunham, D. W. Latham, G. Torres, A. Sozzetti, T. M. Brown, J. T. Trauger, J. A. Belmonte, M. Rabus, J. M. Almenara, R. Alonso, H. J. Deeg, G. A. Esquerdo, E. E. Falco, L. A. Hillenbrand, A. Roussanova, R. P. Stefanik, and J. N. Winn. TrES-2: The First Transiting Planet in the Kepler Field. *ApJ*, 651:L61–L64, November 2006. doi: 10.1086/509123.
- [146] J. C. Owens. Optical refractive index of air: dependence on pressure, temperature, and composition. *Appl. Opt.*, 6:51–+, January 1967.
- [147] G. F. Porto de Mello and L. da Silva. HR 6094: A Young, Solar-Type, Solar-Metallicity Barium Dwarf Star. *ApJ*, 476:L89+, February 1997. doi: 10.1086/310504.

- [148] M. S. Povich, M. S. Giampapa, J. A. Valenti, T. Tilleman, S. Barden, D. Deming, W. C. Livingston, and C. Pilachowski. Limits on Line Bisector Variability for Stars with Extrasolar Planets. *AJ*, 121:1136–1146, February 2001. doi: 10.1086/318745.
- [149] S. H. Pravdo and S. B. Shaklan. Astrometric Detection of Extrasolar Planets: Results of a Feasibility Study with the Palomar 5 Meter Telescope. *ApJ*, 465: 264–+, July 1996. doi: 10.1086/177417.
- [150] S. H. Pravdo and S. B. Shaklan. An ultracool Star’s Candidate Planet. *ApJ*, 700: 623–632, July 2009. doi: 10.1088/0004-637X/700/1/623.
- [151] W. H. Press. *Numerical Recipes 3rd Edition: The Art of Scientific Computing*. 2002.
- [152] S.-B. Qian, W.-P. Liao, L.-Y. Zhu, Z.-B. Dai, L. Liu, J.-J. He, E.-G. Zhao, and L.-J. Li. A giant planet in orbit around a magnetic-braking hibernating cataclysmic variable. *MNRAS*, 401:L34–L38, January 2010. doi: 10.1111/j.1745-3933.2009.00780.x.
- [153] D. Queloz, M. Mayor, L. Weber, A. Blécha, M. Burnet, B. Confino, D. Naef, F. Pepe, N. Santos, and S. Udry. The CORALIE survey for southern extra-solar planets. I. A planet orbiting the star Gliese 86. *A&A*, 354:99–102, February 2000.
- [154] D. Queloz, D. Anderson, A. Collier Cameron, M. Gillon, L. Hebb, C. Hellier, P. Maxted, F. Pepe, D. Pollacco, D. Ségransan, B. Smalley, A. H. M. J. Triaud, S. Udry, and R. West. WASP-8b: a retrograde transiting planet in a multiple system. *A&A*, 517:L1+, July 2010. doi: 10.1051/0004-6361/201014768.
- [155] C. F. Quist. Astrometric detection of sub-stellar companions with GAIA. *A&A*, 370:672–679, May 2001. doi: 10.1051/0004-6361:20010257.
- [156] G. Rabl and R. Dvorak. Satellite-type planetary orbits in double stars - A numerical approach. *A&A*, 191:385–391, February 1988.
- [157] D. Raghavan, T. J. Henry, B. D. Mason, J. P. Subasavage, W.-C. Jao, T. D. Beaulieu, and N. C. Hambly. Two Suns in The Sky: Stellar Multiplicity in Exoplanet Systems. *ApJ*, 646:523–542, July 2006. doi: 10.1086/504823.
- [158] D. Raghavan, H. A. McAlister, T. J. Henry, D. W. Latham, G. W. Marcy, B. D. Mason, D. R. Gies, R. J. White, and T. A. ten Brummelaar. A Survey of Stellar Families: Multiplicity of Solar-type Stars. *ApJS*, 190:1–42, September 2010. doi: 10.1088/0067-0049/190/1/1.
- [159] S. Rasouli and M. T. Tavassoly. Measurement of the refractive-index structure constant,  $C_n^2$ , and its profile in the ground level atmosphere by moire technique. In *Society of Photo-Optical Instrumentation Engineers (SPIE) Conference Series*, volume 6364 of *Society of Photo-Optical Instrumentation Engineers (SPIE) Conference Series*, October 2006. doi: 10.1117/12.683873.

## Bibliography

- [160] H. G. Roe. Implications of Atmospheric Differential Refraction for Adaptive Optics Observations. *PASP*, 114:450–461, April 2002. doi: 10.1086/342495.
- [161] T. Roell, A. Seifahrt, and R. Neuhäuser. Search for extrasolar planets with high-precision relative astrometry by ground-based and single-aperture observations. In Y.-S. Sun, S. Ferraz-Mello, & J.-L. Zhou, editor, *IAU Symposium*, volume 249 of *IAU Symposium*, pages 57–60, May 2008. doi: 10.1017/S1743921308016372.
- [162] T. Röhl, A. Seifahrt, R. Neuhäuser, R. Köhler, and J. Bean. Ground based astrometric search for extrasolar planets in stellar multiple systems. In *EAS Publications Series*, volume 45 of *EAS Publications Series*, pages 429–432, February 2011. doi: 10.1051/eas/1045076.
- [163] G. Rousset, F. Lacombe, P. Puget, N. N. Hubin, E. Gendron, T. Fusco, R. Arsenault, J. Charton, P. Feautrier, P. Gigan, P. Y. Kern, A.-M. Lagrange, P.-Y. Madec, D. Mouillet, D. Rabaud, P. Rabou, E. Stadler, and G. Zins. NAOS, the first AO system of the VLT: on-sky performance. In P. L. Wizinowich & D. Bonaccini, editor, *Society of Photo-Optical Instrumentation Engineers (SPIE) Conference Series*, volume 4839 of *Presented at the Society of Photo-Optical Instrumentation Engineers (SPIE) Conference*, pages 140–149, February 2003. doi: 10.1117/12.459332.
- [164] C. Saffe, M. Gómez, and C. Chavero. On the ages of exoplanet host stars. *A&A*, 443:609–626, November 2005. doi: 10.1051/0004-6361:20053452.
- [165] N. C. Santos, M. Mayor, D. Naef, F. Pepe, D. Queloz, S. Udry, M. Burnet, and Y. Revaz. The CORALIE survey for Southern extra-solar planets. III. A giant planet in orbit around HD 192263. *A&A*, 356:599–602, April 2000.
- [166] N. C. Santos, M. Mayor, D. Naef, F. Pepe, D. Queloz, S. Udry, and M. Burnet. The CORALIE survey for southern extra-solar planets VI. New long period giant planets around HD 28185 and HD 213240. *A&A*, 379:999–1004, December 2001. doi: 10.1051/0004-6361:20011366.
- [167] N. C. Santos, S. Udry, M. Mayor, D. Naef, F. Pepe, D. Queloz, G. Burki, N. Cramer, and B. Nicolet. The CORALIE survey for southern extra-solar planets. XI. The return of the giant planet orbiting HD 192263. *A&A*, 406:373–381, July 2003. doi: 10.1051/0004-6361:20030776.
- [168] B. Sato, H. Izumiura, E. Toyota, E. Kambe, Y. Takeda, S. Masuda, M. Omiya, D. Murata, Y. Itoh, H. Ando, M. Yoshida, M. Ikoma, E. Kokubo, and S. Ida. A Planetary Companion to the Hyades Giant  $\epsilon$  Tauri. *ApJ*, 661:527–531, May 2007. doi: 10.1086/513503.
- [169] B. Sato, E. Toyota, M. Omiya, H. Izumiura, E. Kambe, S. Masuda, Y. Takeda, Y. Itoh, H. Ando, M. Yoshida, E. Kokubo, and S. Ida. Planetary Companions to Evolved Intermediate-Mass Stars: 14 Andromedae, 81 Ceti, 6 Lyncis, and HD167042. *PASJ*, 60:1317–, December 2008.



- [170] T. O. B. Schmidt, R. Neuhäuser, A. Seifahrt, N. Vogt, A. Bedalov, C. Helling, S. Witte, and P. H. Hauschildt. Direct evidence of a sub-stellar companion around CT Chamaeleontis. *A&A*, 491:311–320, November 2008. doi: 10.1051/0004-6361:20078840.
- [171] J. Schneider. The extrasolar planets encyclopaedia. Website, 1995. <http://exoplanet.eu>, October 2010.
- [172] D. Ségransan, X. Delfosse, T. Forveille, J.-L. Beuzit, S. Udry, C. Perrier, and M. Mayor. Accurate masses of very low mass stars. III. 16 new or improved masses. *A&A*, 364:665–673, December 2000.
- [173] A. Seifahrt, T. Röhl, R. Neuhäuser, A. Reiners, F. Kerber, H. U. Käufl, R. Siebenmorgen, and A. Smette. Improved orbital solution and masses for the very low-mass multiple system LHS 1070. *A&A*, 484:429–434, June 2008. doi: 10.1051/0004-6361:20078875.
- [174] A. Seifahrt, H. U. Käufl, G. Zängl, J. L. Bean, M. J. Richter, and R. Siebenmorgen. Synthesising, using, and correcting for telluric features in high-resolution astronomical spectra . A near-infrared case study using CRIRES. *A&A*, 524:A11+, December 2010. doi: 10.1051/0004-6361/200913782.
- [175] D. M. Seymour, B. D. Mason, W. I. Hartkopf, and G. L. Wycoff. Binary Star Orbits. II. Preliminary First Orbits for 117 Systems. *AJ*, 123:1023–1038, February 2002. doi: 10.1086/338441.
- [176] B. A. Skiff. Catalogue of Stellar Spectral Classifications (Skiff, 2010). *VizieR Online Data Catalog*, 1:2023–+, February 2009.
- [177] M. F. Skrutskie, R. M. Cutri, R. Stiening, M. D. Weinberg, S. Schneider, J. M. Carpenter, C. Beichman, R. Capps, T. Chester, J. Elias, J. Huchra, J. Liebert, C. Lonsdale, D. G. Monet, S. Price, P. Seitzer, T. Jarrett, J. D. Kirkpatrick, J. E. Gizis, E. Howard, T. Evans, J. Fowler, L. Fullmer, R. Hurt, R. Light, E. L. Kopan, K. A. Marsh, H. L. McCallon, R. Tam, S. Van Dyk, and S. Wheelock. The Two Micron All Sky Survey (2MASS). *AJ*, 131:1163–1183, February 2006. doi: 10.1086/498708.
- [178] R. Soummer and A. Ferrari. The Strehl Ratio in Adaptive Optics Images: Statistics and Estimation. *ApJ*, 663:L49–L52, July 2007. doi: 10.1086/519080.
- [179] S. G. Sousa, N. C. Santos, M. Mayor, S. Udry, L. Casagrande, G. Israelian, F. Pepe, D. Queloz, and M. J. P. F. G. Monteiro. Spectroscopic parameters for 451 stars in the HARPS GTO planet search program. Stellar [Fe/H] and the frequency of exo-Neptunes. *A&A*, 487:373–381, August 2008. doi: 10.1051/0004-6361:200809698.
- [180] R. C. Stone. An Accurate Method for Computing Atmospheric Refraction. *PASP*, 108:1051–1058, November 1996. doi: 10.1086/133831.

## Bibliography

- [181] R. Suzuki, T. Kudo, J. Hashimoto, J. Carson, S. Egner, M. Goto, M. Hattori, Y. Hayano, K. Hodapp, M. Ito, M. Iye, S. Jacobson, R. Kandori, N. Kusakabe, M. Kuzuhara, T. Matsuo, M. McElwain, J.-I. Morino, S. Oya, Y. Saito, R. Shelton, V. Stahlberger, H. Suto, H. Takami, C. Thalmann, M. Watanabe, H. Yamada, and M. Tamura. Performance characterization of the HiCIAO instrument for the Subaru Telescope. In *Society of Photo-Optical Instrumentation Engineers (SPIE) Conference Series*, volume 7735 of *Society of Photo-Optical Instrumentation Engineers (SPIE) Conference Series*, July 2010. doi: 10.1117/12.857361.
- [182] O. Tamuz, D. Ségransan, S. Udry, M. Mayor, A. Eggenberger, D. Naef, F. Pepe, D. Queloz, N. C. Santos, B.-O. Demory, P. Figuera, M. Marmier, and G. Montagnier. The CORALIE survey for southern extra-solar planets. XV. Discovery of two eccentric planets orbiting HD 4113 and HD 156846. *A&A*, 480:L33–L36, March 2008. doi: 10.1051/0004-6361:20078737.
- [183] I. B. Thompson, J. Kaluzny, S. M. Rucinski, W. Krzeminski, W. Pych, A. Dotter, and G. S. Burley. The Cluster AgeS Experiment (CASE). IV. Analysis of the Eclipsing Binary V69 in the Globular Cluster 47 Tuc. *AJ*, 139:329–341, February 2010. doi: 10.1088/0004-6256/139/2/329.
- [184] C. G. Tinney, R. P. Butler, G. W. Marcy, H. R. A. Jones, A. J. Penny, C. McCarthy, and B. D. Carter. Two Extrasolar Planets from the Anglo-Australian Planet Search. *ApJ*, 571:528–531, May 2002. doi: 10.1086/339916.
- [185] G. Torres, J. Andersen, and A. Giménez. Accurate masses and radii of normal stars: modern results and applications. *A&A Rev.*, 18:67–126, February 2010. doi: 10.1007/s00159-009-0025-1.
- [186] G. Torres, F. Fressin, N. M. Batalha, W. J. Borucki, T. M. Brown, S. T. Bryson, L. A. Buchhave, D. Charbonneau, D. R. Ciardi, E. W. Dunham, D. C. Fabrycky, E. B. Ford, T. N. Gautier, III, R. L. Gilliland, M. J. Holman, S. B. Howell, H. Isaacson, J. M. Jenkins, D. G. Koch, D. W. Latham, J. J. Lissauer, G. W. Marcy, D. G. Monet, A. Prsa, D. Ragozzine, J. F. Rowe, D. D. Sasselov, J. H. Steffen, and W. F. Welsh. Modeling Kepler transit light curves as false positives: Rejection of blend scenarios for Kepler-9, and validation of Kepler-9d, a super-Earth-size planet in a multiple system. *ArXiv e-prints*, August 2010.
- [187] S. Trippe, S. Gillessen, O. E. Gerhard, H. Bartko, T. K. Fritz, H. L. Maness, F. Eisenhauer, F. Martins, T. Ott, K. Dodds-Eden, and R. Genzel. Kinematics of the old stellar population at the Galactic centre. *A&A*, 492:419–439, December 2008. doi: 10.1051/0004-6361:200810191.
- [188] R. N. Tubbs. Lucky exposures: diffraction-limited astronomical imaging through the atmosphere. *The Observatory*, 124:159–160, April 2004.
- [189] V. G. Turyshev. Relativistic gravitational deflection of light and its impact on the modeling accuracy for the Space Interferometry Mission. *Astronomy Letters*, 35:215–234, April 2009. doi: 10.1134/S106377370904001X.

- [190] R. K. Tyson. *Introduction to Adaptive Optics*. 2000.
- [191] U. S. Government Printing Office. *The Astronomical Almanac for the year 2008*. 2006.
- [192] S. Udry, M. Mayor, D. Naef, F. Pepe, D. Queloz, N. C. Santos, M. Burnet, B. Confino, and C. Melo. The CORALIE survey for southern extra-solar planets. II. The short-period planetary companions to HD 75289 and HD 130322. *A&A*, 356:590–598, April 2000.
- [193] P. van de Kamp. Planetary companions of stars. *Vistas in Astronomy*, 2:1040–1048, 1956. doi: 10.1016/0083-6656(56)90030-7.
- [194] P. van de Kamp. Astrometric study of Barnard’s star from plates taken with the 24-inch Sproul refractor. *AJ*, 68:515–521, September 1963. doi: 10.1086/109001.
- [195] P. van de Kamp. The planetary system of Barnard’s star. *Vistas in Astronomy*, 26:141–157, 1982. doi: 10.1016/0083-6656(82)90004-6.
- [196] R. P. van der Marel, J. Anderson, C. Cox, V. Kozhurina-Platais, M. Lallo, and E. Nelan. Calibration of ACS/WFC Absolute Scale and Rotation for Use in creation of a JWST Astrometric Reference Field. Technical report, July 2007.
- [197] F. van Leeuwen. Hipparcos, the New Reduction (van Leeuwen, 2007). *VizieR Online Data Catalog*, 1311:0–+, September 2008.
- [198] S. S. Vogt, G. W. Marcy, R. P. Butler, and K. Apps. Six New Planets from the Keck Precision Velocity Survey. *ApJ*, 536:902–914, June 2000. doi: 10.1086/308981.
- [199] S. S. Vogt, R. P. Butler, G. W. Marcy, D. A. Fischer, G. W. Henry, G. Laughlin, J. T. Wright, and J. A. Johnson. Five New Multicomponent Planetary Systems. *ApJ*, 632:638–658, October 2005. doi: 10.1086/432901.
- [200] S. S. Vogt, R. A. Wittenmyer, R. P. Butler, S. O’Toole, G. W. Henry, E. J. Rivera, S. Meschiari, G. Laughlin, C. G. Tinney, H. R. A. Jones, J. Bailey, B. D. Carter, and K. Batygin. A Super-Earth and Two Neptunes Orbiting the Nearby Sun-like Star 61 Virginis. *ApJ*, 708:1366–1375, January 2010. doi: 10.1088/0004-637X/708/2/1366.
- [201] J. V. Wall and C. R. Jenkins. *Practical Statistics for Astronomers*. November 2003.
- [202] S. Witte, C. Helling, and P. H. Hauschildt. Dust in brown dwarfs and extra-solar planets. II. Cloud formation for cosmologically evolving abundances. *A&A*, 506:1367–1380, November 2009. doi: 10.1051/0004-6361/200811501.
- [203] J. T. Wright, G. W. Marcy, R. P. Butler, and S. S. Vogt. Chromospheric Ca II Emission in Nearby F, G, K, and M Stars. *ApJS*, 152:261–295, June 2004. doi: 10.1086/386283.

## Bibliography

- [204] H. Zimmermann and A. Weigert. *ABC-Lexikon Astronomie*. 1995.
- [205] S. Zucker, D. Naef, D. W. Latham, M. Mayor, T. Mazeh, J. L. Beuzit, G. Drukier, C. Perrier-Bellet, D. Queloz, J. P. Sivan, G. Torres, and S. Udry. A Planet Candidate in the Stellar Triple System HD 178911. *ApJ*, 568:363–368, March 2002. doi: 10.1086/338892.
- [206] S. Zucker, T. Mazeh, N. C. Santos, S. Udry, and M. Mayor. Multi-order TOD-COR: Application to observations taken with the CORALIE echelle spectrograph. I. The system HD 41004. *A&A*, 404:775–781, June 2003. doi: 10.1051/0004-6361:20030499.
- [207] S. Zucker, T. Mazeh, N. C. Santos, S. Udry, and M. Mayor. Multi-order TOD-COR: Application to observations taken with the CORALIE echelle spectrograph. II. A planet in the system HD 41004. *A&A*, 426:695–698, November 2004. doi: 10.1051/0004-6361:20040384.